New Materials for Injected Bolted Connections

A Feasibility Study for Demountable Connections

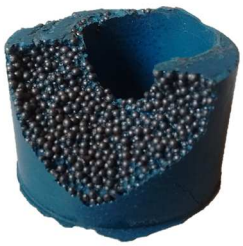

Master's Thesis

M. P. Nijgh

Faculty of Civil Engineering and Geosciences

Delft University of Technology

April 2017, Delft

TU Delft

New Materials for Injected Bolted Connections

A Feasibility Study for Demountable Connections

By

M. P. Nijgh

in partial fulfilment of the requirements for the degree of

Master of Science

in Civil Engineering

at Delft University of Technology,

to be defended publicly on Monday April 3, 2017 at 14:00hrs.

Supervisor:	prof. dr. M. Veljkovic	
Thesis committee:	ir. P. A. de Vries,	TU Delft
	dr. O. Çopuroğlu,	TU Delft

Front page: Shot-reinforced Perspex mould (top) and resin, grout and reinforced resin infill respectively (bottom)

Preface

This thesis is submitted as the last stepping stone towards obtaining a Master's degree in Civil Engineering at Delft University of Technology. The topic of the thesis relates to demountable injected slip-resistant connections, and mainly focuses on the effect of oversize holes, which can be used to ease erection and allow for re-use of structural members.

I started working on this thesis in December 2016, focusing mainly on the state-of-the-art. In January and February 2017 most of the experiments were carried out at the TU Delft Stevin II laboratory. I have used the testing rig continuously, maximizing the amount of experimental results that could be obtained within this period. In March, one long-term test with a duration of multiple weeks was planned. Throughout the entire period of thesis work, I have attempted to directly process all results and relevant information into this report. The month of March has been used to finalize this Master's Thesis, before planned graduation in April 2017.

I would like to thank the members of my Assessment Committee, prof. dr. M. Veljkovic, ir. P.A. de Vries and dr. O. Çopuroğlu for their guidance. Moreover, I would like to express my gratitude towards J. Hermsen and F.J.P Schilperoort for their aid with the preparation and execution of the experiments.

Although no commercial interest was served with the publication of this thesis, I would like to show my appreciation for Verwaard BV for supplying me with 20kgs of PAGEL V1-0HF grout, and Prins Staalhandel for contributing 25kgs of S330 carbon steel shot.

M.P. (Martin) Nijgh
Delft, April 2017

Abstract

The purpose of this thesis is to investigate the short- and long-term behaviour of injected bolted connections (IBCs) with oversize holes for various injection materials. A central theme in this thesis the demountability of IBCs, as a result of which several release agents are tested for their suitability in and effects on IBCs.

Injection bolts have been used successfully in engineering practice using epoxy resin to limit the amount of slip in bolted shear connections with normal clearance holes, but no explicit results are available for connections with oversize or slotted holes. The use of oversize or slotted holes may be beneficial for the (re-)erection process of structures, and thus it is investigated what the effects of such oversize or slotted holes are on the connection behaviour.
First, it is examined if grout is suitable as an injection material in injected bolted connections (IBCs), as well as what precautions are necessary to ensure proper demountability of grout- and (epoxy) resin-injected bolted connections. Secondly, the connection behaviour under short-term loading is determined, on the basis of which long-term creep tests are carried out. Finally, a new injection material is developed based on the preliminary conclusions drawn from the short- and long-term tests.

It is concluded that IBCs can be demounted by treating the connection members with a release agent. The results of the experiments show that the long-term behaviour of resin-injected connections is governing the design, but that modelling of this time-dependent behaviour requires additional testing. The short and long-term performance of the newly developed material (resin reinforced with steel shot) in IBCs with oversize holes is significantly better than that of only resin, on the basis of which it is recommended to further investigate the potential and behaviour of this material in engineering applications.

Table of Contents

List of Symbols and Abbreviations

A	Area	$[L^2]$
	Constant	[-]
A_s	Nominal bolt area in the threaded region	$[L^2]$
C_1	Constant in analytical framework	$[L/F]$
C_2	Constant in analytical framework	$[1/F]$
d	Diameter	$[L]$
d_b	Bolt diameter	$[L]$
E	Young's Modulus	$[F/L^2]$
$E_{app,x}, E_{,x}$	Apparent longitudinal Young's Modulus	$[F/L^2]$
$\Delta E_{app,x,CP}$	Effect of cover plate on apparent Young's Modulus in x-direction	$[F/L^2]$
E_{cc}	Concrete stiffness under multiaxial compression	$[F/L^2]$
E_{cm}	Mean concrete stiffness	$[[F/L^2]$
$f_{b,resin}$	Bearing strength of the resin	$[F/L^2]$
$f_c, f_{c,k}$	(Characteristic) concrete uniaxial compressive strength	$[F/L^2]$
$f_{cc}, f_{ck,c}$	(Characteristic) concrete compressive strength under multiaxial compression	$[F/L^2]$
f_{ub}	Tensile strength of a bolt	$[F/L^2]$
f_1	Confining stress	$[F/L^2]$
F	Force	$[F]$
F_b	Bearing force	$[F]$
$F_{b,Rd}$	Design bearing resistance (plates)	$[F]$
$F_{b,Rd,resin}$	Design bearing resistance of resin	$[F]$
F_{LT}	Load during long-term tests, 90% of F_{ST}	$[F]$
$F_{p,C}$	Nominal pretension force	$[F]$
F_{ST}	Load at 0,15 mm slip based on k_{ini}	$[F]$
$F_{s,Rd}$	Design slip resistance of a pretensioned connection	$[F]$
$F_{v,Rd}$	Design shear resistance of bolt	$[F]$
k	Stiffness	$[F/L]$
k_{ini}	Initial stiffness	$[F/L]$
$k_{ini,FEA}$	Numerically obtained initial connection stiffness	$[F/L]$

$k_{ini,ana}$	Analytically obtained initial connection stiffness	[F/L]
k_s	Coefficient depending on m (injected bolts)	[-]
	Coefficient depending on type of hole (pretensioned bolts)	[-]
k_t	Coefficient depending on the appropriate limit state	[-]
k_1, k_2	Coefficients for determining respect. f_{cc} and ε_{cc}	[-]
K	Compressibility Modulus	[F/L²]
l	Length of bolt within clamping package	[L]
l_{inj}	Nominal clearance between bolt and hole in longitudinal direction	[L]
$\Delta\bar{l}_{cr}$	Order of magnitude of slip due to creep	[L]
L	Length of slotted hole	[L]
m	Coefficient depending on the oversizing/slotting of a hole	[-]
	Time-exponent in creep function	[-]
n	Number of faying surfaces	[-]
	Number of test results	[-]
	Stress-exponent in creep function	[-]
q	Uniaxial equivalent deviatoric stress	[F/L²]
t	Time	[T]
$t_{b,resin}$	Effective height of the resin	[L]
t_p	Plate thickness	[L]
t_1	Thickness of centre plate in a double lap connection	[L]
t_2	Thickness of cover plates in a double lap connection	[L]
u_{FEA}	Slip at CBG in FE-analysis	[L]
x	Longitudinal coordinate	[L]
β	Coefficient depending on the plate thickness ratio	[-]
γ_{M3}	Partial safety factor (1,25)	[-]
γ_{M4}	Partial safety factor (1,0)	[-]
ε_c, ε_{c2}	Strain at which f_c respect. $f_{c,k}$ is reached	[-]
ε_{cc}, $\varepsilon_{c2,c}$	Strain at which f_{cc} respect. $f_{ck,c}$ is reached	[-]
ε_{cr}	Creep strain	[-]
$\varepsilon_{xx,yy,zz}$	Normal strain in x-, y- and z- direction, respectively	[-]

η_{Kepler}	Maximum packing density of equal spheres	[-]
θ	Angle with respect to longitudinal direction	[rad]
μ	Slip factor	[-]
υ	Poisson ratio	[-]
π	Constant (3,14…)	[-]
σ_b	Bearing stress	[F/L²]
$\sigma_{xx,yy,zz}$	Normal stress in x-, y- and z- direction, respectively	[F/L²]
$Ø_{centre}$	Diameter of hole in centre plate	[L]

CBG	Centre Bolt Group
PE	Plate Edge
RCSC	Research Council on Structural Connections
EN	European Norm
ISO	International Standardization Organisation
IBC	Injected Bolted Connection
NAP	Normaal Amsterdams Peil (Dutch Ordnance Datum)
LVDT	Linear Variable Differential Transformer
SMA	Stone Mastic Asphalt

List of Figures

List of Tables

1 Introduction

Injection bolts were invented in the $1970s$ in order to extend the service lifetime of riveted railway bridges. Conventional bolted connections may not be used in such cases due to the cyclic loading, and the use of pretensioned connections is difficult since the condition (slip coefficient) of the faying surfaces is unknown. One of the goals of injection bolts is to limit the connection slip to $0{,}3\ \mathrm{mm}$ during the service lifetime (mostly 50 years), whereas this can easily be $2-3\ \mathrm{mm}$ in case of conventional bolts to even get the bolts in initial bearing [1]. Another key feature of injection bolts above conventional and pretensioned bolts is that no sudden connection slip can occur [2].

Apart from the initial application in railway bridges, injection bolts have later been used in for instance windmills, crane girders [2] and in the Maeslant Storm Surge Barrier.

Given that there is an increasing tendency towards achieving a circular economy, one of the goals in structural engineering is to stimulate re-use of structural members. The connection between re-usable structural members must be such that the structure can (1) be erected initially, (2) be demounted easily and (3) re-erected quickly. One of the ways to achieve a connection that fulfils these demands is to use injection bolts in combination with oversize bolt holes. The oversize holes allow for simple erection, whereas the injection material transfers the force from the member to bolt and vice versa. It shall be noted that the structural members do not necessarily have to be from the same material (e.g. steel), but that also a combination of different element types (e.g. steel beam, concrete floor) can be connected in such a way. In such cases, an additional hole clearance is necessary to take account of the different fabrication tolerances.

The main goals of this thesis are to investigate:

- The demountability of injected bolted connections (IBCs) in general
- The short- and long-term behaviour of IBCs with oversize holes
- The potential of currently non-allowed injection materials in IBCs with oversize holes

If the results of the investigation are promising, it could well be that a completely new field of application is opened up for the use of injection bolts.

1.1 Research Questions

The following research questions have been defined:

- What is the difference between grout-like and resin-like materials? Is it feasible to use grout-like materials in injected bolted connections?
- What is the effect of oversize or slotted holes on the structural behaviour of injected bolted connections?
- What is the strength/stiffness of injected bolted connections with oversize or slotted holes?
- What is the creep/long-term behaviour of injected bolted connections?
- Can injected bolted connections be easily demounted? If not, what measures need to be taken to allow for easy demounting?
- What is the effect of the cover plate that shall be used in case of oversize or slotted holes?
- What alternative injection materials may yield better results than conventional epoxy resins or grout?

1.2 Reader's Guide

Chapter 2 discusses the state of the art on injected bolted connections. In Chapter 3, the methods are defined that are used to answer the research questions presented in Chapter 1. Chapter 4 displays the results obtained using the methods, on the basis of which a numerical model is verified in Chapter 5. Moreover, chapter 5 presents several factors that have an apparent influence on the connection behaviour. Based on the results from Chapter 4, a new material is developed in Chapter 6, where also results are presented. Finally, discussion of all results takes place in Chapter 7, leading to the conclusions and recommendations posed in Chapter 8. The overall structure of this thesis is presented in the flowchart below.

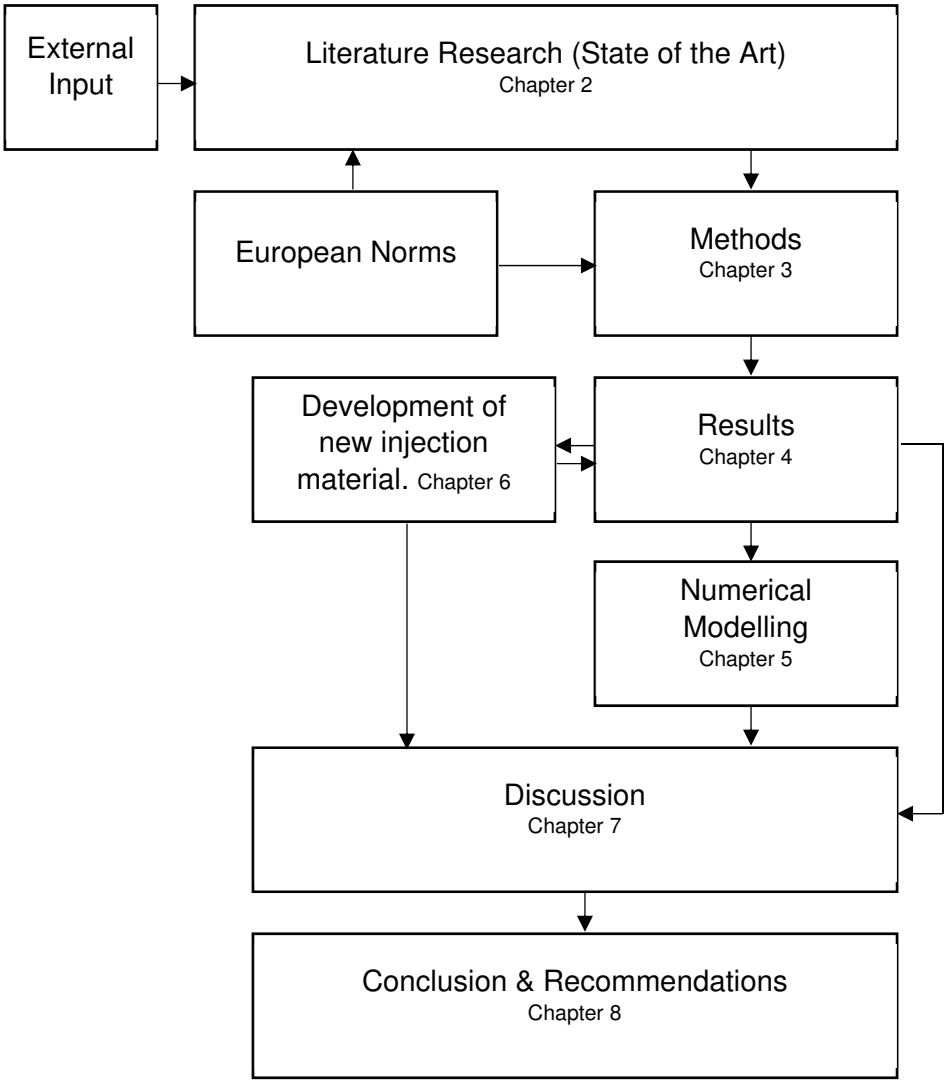

2 State of the Art

2.1 Current Regulation on Injection Bolts

The current regulations regarding injection bolts are laid down in EN 1993-1-8 [3] and EN 1090-2 [4]. The first discusses the calculation rules for the design resistance of a connection with injected bolts, whereas the latter provides executional information on the detailing of the bolt and bolt hole itself.

2.1.1 Connection Components

In Figure 1, an overview of all components in a resin-injected bolted connection are shown. The components are discussed one by one in the subsequent sections.

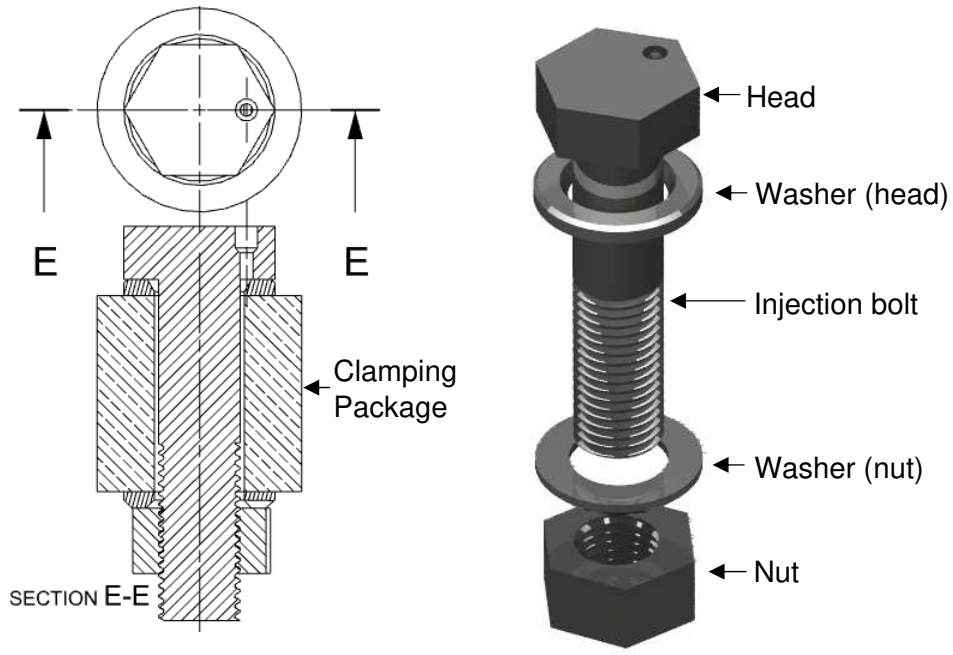

Figure 1 - Left: cross section of an assembly with an injection bolt. Right: exploded view indicating differing components within the assembly.

Fasteners

In principle, all fasteners of steel grades 8.8 and 10.9 that are allowed for preloaded and non-preloaded connections may be used in resin-injected bolted connections. Such fasteners are laid down in respectively EN 14399 and EN 15048. In order to be able to inject the bolted assembly with resin, a hole is present in the head of the bolt, as indicated in Figure 2 (hole dimensions cf. Annex K of EN 1090-2 [4]). In case the bolts are designed to be preloaded, the tightening should occur before the injection of the resin.

Washers

In case of resin-injected bolted connections, the use of special washers is prescribed under both the head and nut. The washers must fulfil the requirements of EN 1090-2 Annex K. The washer under the head of the bolt promotes easy ingress of resin into the open space between bolt and plate package, whereas the washer under the nut includes a groove through which the air can escape during the injection of the resin. Both types of washers are shown in Figure 3.

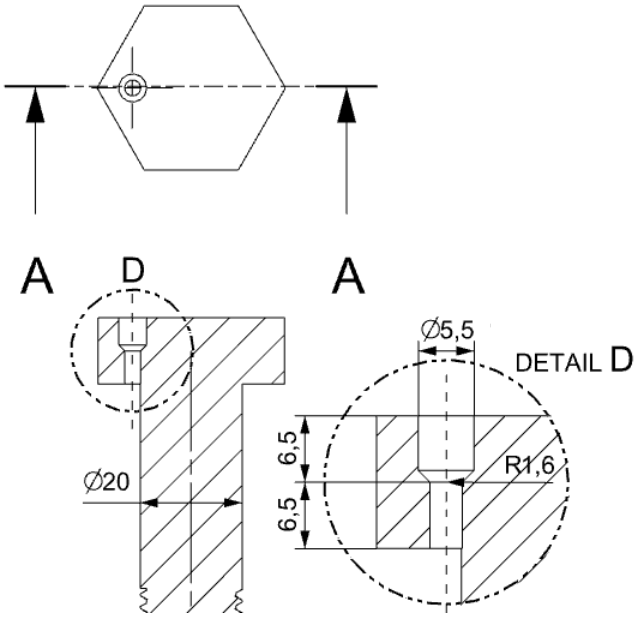

Figure 2 - Bolt head with resin channel. Dimensions in mm for an M20 bolt. Diameter of resin channel is invariant with differing bolt sizes.

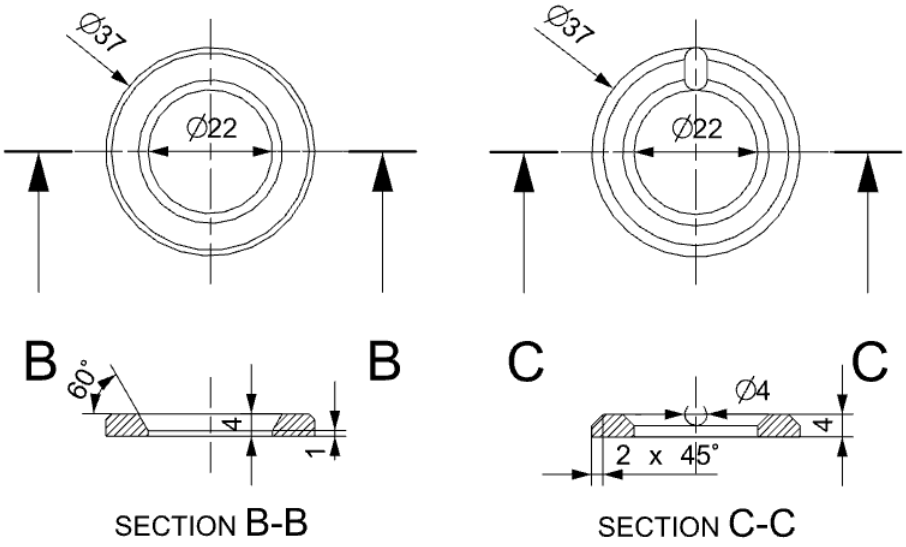

Figure 3 - Special washers used in injected assemblies, dimensions in mm for use in combination with M20 bolts. Left: washer under bolt head. Right: washer under nut (groove facing towards the nut)

Plate Package

The prescriptions regarding the hole diameter for injected assemblies are the same as for regular bolted assemblies, and are laid down in Table 11 of EN 1090-2 [4]. The nominal diameter of the holes in the clamping package must be 3 mm more than the nominal bolt diameter. An exception is applicable for bolt smaller than M27: in this case the minimum nominal hole diameter may be reduced to 2 mm more than the nominal bolt diameter.

Resin

It is prescribed that a two component epoxy resin with a pot life of at least 15 minutes should be used to inject the bolted assembly. The type of resin itself is not further defined, however end result specifications apply: the resin should fill all cavities in the connection and stop flowing after removal of the injection pressure. Epoxy resins are thermosetting polymers, meaning that they will not melt after heating up, but rather burn.

2.1.2 Design Resistance

Static Resistance

The design resistance of a resin-injected bolted connection is dependent on the connection category. In case of a non-preloaded injected shear connection (cat. A), the design resistance of a bolt is the smallest value of the design shear resistance $\mathrm{F_{v,Rd}}$ of the bolt and the design bearing resistance $F_{b,Rd,resin}$ (Eq. 3) of the resin. The design shear resistance of a cat. A connection is given by Eq. 1.

$$F_{Rd,A} = \min(F_{b,Rd,resin}, F_{v,Rd}) \qquad \text{Eq. 1}$$

In case of a preloaded injected shear connection (cat. B/C), the design resistance is the sum of the design slip resistance $F_{s,Rd}$ due to the clamping force (see Section 2.1.2) and the design bearing resistance $F_{b,Rd,resin}$ of the resin. In the case of category B and C connections, the design ultimate shear load in a bolt may not exceed either the bolt design shear resistance $F_{v,Rd}$ or the design bearing resistance $F_{b,Rd}$. The mathematical representation of the design resistance for cat. B/C connections is given by Eq. 2.

$$F_{Rd,B/C} = \min(F_{s,Rd} + F_{b,Rd,resin}, F_{v,Rd}, F_{b,Rd}) \qquad \text{Eq. 2}$$

The bearing resistance of the resin is expressed by Eq. 3.

$$F_{b,Rd,resin} = \frac{k_t \cdot k_s \cdot d \cdot t_{b,resin} \cdot \beta \cdot f_{b,resin}}{\gamma_{M4}} \qquad \text{Eq. 3}$$

with:

β and $t_{b,resin}$	are given by Table 1.
$f_{b,resin}$	is the bearing strength of the resin, to be determined using Annex G of EN 1090-2 (for The Netherlands, see the National Annex of EN 1993-1-8).
k_t	$k_t = \begin{cases} 1{,}0 & \text{for SLS (long duration)} \\ 1{,}2 & \text{for ULS} \end{cases}$
k_s	k_s is 1,0 for holes with normal clearances, or $1{,}0 - 0{,}1 \cdot m$ for oversized holes
m	m is the difference (in mm) between the normal and oversized hole dimensions. For short slotted holes m is half the difference between slot length and width [5].

Table 1 - Values of β and $t_{b,resin}$ as a function of ratio t_1/t_2 [3] in double lap shear connections. The definition of t_1 and t_2 is given in Figure 4.

t_1/t_2	β	$t_{b,resin}$
$\geq 2{,}0$	$1{,}0$	$\min(2 \cdot t_2; 1{,}5 \cdot d)$
$1{,}0 < t_1/t_2 < 2{,}0$	$1{,}66 - 0{,}33 \cdot (t_1/t_2)$	$\min(t_1; 1{,}5 \cdot d)$
$\leq 1{,}0$	$1{,}33$	$\min(t_1; 1{,}5 \cdot d)$

The length $t_{b,resin}$ is the length over which the resin is considered to be effective. It is assumed that for $l/d > 3$ bending deformation of the bolt may induce an uneven bearing stress distribution, and therefore $t_{b,resin}$ is currently limited to $2 \cdot 1{,}5d$ for a double lap connection, as indicated in Figure 5.

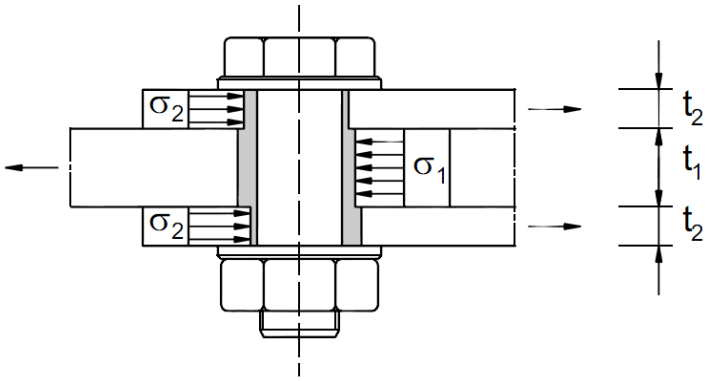

Figure 4 - Definition of t_1 and t_2 according to EN 1090-2 [4]

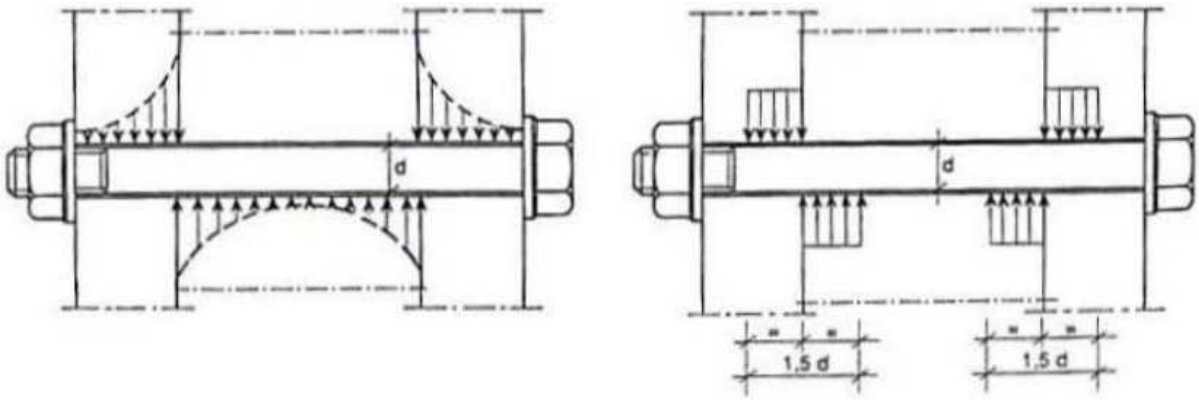

(a) (b)

Figure 5 - Bearing stress distribution in case of long bolts [5], (a) schematized true stress situation, (b) idealized calculation model

Fatigue

The structural resistance against failure due to fatigue is governed by EN 1993-1-9. Resin-injected bolted double lap connections have detail category 90, unless the bolts are also preloaded. In this case the detail category may be assumed to be 112. In case of single lap connection without preloaded bolts, the detail category is 80, and is raised to category 90 when the bolts are also preloaded. The detail category per connection type is summarized in Table 2.

Table 2 - Detail category according to EN 1993-1-9 for different connection detailing.

	Non-Preloaded		Preloaded	
Connection Type	Double-lap	Single-lap	Double-lap	Single-lap
Non-Injected	50	50	112	90
Injected	90	80	112	90

Although EN 1993-1-9 does not distinguish between preloaded and preloaded resin-injected connections, experimental research on connections taken from existing bridges has indicated that in case of the latter the fatigue strength is considerably reduced [6]. However, more recent numerical experiments have been carried out, indicating resin-injecting a preloaded connection has a beneficial effect on its fatigue strength [7], which is also supported by current TU Delft research.

2.2 Current Regulation on Pretensioned Connections

The current regulation on pretensioned connections is only briefly touched upon in this thesis, since most of the background information on this topic can be found in earlier work (i.e. Nijgh (2016) [8]). However, the following section does include the most important information.

2.2.1 Connection Components

Fasteners

All fasteners used in pretensioned connections must fulfil the requirements prescribed in EN 14399 [9]. Only bolts of property class 8.8 and 10.9 are allowed to be pretensioned. In order not to have problems regarding thread stripping, it is mandatory to leave a minimum of four threads sticking out at the free surface of the nut.

Washers

It is prescribed that a washer must be installed at the surface on which the pretension is applied. In case of 10.9 grade bolts, a washer must be present under both the bolt head an nut, regardless of the side that is used to achieve the pretension.

2.2.2 Design Resistance

Tightening of the bolts should be done according to EN 1090-2, which results in the initial pretension level of Eq. 4 [4] [3].

$$F_{p,C} = 0{,}7 \cdot f_{ub} \cdot A_s \qquad \text{Eq. 4}$$

With:

$F_{p,C}$	Nominal preload force in the bolt $[\mathrm{F}]$
f_{ub}	Tensile strength of the bolt $[\mathrm{F/L^2}]$
A_s	Tensile stress area $[\mathrm{L^2}]$

The design slip resistance of pretensioned connections is given by Eq. 5 [3].

$$F_{s,Rd} = \frac{k_s \cdot n \cdot \mu}{\gamma_{M3}} \cdot F_{p,C} \qquad \text{Eq. 5}$$

With:

$F_{s,Rd}$	Design slip resistance $[\mathrm{F}]$
k_s	Coefficient depending on the type of hole (see Section 2.7) $[-]$
μ	Slip factor (Figure 7) $[-]$
n	Number of faying surfaces $[-]$
γ_{M3}	Partial safety factor $[-]$
$F_{p,C}$	See Eq. 4

Description	k_s
Bolts in normal holes.	1,0
Bolts in either oversized holes or short slotted holes with the axis of the slot perpendicular to the direction of load transfer.	0,85
Bolts in long slotted holes with the axis of the slot perpendicular to the direction of load transfer.	0,7
Bolts in short slotted holes with the axis of the slot parallel to the direction of load transfer.	0,76
Bolts in long slotted holes with the axis of the slot parallel to the direction of load transfer.	0,63

Figure 6 - Coefficient k_s used to determine the design slip resistance of pretensioned connections conform EN 1993-1-8 [4] [3]

If one were to use a different surface treatment than mentioned in Figure 7, tests have to be carried out in compliance with Annex G of EN 1090-2 in order to prove that the long-term connection slip as a result of creep remains sufficiently small (maximum 0,3 mm slip after the service lifetime, mostly 50 years).

Surface treatment	Class	Slip factor μ
Surfaces blasted with shot or grit with loose rust removed, not pitted.	A	0,50
Surfaces blasted with shot or grit: a) spray-metallized with a aluminium or zinc based product; b) with alkali-zinc silicate paint with a thickness of 50 µm to 80 µm	B	0,40
Surfaces cleaned by wire-brushing or flame cleaning, with loose rust removed	C	0,30
Surfaces as rolled	D	0,20

Figure 7 - Slip factor μ for surface treatment classes A-D (EN 1090-2) [4] [3]

2.3 Current Applications

This section briefly discusses two distinct projects in which injection bolts have been implemented. For more examples, reference is made to the ECCS Recommendations (1994) [5].

2.3.1 Repair of Riveted Connections Using Injection Bolts

Damaged riveted connections have been replaced with injection bolts in The Netherlands since the 1970s. The choice for using resin-injected bolted connections as a replacement rather than using the new rivets lies in the fact that riveting was not a very common connection method anymore, and thus that it was hard to find skilled workers. An example of a (German) bridge in which rivets are replaced with resin-injected bolts is shown in Figure 8. Numerical research has shown that replacement of rivets with injection bolts leads to an increase of load transferred by the rivets, which is mainly related to the relatively low stiffness of the resin [10]. In case the resin does not fully fill the cavity between the hole and bolt (e.g. due to too little injected resin, too high resin viscosity), the differential load distribution is aggravated.

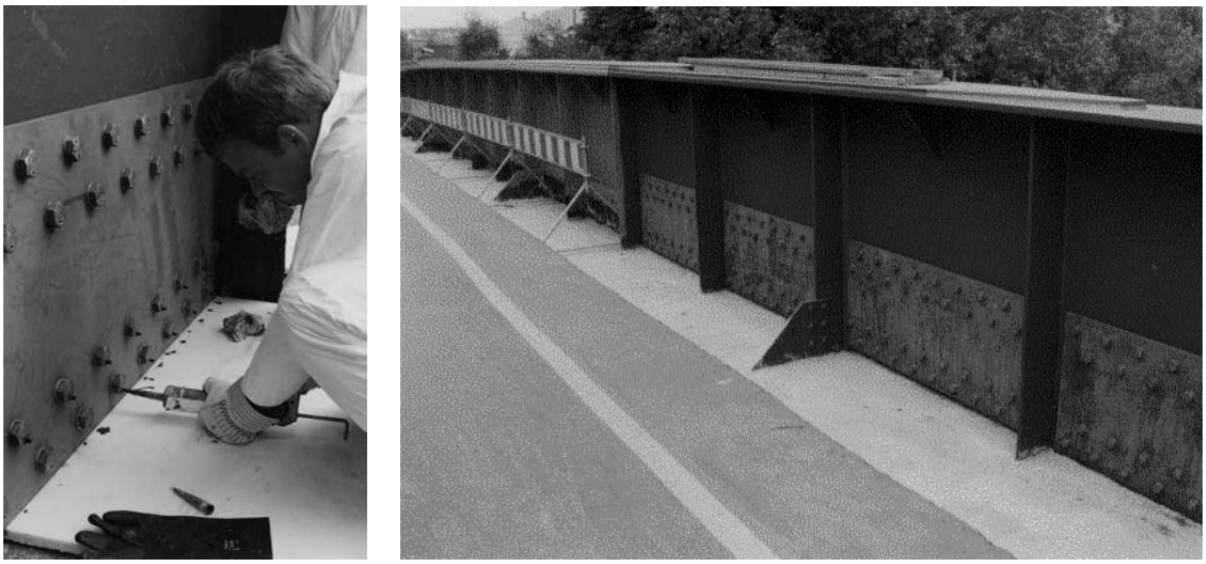

Figure 8 - Injection bolts in the Schlossbrücke Oranienburg (Germany). Left: injection process, Right: general overview of the final result [60]

2.3.2 Slip-resistant Connection in Maeslant Storm Surge Barrier

The Maeslant Storm Surge Barrier (Figure 9) protects two million people against storm surges in the province of South-Holland in The Netherlands. Located at the mouth of the Rhein-Meuse estuary, it keeps the seawater from entering into the river system, hereby reducing the water levels in Rotterdam and its vicinity. The gates are usually open: only storms causing water levels of more than $3\ \mathrm{m}\ +\mathrm{NAP}$ (ordnance datum) cause the gates to close, which happens on average every 5-10 years. The force of the water on the gates can be as large as $36\ \mathrm{MN}$, which has to be transferred through a truss to the system's ball bearing into the foundation. In order to prevent connection slip at the connection between the truss and ball bearing, resin-injected preloaded bolts have been used of metric sizes $\mathrm{M56}$, $\mathrm{M64}$, $\mathrm{M72}$ and even $\mathrm{M80}$. The main reason for such large bolt sizes is that the plate package is rather thick, and the contractors wanted to stay within the range $l/d \leq 3$.

An overview of the Maeslant Storm Surge Barrier is given in Figure 9. The connection between the truss and ball bearing is illustrated in Figure 10

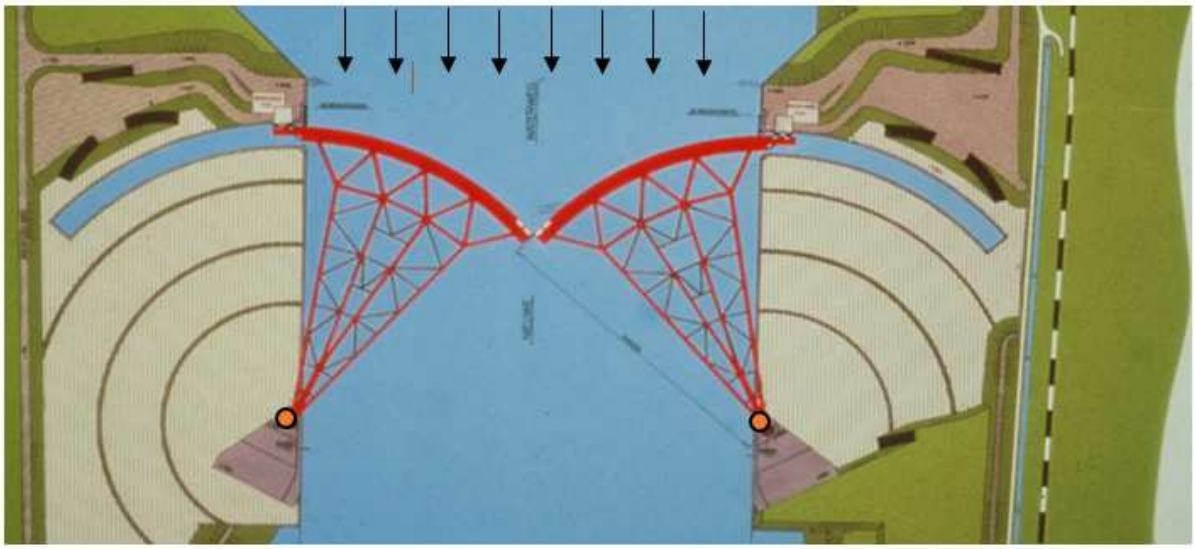

Figure 9 - Top view of the Maeslant Storm Surge Barrier in Hoek van Holland (The Netherlands) in closed condition [68]. Resin-injected preloaded bolts can be found in the connection between the trusses (red) with the ball bearing (orange)

Figure 10 – Detail image of resin-injected preloaded bolts in the Maeslant Storm Surge Barrier [75]

2.4 Installation & Costs

The installation of injection bolts consists of several steps. Most of the steps are equal to the steps taken during installation of conventional bolts, however in case of injection bolts the resin needs to be injected after tightening of the bolt(s). In case the connection is designed to be both pretensioned and injected, pretensioning to the specified level [3] [4] should be done prior to the injection. In any case, the plate package must be subjected by a small bolt preload in order to prevent the injection material from escaping between the connection members during injection.

In the ECCS Recommendations [5] the costs of (installing) a resin-injected bolted connection are broken down to:

1. The buying of the standard bolts
2. Adapting the standard bolts and washers to be able to inject the connection
3. The buying of the resin
4. The preparation of the resin
5. The application of the resin in the connection

The total costs for injection per bolt depend on the total amount of bolts, the accessibility of the bolts and the volume of resin needed to fill the cavity in the bolt hole [5]. It should be noted that it is also possible to purchase custom injection bolts which makes the adaptation process unnecessary. In the ECCS Recommendations (1994) [5] it is stated that generally speaking the labour time for injecting a single bolt with resin is between 1-2 minutes.

In order to make bolt holes in plates, often drilling or laser cutting is used. The costs of laser cutting of steel is proportional to the circumference of the desired shape [11] and other characteristics such as the plate thickness. It should be noted that laser cutting is generally more expensive than drilling. In order to obtain a slotted hole by drilling, one would drill two circular holes and mill away the material between these holes. The costs of the resin needed to fill the cavities between the holes and bolts is depending on the total volume of resin. Although a connection with injection bolts is more expensive than a normal bolted connection, it should be noted that (1) the purpose of the connection is different (e.g. slip resistant) or (2) that the re-use value of the members is increased (in case of demountable connections).

In Section 3.1 more attention is given to the costs of injection materials in general.

2.5 Material Properties

This section mainly discusses the material properties of resin and other materials that have the potential to be used as injection materials. Of particular interest are the compressive strengths, the Young's Modulus and the time-dependent behaviour of the materials under consideration. Before going into detail on the material properties of the distinct materials, first an introduction to the field of compressibility is given.

Compressibility of resin material is unwanted in slip-resistant connections, since the compressibility of the resin material yields additional connection slip. For isotropic linear elastic materials, the compressibility modulus K of a material is related to the Young's Modulus and Poisson Ratio through Eq. 6. Values of the Young's Modulus E and the Poisson Ratio υ can be derived from experimental results and product sheets.

$$K = \frac{E}{3 \cdot (1 - 2 \cdot \upsilon)} \qquad \text{Eq. 6}$$

With:

K	Compressibility Modulus $[\mathrm{F/L^2}]$
E	Young's Modulus $[\mathrm{F/L^2}]$
υ	Poisson ratio $[-]$

If one were to take the product sheet of $\mathrm{Araldite/RenGel\ SW\ 404 + HY\ 2404}$ [12], which indicates $E = 9000\ \mathrm{MPa}$, and literature indicating $\upsilon \approx 0.3$, using Eq. 6 would yield a compressibility modulus of $K = 7{,}5 \cdot 10^3\ \mathrm{MPa}$. Under uniform compression of $75\ \mathrm{MPa}$ this would lead to a volume reduction of 1%, which is a rather low stress for quite a significant volume reduction compared to e.g. steel, in which case a uniform compressive stress of $1750\ \mathrm{MPa}$ would be necessary to give the same volume reduction and thus the same negative effect.

2.5.1 Epoxy Resin

One of the most commonly used two component epoxy resins in injected bolted connections is $\mathrm{Araldite/RenGel\ SW\ 404}$ in combination with hardening agent $\mathrm{Ren\ HY\ 2404}$. It is the only two component resin that has been approved by the Dutch Ministry of Infrastructure (Rijkswaterstaat) to be used in injection bolts applied in their infrastructural works. $\mathrm{SW\ 404}$ in combination with $\mathrm{HY\ 2404}$ is an epoxy gelcoat which offers a high level of durability and has a pot life of 25-30 minutes. Other authors (e.g. Gresnigt & Beg (2013) [13]) have shown that for this specific two component resin, the long duration bearing stress can be taken as $f_{b,resin,LT} = 200\ \mathrm{MPa}$ and the short-term bearing stress as $f_{b,resin,ST} = 280\ \mathrm{MPa}$ [13]. According to the manufacturer, the Young's Modulus ranges between $E = 9 - 9{,}5\ \mathrm{GPa}$ whereas the uniaxial compressive strength ranges between $110 - 125\ \mathrm{MPa}$ [12]. However, several authors have found significantly different Young's Moduli, i.e. $E = 4{,}5 - 5\ \mathrm{GPa}$ (Kortis, 2011) [10] and $E = 3{,}2\ \mathrm{GPa}$ (de Freitas et al., 2012) [14]

Another potentially suitable resin for injection bolts is $\mathrm{Sikadur\ 30}$, which according to the manufacturer, has a high creep resistance under permanent load and has a very good adhesion to for example steel. The properties of cured Sikadur 30 are given by the manufacturer, and are indicated in Table 3. The pot life of this resin is 90 minutes at room temperature. Research at TU Delft has indicated that the workability of $\mathrm{Sikadur\ 30}$ is rather low [15] if used in normal clearance holes. In order to facilitate the injection process to prevent workability issues, researchers at University of East London and Warwick University (Qureshi & Mottram, 2012) [16] have come up with an alternative washer design as illustrated in Figure 11.

Table 3 - Properties of Sikadur 30 [17] and Araldite/Rengel SW404 + HY2404 [12] according to manufacturers

Property	Sikadur 30	Araldite SW404+HY2404	Unit
Tensile Strength	24-27	-	MPa
Compressive Strength	70-80	110-125	MPa
Shear Strength	14-17	-	MPa
Shear Modulus	11,2	-	GPa
E-Modulus (compression)	9,6	9,0-9,5	GPa

The stress-strain curve of Sikadur 30 has been obtained by several authors by performing tensile and compressive tests on the cured resin material. Figure 12 shows the stress-train curve of Sikadur 30 [18] [19] under uniaxial tension and compression. It can be observed that under uniaxial tension the resin behaves rather brittle, and that under uniaxial compression, the material behaves more ductile. The shape of the stress-strain diagram does not differ significantly between different epoxy resins [18]. Carvalho (2007) [19] has suggested to describe the behaviour of Sikadur 30 under confined compression using hardening models, however such effects are only apparent at very large connection slip (> 4 mm). If one were to draw the stress-strain diagram of polymer material (such as polycarbonate) based on a specimen that has been confined laterally, one would find the diagram illustrated in Figure 14. To the authors knowledge, no confined compression test have been carried out yet on epoxy resins.

Koper (2017) [15] has carried out research in other resins that are not well-known in the field of resin-injected bolted connections, such as Edilon DEX G20 and Edilon DEX R2K. Also Araldite/RenGel SW 404 + HY 2404 and Sikadur 30 have been tested in this research. All double lap connections with the abovementioned resins initially show a linear relationship between force and connection slip when loaded in shear. Later, the behaviour tends to be more non-linear. One of the test results of Araldite/RenGel SW 404 in a double lap connection has been included in Figure 13 (Koper, 2017) [15].

The mechanical properties of epoxy resins are known to vary in time due to ageing processes. An extensive work is written on this topic by Kajorncheappunngam (1999) [20]. Ageing process may be initiated by aggressive media, such as acids or salt solutions. However, also water and temperature have an effect on the mechanical properties of epoxy resins. Generally, an increase in temperature after the initial curing has finished causes the glass transition temperature T_g to increase [20]. As a result of additional curing at higher temperatures, also the stiffness is found to increase [20]. On the contrary, cured epoxy resin submerged in water is found to have a lower T_g and a lower stiffness, however this is not explicitly quantified in the mentioned research. Also, it is concluded that at room temperature water has the most negative influence on the mechanical properties [20].

Figure 11 - Alternative designs for washer under bolt head to facilitate injection process [16]

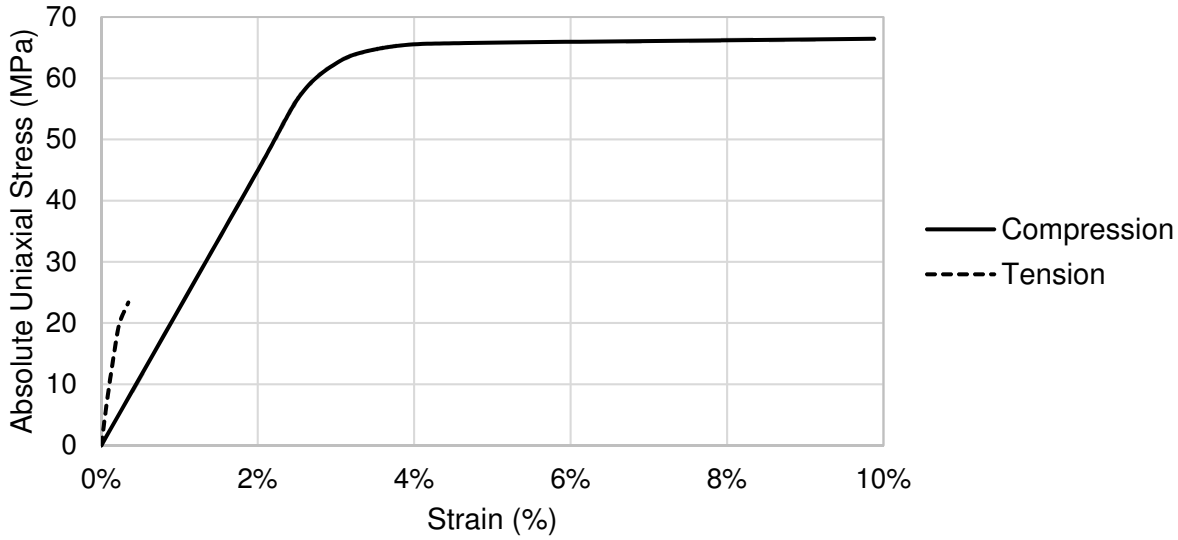

Figure 12 - Stress-Strain curve of Sikadur 30 for uniaxial (unconfined) tension [18] and compression [19]

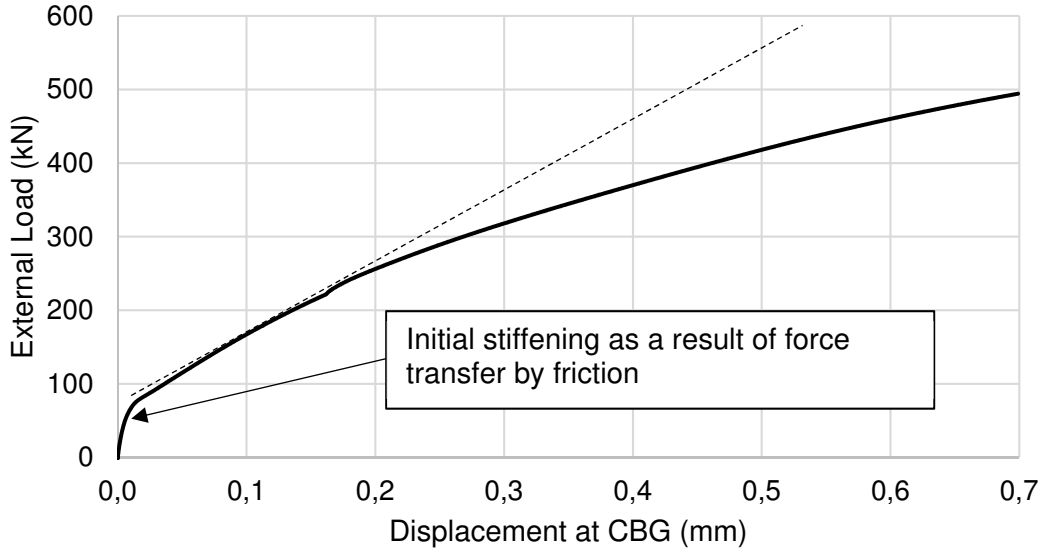

Figure 13 - Force-displacement relationship for a resin-injected double lap shear connection test according to Annex G of EN 1090-2 using Araldite/RenGel SW 404 + HY 2404 [15]

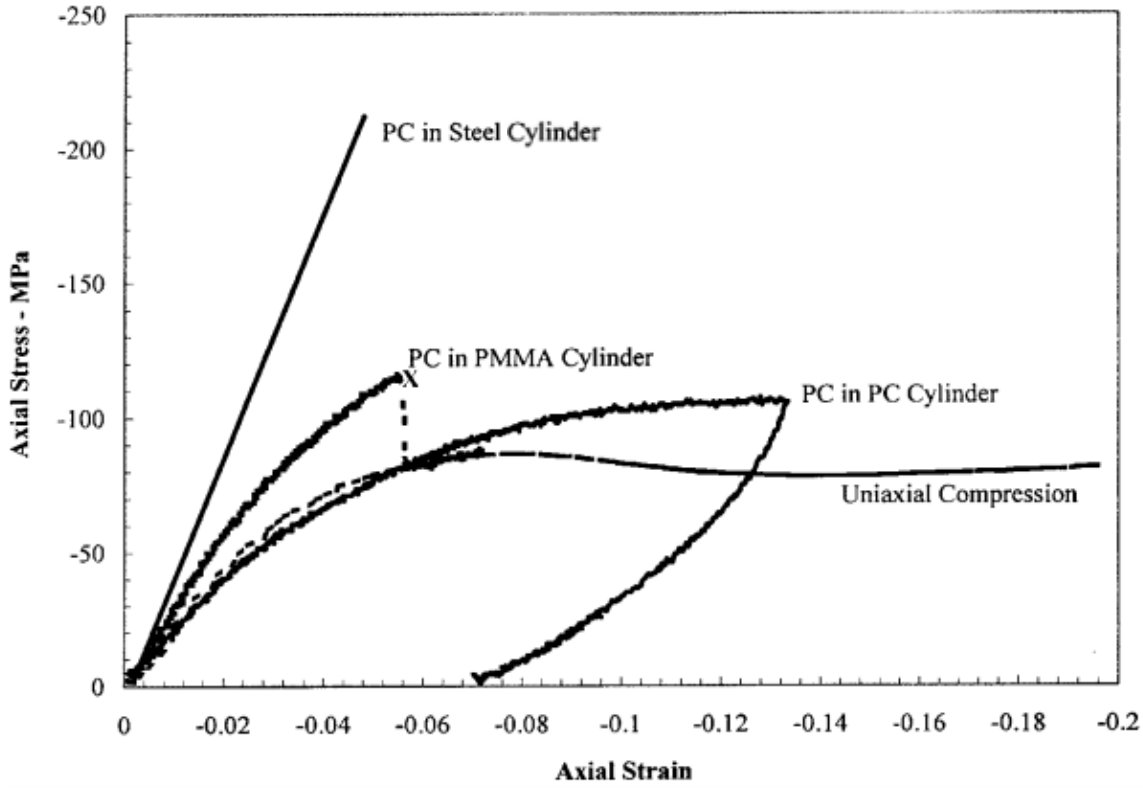

Figure 14 - Stress-Strain diagram for a polymer (PC, Polycarbonate) under different confinement conditions [62]. PMMA stands for acrylic (commonly known as Plexiglas). The stress-strain diagram clearly indicates the effect of confinement on the relationship between stress and strain.

Creep

All polymers, including epoxies, deform plastically over time due to creep (Daniels, 1989) [21]. Polymers are generally more sensitive to creep than metals and their creep rate is mostly dependent on stress, time and temperature.

The creep strain of epoxy resins can be approximated by a power law (Osswald, 2010) [22], which has been successfully done in earlier work [23]. The creep strain can be approximated by Eq. 7.

$$\varepsilon_{cr} = \frac{A}{m+1} \cdot q^n \cdot t^{m+1} \qquad \text{Eq. 7}$$

With:

A	Material constant $[\mathrm{L}^{2\mathrm{n}}/(\mathrm{F}^{\mathrm{n}} \cdot \mathrm{T}^{1+\mathrm{m}})]$
q	Uniaxial equivalent deviatoric stress (Mises stress) $[\mathrm{F}/\mathrm{L}^2]$
t	Time $[\mathrm{T}]$
m	Time exponent (material property) $[-](-1 < m < 0)$
n	Stress exponent (material property) $[-]$ $(n > 1)$

A potential consequence of creep is that the epoxy resin moves around the bolt to the non-bearing side of the connection (Bouwman, 1974) [24]. As a result, the bolt is able to move slightly in the direction of load transfer which induces connection slip, as indicated in Figure 15

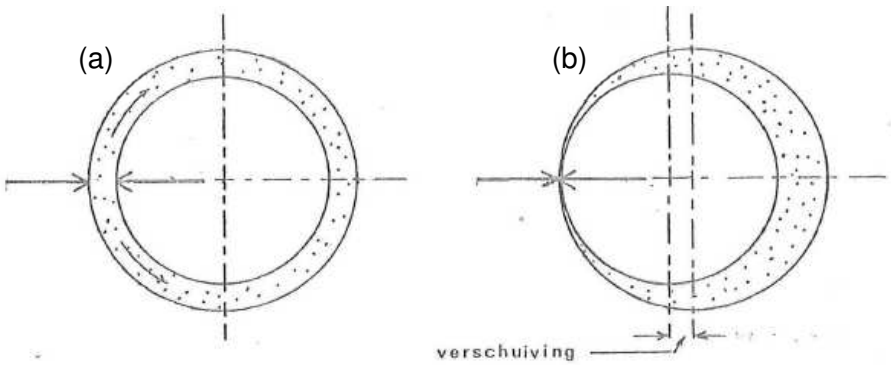

Figure 15 – (a) original situation, (b) slip (verschuiving) as a result of resin creep [24]

2.5.2 Grout

Currently, the use of grout in injected bolted connections is prohibited for the simple reason that grout is not a two component epoxy resin. However, grout may be a suitable injection material, because of its high compressive strength and Young's Modulus. Apart from the general problem of creep in injection materials, particular attention should be paid to the shrinkage of the mortar used for injection.

Generally, for materials that are subjected to multiaxial compression, higher external loads can be withstood than in case of uniaxial compression. For concrete, Ellobody & Young (2006) [25] have suggested the stress-strain diagram illustrated in Figure 16. The terms f_{cc} and ε_{cc} that are indicated in Figure 16 can be computed using the relations of Eq. 8 and Eq. 9, suggested by Manders et al. (1988) [26].

$$f_{cc} = f_c + k_1 \cdot f_1 \qquad \text{Eq. 8}$$

$$\varepsilon_{cc} = \varepsilon_c \cdot \left(1 + k_2 \cdot \frac{f_1}{f_c}\right) \qquad \text{Eq. 9}$$

With:

f_{cc}	Confined concrete compressive strength $[\mathrm{F/L^2}]$
ε_{cc}	Strain at f_{cc} $[-]$
f_c	Uniaxial concrete compressive strength $[\mathrm{F/L^2}]$
ε_c	Strain at f_c $[-]$
f_1	Lateral confining pressure $[\mathrm{F/L^2}]$
k_1, k_2	Constants $[-]$ ($k_1 \approx 4.1$ and $k_2 \approx 20.5$ [27])

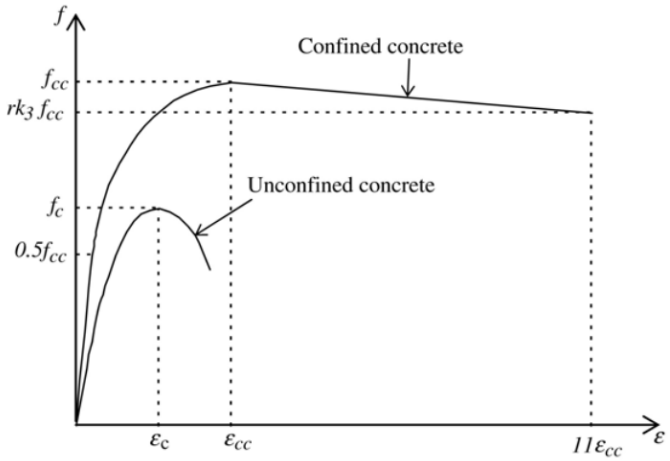

Figure 16 - Stress-strain diagram for concrete under uniaxial and confined (multiaxial) compression [25]

The initial concret concrete compressive stiffness E_{cc} is constant up to $0{,}5 \cdot f_{cc}$ and can be expressed as Eq. 10.

$$E_{cc} = 4700\sqrt{f_{cc}}\ [\mathrm{MPa}] \qquad \text{Eq. 10}$$

The stress-strain path is further defined by Eq. 11 [28] with the parameters of Eq. 12 and Eq. 13 for the stress interval between $0{,}5 \cdot f_{cc}$ and f_{cc}. The parameters R_σ and R_ε are recommended to be taken as 4 by Hui & Schnobrich (1989) [29]. The definition of all other parameters can be found from Figure 16.

$$f = \frac{E_{cc}\varepsilon_{cc}}{1 + (R + R_E - 2)\left(\frac{\varepsilon}{\varepsilon_{cc}}\right) - (2R - 1)\left(\frac{\varepsilon}{\varepsilon_{cc}}\right)^2 + R\left(\frac{\varepsilon}{\varepsilon_{cc}}\right)^3} \quad \text{Eq. 11}$$

$$R_E = \frac{E_{cc}\varepsilon_{cc}}{f_{cc}} \quad \text{Eq. 12}$$

$$R = \frac{R_E(R_\sigma - 1)}{(R_\varepsilon - 1)^2} - \frac{1}{R_\varepsilon} \quad \text{Eq. 13}$$

EN 1992-1-1 [30] allows for the stress-strain relationship of confined concrete shown in Figure 17. Eq. 14, Eq. 15 and Eq. 16 may be used to define the stress-strain curve of confined concrete. The equations from the Eurocode have more or less the same build-up as suggested by Manders et al. (1988) [26], and have slightly lower admissible compressive stress compared to the suggestions of Richart et al. (1928) [27]. However, if more detailed test results are available, the compressive strength under confinement may be determined using this data.

$$f_{ck,c} = f_{ck}\left(1 + 2{,}5 \cdot \frac{\sigma_2}{f_{ck}}\right) \quad \text{Eq. 14}$$

$$\varepsilon_{c2,c} = \varepsilon_{c2} \cdot \left(\frac{f_{ck,c}}{f_{ck}}\right)^2 \quad \text{Eq. 15}$$

$$\varepsilon_{cu2,c} = \varepsilon_{c2} + 0{,}2 \cdot \frac{\sigma_2}{f_{ck}} \quad \text{Eq. 16}$$

With:

$f_{ck,c}$	Characteristic compressive concrete strength under confinement $[\mathrm{F/L^2}]$
f_{ck}	Uniaxial compressive concrete strength $[\mathrm{F/L^2}]$
σ_2	Confining stress $[\mathrm{F/L^2}]$
$\varepsilon_{c2,c}$	Strain upon reaching $\mathrm{f_{ck,c}}$ $[-]$
ε_{c2}	Strain at $\mathrm{f_{ck}}$ $[-]$
$\varepsilon_{cu2,c}$	Ultimate strain of compressed and confined concrete $[-]$

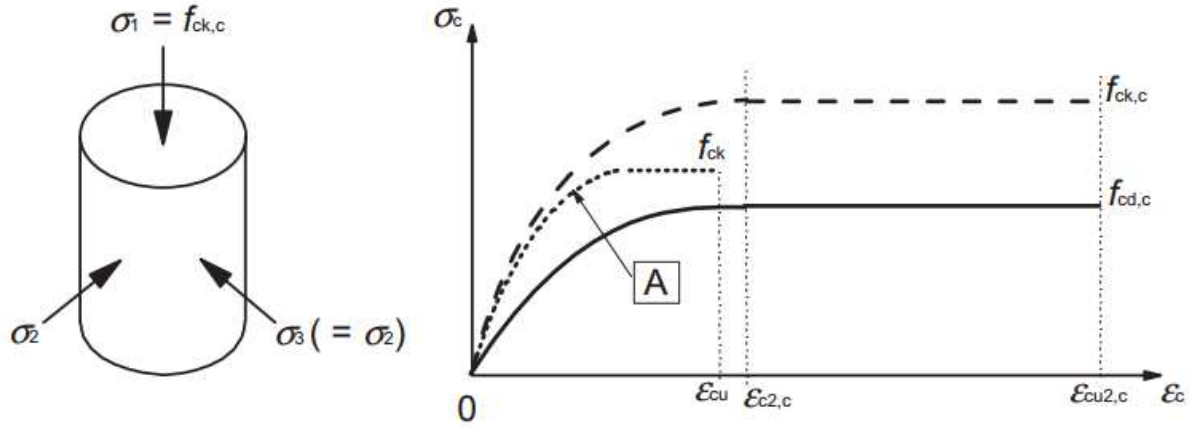

Figure 17 - Characteristic stress-strain curve of confined (top curve) and unconfined (middle curve) concrete according to EN 1992-1-1 [30]

It should be noted that the tensile strength of concrete is rather low compared to its compressive strength. In most calculations, the contribution of the concrete to the tensile resistance (e.g. axial or bending) is ignored.

One of the potential issues with using grouts is their shrinkage upon hydration, which is often referred to as hardening or chemical shrinkage. The reduction of volume of cementitious materials during hydration was first observed by Le Chatelier (1900) [31]. Chemical shrinkage occurs due to the volume of the original components (water and cementitious material) is larger than the volume of the hardened end-product. The magnitude of chemical shrinkage can calculated using the chemical equations of the hardening process, as is exemplified through Figure 18

$$2C_2S + 6H_2O \longrightarrow C_3S_2H_3 + 3Ca(OH)_2$$

Weight	456.6	108.1	342.5	222.3
Specific gravity	3.15	1.0	2.71	2.24
Volume	145.0	108.1	126.4	99.2
	253.1		225.6	

$$\text{Chemical Shrinkage} \quad \frac{(253.1 - 225.6)}{253.6} \times 100 = 10.87\ (\%)$$

Figure 18 - Sample calculation of chemical or hardening shrinkage for a portland cement [66]

Since shrinkage in general will allow for additional connection slip, it is best if shrinkage can all together be avoided. Special shrinkage-compensating grouts are available on the market, which prevent shrinkage from occurring. The underlying principle is the use of expansive cement or a combination of an expensive component and normal cement [32]. Such shrinkage-compensating grouts have a higher hardened end-product volume than the volume of the original components. Apart from the benefits of not having shrinkage, the expansion may also contribute to the complete filling of any voids. Other characteristics shared among most shrinkage-compensation grouts are a high early strength and a high final strength. Moreover, shrinkage-compensation grouts are usually full pre-mixes, meaning only water is to be added before casting.

Creep

It is generally acknowledged that concrete creeps in time. It has been found that creep in concrete subjected to compression is about one seventh of that under tension [33]. Also, research has indicated that higher compressive creep occurs at lower stress levels than at higher stress levels [33] [34]. It is suggested that this phenomenon occurs due to the fact that at low compressive stress the interlayer water is pushed away, reducing the total volume and causing creep, whereas a higher compressive stress causes new bonds to form between subsequent surfaces. [34].

Creep in the concrete/grout may aid in the same deformation process discussed in Section 2.5.1 which is shown in Figure 15 (p.17).

2.5.3 Shape Memory Alloys

Shape memory alloys (SMAs) mostly consist of Nickel and Titanium [35]. As the name suggests, shape memory alloys have the characteristic of being able to divert to their original state. In order to reach their original state, a heat source is necessary in order to obtain a temperature that lies above the transition temperature, which can range between $-200℃$ and $+200℃$ depending on the material composition [36]. Recoverable strains of $3-8\%$ are not uncommon for SMAs. Nickel and Titanium-based SMAs have a Young's Modulus of $80\ \mathrm{GPa}$, which is substantially higher than that of resin or grout.

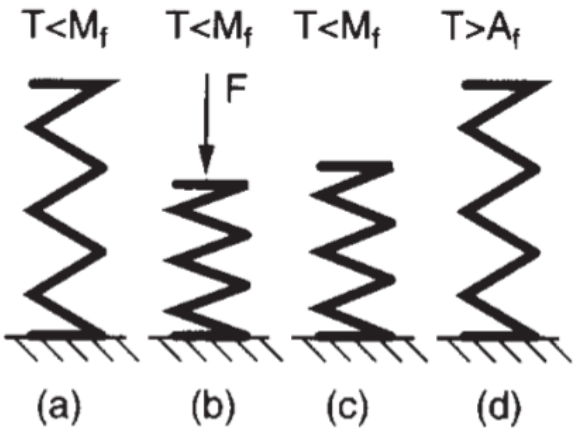

Figure 19 - One-way memory effect. (a) → (b), the sample is deformed, (b) → (c) the sample is unloaded, (c) → (d) at a temperature above A_f (the transition temperature) the sample will go back to its original shape [36]

Given their high Young's Modulus, shape memory alloys may be suitable for use in slip-resistant bolted connections. However, SMAs cannot be injected in liquid state, given that the melting temperature lays in the range of $+1200℃$ [35]. An alternative may be the insertion of small compressed SMA blocks or balls within the connection assembly. If the transition temperature is sufficiently low, the SMA block will at all times exert a compressive force on the connection components due to the confinement of the material, which at the same time guarantees that the total volume is filled. The effect is illustrated in Figure 19. The same principle is currently used in mending broken bones in the human body [37], in which case a tensile force is strived for rather than a compressive.

Currently, the main issue with SMAs is their high cost [36]. However, potential application may seem promising in the future, given that it is possible to apply the SMA-filler material at the right temperature. In this thesis, no further explicit attention is given to the feasibility of SMA-like materials in bolted connections.

2.5.4 Comparison

Resins and grouts share the characteristic of needed time to cure/harden before sufficient strength has been achieved to deliver the demanded functionality. However, generally for resins (24hrs) this curing time is much shorter than for grout. Grouts take a few days before reaching a compressive strength of any significance, whereas rapid strength developing grouts may still take a day to reach a compressive strength of $30 - 50$ MPa [38] [39].

The Young's Modulus of Araldite/RenGel SW 404 + HY 2404 is $E = 9000 - 9500$ MPa [12] and can vary between resins with the same ultimate strength, whereas the Young's Modulus of concrete is independent of the type of concrete used and mainly depends on the compressive strength via Eq. 17 (EN 1992-1-1 [30]). It should be noted that Eq. 17 only holds for concrete, and that in case of grout the stiffness is expected to be less due to a smaller amount of stiff aggregates. Often no data on the Young's Modulus of grouts is given in product sheets, however a few data points (strength, Young's Modulus) are plotted in Figure 20 .

$$E_{cm} = 22 \cdot \left(\frac{f_{cm}}{10}\right)^{0,3} \text{ (GPa)} \qquad \text{Eq. 17}$$

With:

f_{cm} The mean compressive strength of concrete (MPa).

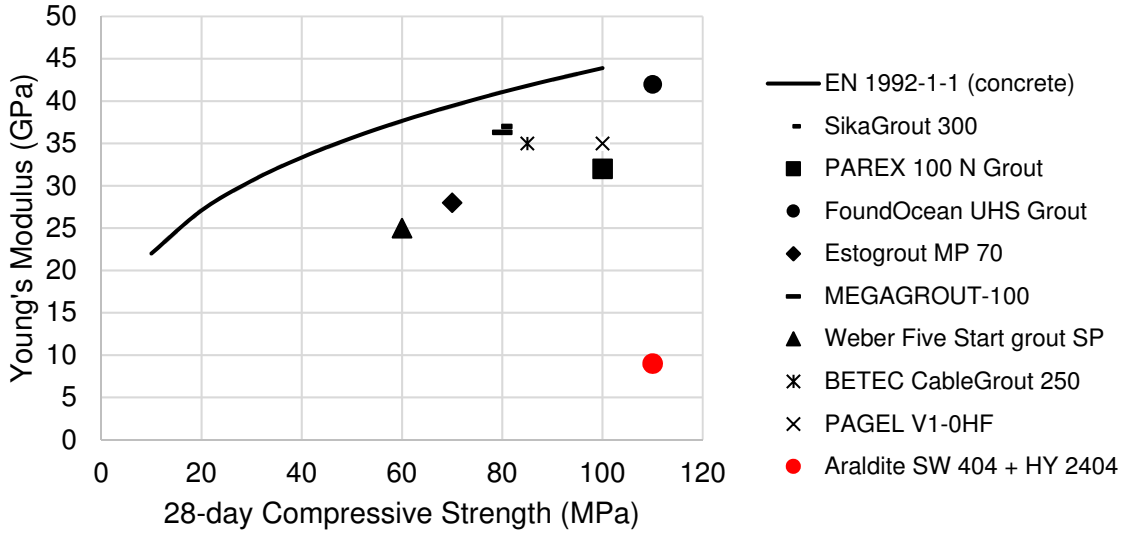

Figure 20 - Young's Modulus versus 28-day compressive strength for different grouts. Strength and stiffness of Araldite SW 404 + HY 2404 included for comparison.

Figure 20 clearly shows that grouts do not exceed the stiffness of concrete according to EN 1992-1-1 [30]. Also, it can be observed that the Young's Modulus of Araldite/RenGel SW 404 + HY 2404 is significantly lower than that of grouts with a similar strength. From a connection stiffness point of view, it is expected that grouts will lead to a better performance.

2.6 Demountability

The demountability of a structure relates to what extend a structure can be taken apart and re-assembled. Research done at TU Delft in the 1970s [40] has indicated that it is possible to dismantle resin-injected bolted connections, i.e. separating the bolts from the bolt hole without excessive force necessary to do so. In order to dismantle the connection, the components of the connection that come into contact with the resin have been treated with a mould release agent (e.g. Deitermann Relax 6 [40], as in the 1970s TU Delft research).

Several materials have the potential to function as a mould release agent. Commonly used are [41]:

- Teflon-based products, which function based on the polarity of the epoxy resin and the non-polarity of the Teflon-based product (see Figure 21).
- Wax-based products, functions in a similar way to Teflon-based products. Care should be taken to choose a wax with a melting temperature above the curing temperature of the epoxy.
- Silicone-based products, however not used as often as Teflon-based or waxy products, since the interaction between epoxy and silicon may degrade the final epoxy properties.

Of all three types commercial products are available on the market. However, some household product can reportedly lead to the same demountability/demouldability, since they are ingredients in commercial products. An example of such an household product is Carnauba wax, which is often used as automobile wax, shoe polish or in food products.

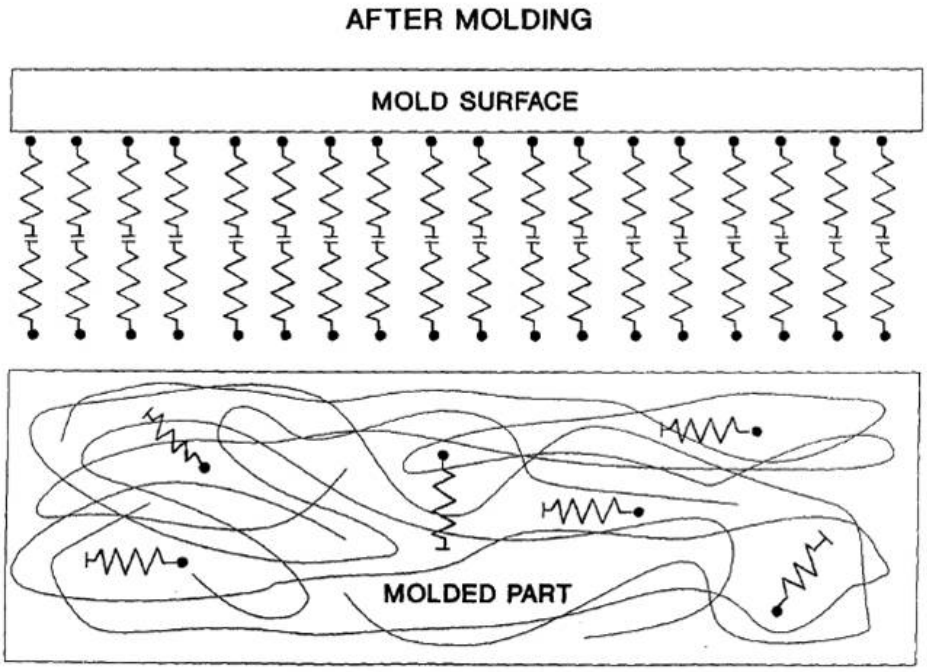

Figure 21 - Effect of using Teflon- and wax-based products. The non-polarity of the mould release agent forms a barrier between the mould surface and the polar injection material [67]

It should be noted that separation liquid may induce additional slip in the connection when it is forced aside [40], as is illustrated through Figure 22. Also, it is theoretically possible for the resin to slide along the separation liquid without considerable friction, which may or may not aggravate the connection slip and is further investigated in this thesis. A possible danger of using separation liquids is that it may come between two plates, hereby reducing the coefficient of friction in case of injected friction connections [42].

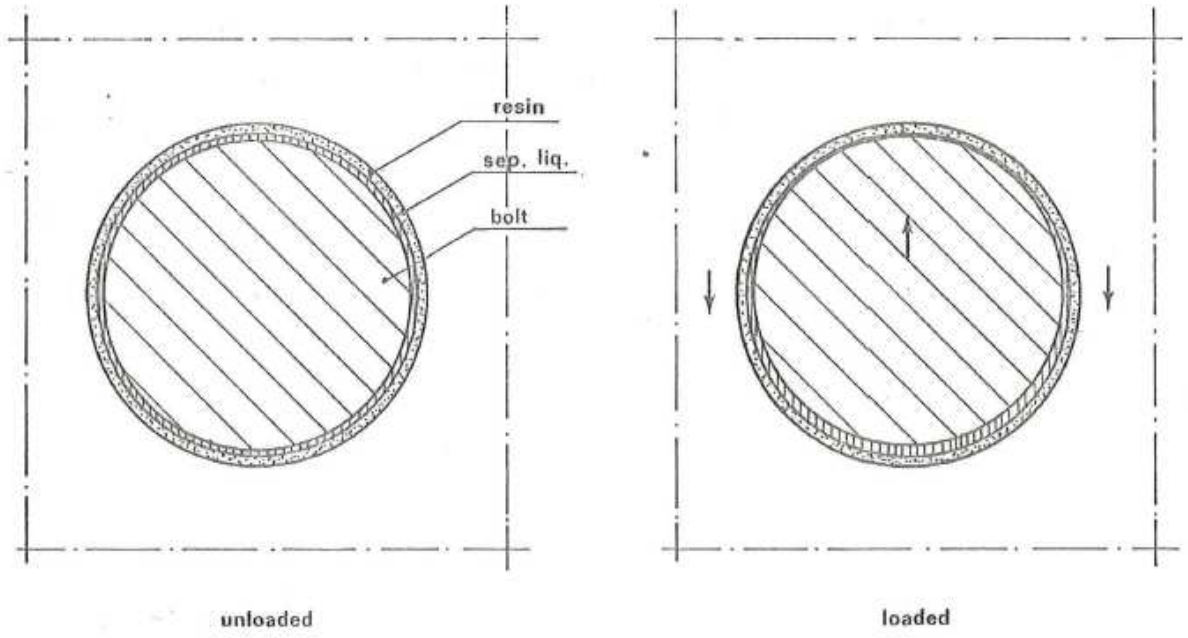

Figure 22 - Potential additional slip of connection due to the separation liquid being pushed aside as a result of external loading [40] [42]

For concrete/grout, it is also possible to allow for easy demountability of the structure. Generally used in formwork, release agents or 'formwork oil' prevent the concrete from adhering to the formwork or substrate. Two main types of such release agents exist:

- Barrier type
    - Creates a barrier between the substrate and the concrete, hereby preventing any contact between the substrate and concrete
- Chemically reactive type
    - Chemically reactive release agents react with the lime in the concrete. Often fatty acids are used, which upon reaction with lime form a soapy layer that prevents any adhesion between concrete and substrate.

2.7 Oversized and Slotted Holes

The definition of oversized hole is taken in this thesis as “a hole that has a nominal clearance larger than the nominal clearance for normal round holes”. The nominal clearance for normal round holes is given by Table 11 of EN 1090-2, which is presented in Figure 23 and of which an example is illustrated in Figure 24. Oversized and slotted holes (Figure 24) allow for an easier assembly process of pre-fabricated members, since the chance that holes of different members overlap increases with increasing hole size.

Nominal bolt or pin diameter d (mm)	12	14	16	18	20	22	24	27 and over
Normal round holes [a]	1 [b c]		2					3
Oversize round holes	3		4				6	8
Short slotted holes (on the length) [d]	4		6				8	10
Long slotted holes (on the length) [d]	1,5 d							

[a] For applications such as towers and masts the nominal clearance for normal round holes shall be reduced by 0,5 mm unless otherwise specified.

[b] For coated fasteners, 1 mm nominal clearance can be increased by the coating thickness of the fastener.

[c] Bolts with nominal diameter 12 and 14 mm, or countersunk bolts may also be used in 2 mm clearance holes under conditions given in EN 1993-1-8.

[d] For bolts in slotted holes the nominal clearances across the width shall be the same as the clearances on diameter specified for normal round holes.

Figure 23 - Nominal clearances for bolts and pins (mm) [4]

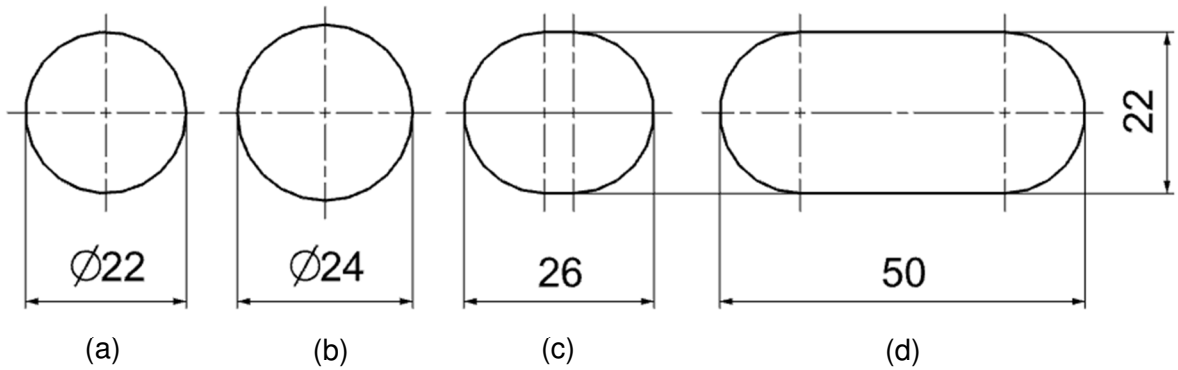

Figure 24 - Bolt hole dimensions for a (a) normal round, (b) oversize, (c) short slotted and (d) long slotted hole. Dimensions according to EN 1090-2 [4] and given in millimetres.

In case oversized or slotted holes are used, it is prescribed that a plate washer with a minimum thickness of $4\ \mathrm{mm}$ must be used [4]. An example is given in Figure 25. Alternatively, a cover plate can be used, as is for instance done in the assembly shown in Figure 26.

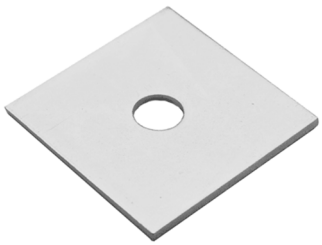

Figure 25 - Square M20 plate washer with a thickness of 4 mm [64]

A particular useful application of slotted holes is in the connection between members of wind turbine shell elements, as has been investigated in the HISTWIN+ [43] project. In this particular application, the shear force is transferred by friction between the subsequent members. An illustration of a connection design in the HISTWIN+ [43] is included in Figure 26. It should be noted that in this case the hole is not purely slotted, but open at one end (finger connection), in order to further ease the assembly process.

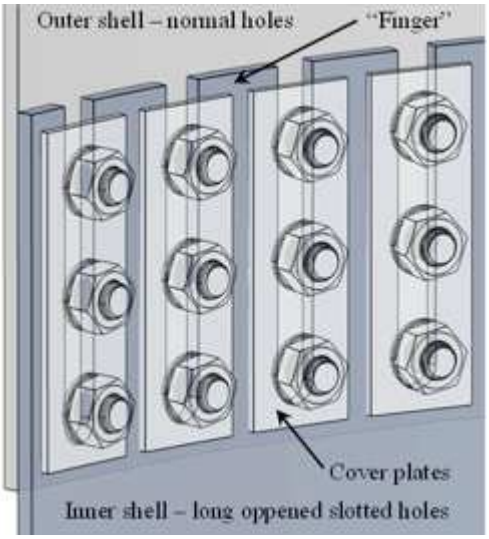

Figure 26 - Example of an application of slotted holes in a wind turbine connection [43] (open at one end)

Although oversized and slotted holes aid the erection process, a consequence of the use of oversized/slotted holes is that significant slip can occur between connection members, and that large deformations may occur once the bolt and plates are in contact [44]. The slip that can occur in the connection is theoretically limited to twice the hole clearance, but is often not more than one time the hole clearance [1]. In order to overcome any deformation issues related to the use of oversized holes, connections with oversized holes are required to be designated as slip-critical by the (American) Research Council on Structural Connections [1]. In the European codes EN 1090-2 and EN 1993-1-8 it is not explicitly stated that connections with oversized holes must be detailed as slip-critical, however in such cases the bearing resistance of the connection is reduced by 20%. Both the American and European specifications prescribe a reduction of 15% of the slip load in case of pretensioned connections with oversized holes. With respect to pretensioned connections with slotted holes, EN 1993-1-8 [3] reduces the shear resistance with 37% for long slotted holes parallel to the direction of load transfer, whereas the RCSC [1] reduces the resistance by 30%. The different European reduction values are summarized in Table 4.

Table 4 - Multiplication factor of resistance of oversized and slotted holes compared to normal holes according to EN 1993-1-8 [3]

Hole type	Bearing	Friction
Normal Holes	1	1
Oversize holes	0,8	0,85
Short slotted holes (parallel to direction of load transfer)	1	0,76
Long slotted holes (parallel to direction of load transfer)	1	0,63

In the $1960s$ research has been carried out to investigate the effect of oversized and slotted holes on preload loss of pretensioned bolts. By Allan et al. (1967) [45] and Chesson et al. (1965) [46] , it was concluded that nor oversized nor slotted holes have a significant influence on the preload loss in time [45] [46]. The results of the research of Allan et al. (1967) [45] have been illustrated in Figure 27. It must be noted that Allan et al. (1967) were not able to pre-tension the bolts in oversized holes without the installation of a washer. Although the preload loss is mostly unaffected by oversized holes, the slip factor was reported to decrease with increasing oversize of the hole. Especially in case of slotted holes, the observed slip factor is significantly $(22\%\text{-}33\%)$ lower [45]. Allan et al. (1967) suggest that the reduction in slip factor is due to the higher surface pressure in the region directly next to the bolt hole/slot, which tends to compress the surface irregularities.

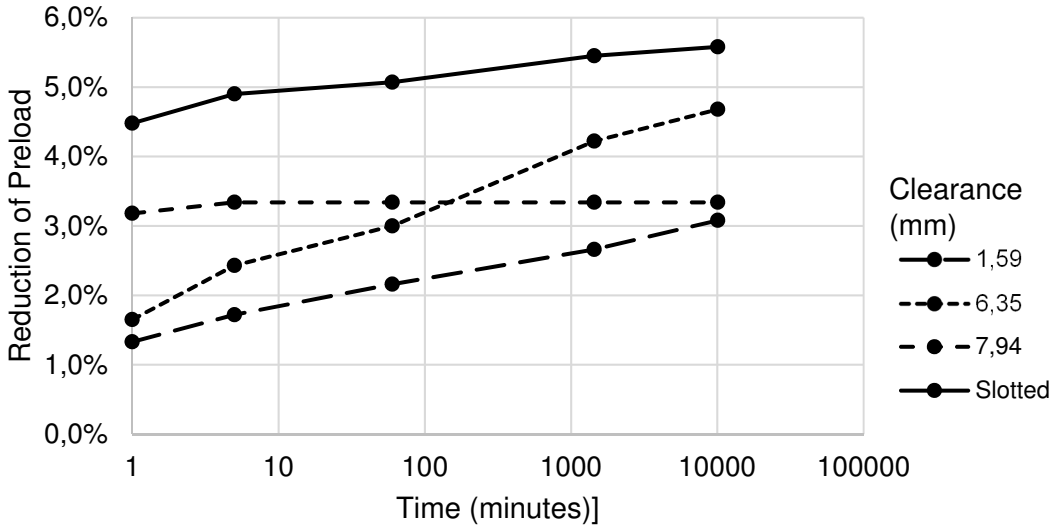

Figure 27 - Preload loss for oversized and slotted holes [45] [46]

2.8 Bearing Stress

The equivalent bearing stress σ_b, indicated in Eq. 18 and Figure 28b , is often used as an indicator for the maximum long-term load that can be transferred through the resin without excessive connection slip. However, the bearing stress is not equally distributed along the width of the hole, as indicated in Figure 28a. The constant stress distribution cf. Eq. 18 and Figure 28b is only valid in case of rigid connection members [47] [48].

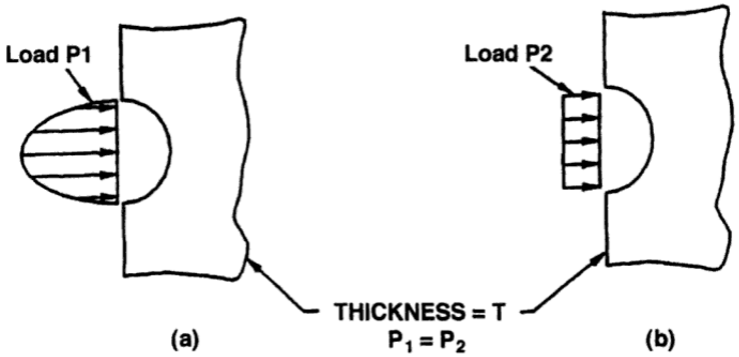

Figure 28 - Bearing stress distribution as a result of loading by a bolt, (a) true stress distribution, (b) equivalent stress distribution

$$\sigma_b = \frac{F_b}{d_b \cdot t_p} \qquad \text{Eq. 18}$$

With:

σ_b	Equivalent bearing stress $[\mathrm{F/L^2}]$
F_b	External load $[\mathrm{F}]$
d_b	Bolt diameter $[\mathrm{L}]$
t_p	Plate thickness $[\mathrm{L}]$

In case of a marginal clearance between the bolt and the bolt hole, the bearing stress distribution can be approximated by Eq. 19 [47] [49]. In case the clearance between the bolt and the surrounding material cannot be neglected, the bearing stress distribution becomes more complex and cannot be obtained from mere theory. In this case the angle in between which the bearing stress is transferred must be determined by testing [47]. For the case of injected bolted connections, it is assumed that the clearance is non-existent, as the injection material is both in contact with the bolt and bolt hole.

$$\sigma_b(\theta) = \frac{4}{\pi} \cdot \frac{F}{d_b \cdot t_p} \cdot cos(\theta) \qquad \text{Eq. 19}$$

With:

$\sigma_b(\theta)$	Bearing stress as a function of θ $[\mathrm{F/L^2}]$
F, d_b, t_p	As defined in Eq. 18
θ	Angle with respect to direction of force

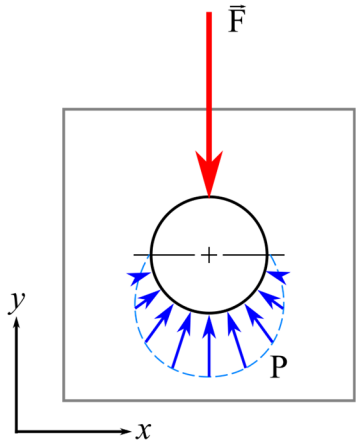

Figure 29 - Bearing stress distribution for negligible clearance between elastic bodies [63]

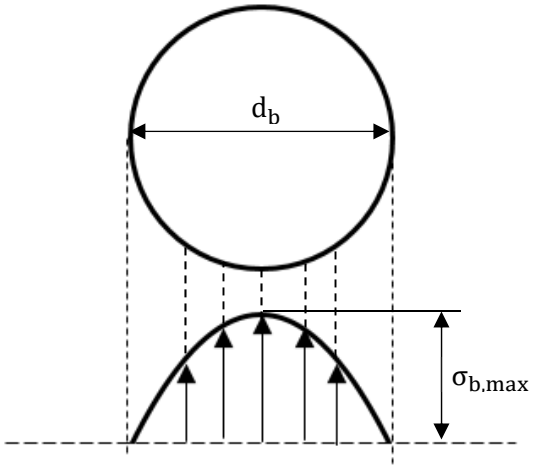

Figure 30 – Sketch of longitudinal component of bearing stress, indicative

Integrating Eq. 19 over the perimeter of the bolt whilst taking only the longitudinal components, one can prove that indeed the expression of Eq. 19 leads to longitudinal force equilibrium. Based on the same considerations, the longitudinal component of the bearing stress can be sketched using Eq. 21, as is illustrated in Figure 30.

$$F_y = \int_{-\frac{\pi}{2}}^{\frac{\pi}{2}} \sigma_b(\theta) \cdot \frac{1}{2} d_b \cdot t_p \cdot cos(\theta)\, d\theta$$
$$= \left[\frac{4}{\pi} \cdot \frac{F}{d_b t_p}\right] \cdot \frac{1}{2} d_b \cdot L \cdot \int_{-\frac{\pi}{2}}^{\frac{\pi}{2}} cos^2(\theta)\, d\theta \qquad \text{Eq. 20}$$
$$= \frac{2}{\pi} \cdot F \cdot \frac{\pi}{2} = F_y$$

$$\sigma_{b,lt}(\theta) = \sigma_b(\theta) \cdot cos(\theta) = \frac{4}{\pi} \cdot \frac{F}{d_b t_p} \cdot cos^2(\theta) \qquad \text{Eq. 21}$$

With:

$\sigma_{b,lt}(\theta)$	Longitudinal component of bearing stress $[\mathrm{F/L^2}]$
$\sigma_b(\theta), F, d_b, t_p$	Defined as in Eq. 18 and Eq. 19

2.9 Structural behaviour of Resin-Injected Connections

The structural behaviour of resin-injected connection has been studied by several authors. All present studies on the structural behaviour of resin-injected connections focus on M20 bolts in normal clearance holes, with specimen dimensions (Figure 31) cf. Annex G of EN 1090-2 [4]. Moreover, all results come from eccentric tests (as specified in EN 1090-2 [4]), i.e. tests in which the bolt has been placed in the position with maximum slip potential, as is illustrated in Figure 32. The underlying reason behind the bolt eccentricity is that this positioning is required to determine the maximum allowable bearing stress $f_{b,resin}$.

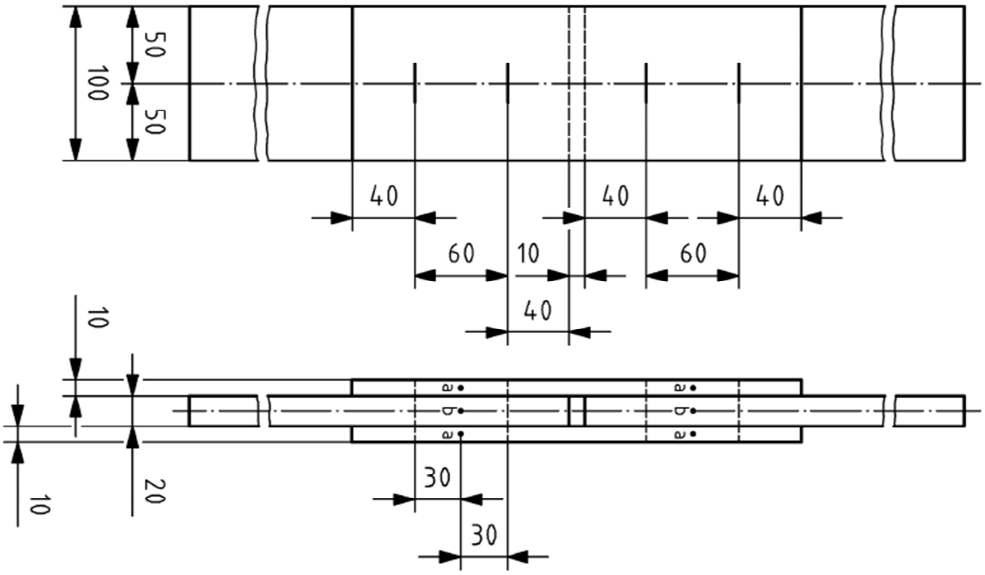

Figure 31 - Test set-up from Annex G of EN 1090-2 [4]. Bolts M20 (4x) in normal clearance holes. Points a and b indicate measurement points for connection slip.

Figure 34 shows the relationship between applied tensile force and connection slip found by Koper (2017) [15]. The test results initially show a stiffer behaviour due to load transfer by friction rather than bearing. The average connection stiffness observed between $0{,}05$ mm and $0{,}15$ mm of slip is $k = 9{,}8 \cdot 10^2$ kN/mm. From similar experiments carried out by Ragelj & Beg (2008) [50], a connection stiffness of $k = 10 \cdot 10^2$ kN/mm is found (Figure 35).

Figure 35 does not only show results for resin-injected connections, but also for pretensioned, combined pretensioned and resin-injected connections. Pretensioned connections provide a higher slip load than resin-injected connections, but the combination of pretensioning and resin injecting yields the most favourable results. It is noted that in case of the combination of a pretensioned and resin-injected connection, initially the load-displacement paths are similar, which indicates that the force is first mostly transferred by friction, and later by bearing of the resin. The combination of pretensioning and injecting leads to a design load that is respectively 35% and 90% higher than in case of only pretensioning or injecting. However, Figure 35 indicates that the slip load for a combination of force transfer by friction and resin bearing is less than the sum of both individual slip capacities, which is in contrast to the design resistance according to EN 1993-1-8 [3]. Other authors (e.g. [13]) have made the same observation and conclude that it is not a major issue since the design resistance according to EN 1993-1-8 [3] can be resisted at higher slip levels $(0{,}2 - 0{,}25$ mm$)$.

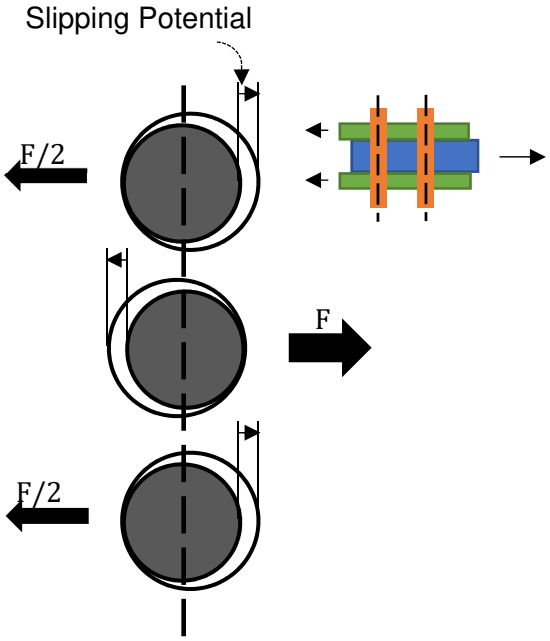

Figure 32 – Eccentric position of the bolt (grey) with respect to the bolt hole, causing the greatest potential of connection slip

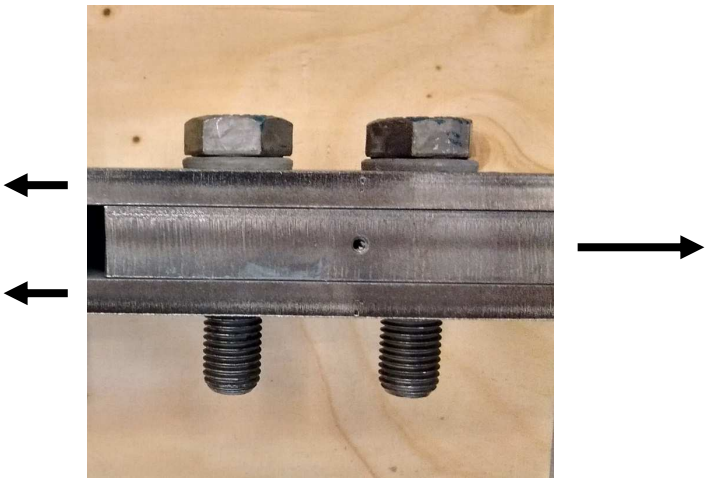

Figure 33 - Side view of a resin-injected connection (half specimen) tested in the experimental programme of Koper (2017) [15]

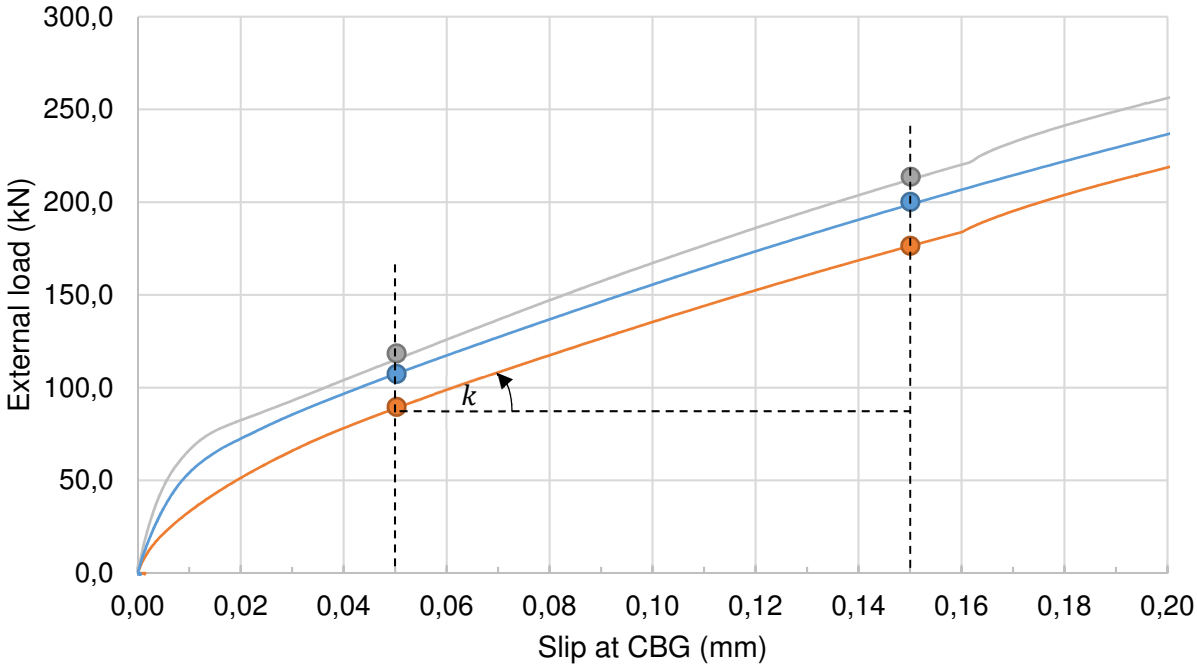

Figure 34 - Force-displacement diagram obtained by Koper (2017) [15] for three double lap shear tests cf. Annex G of EN 1090-2 for M20 bolts

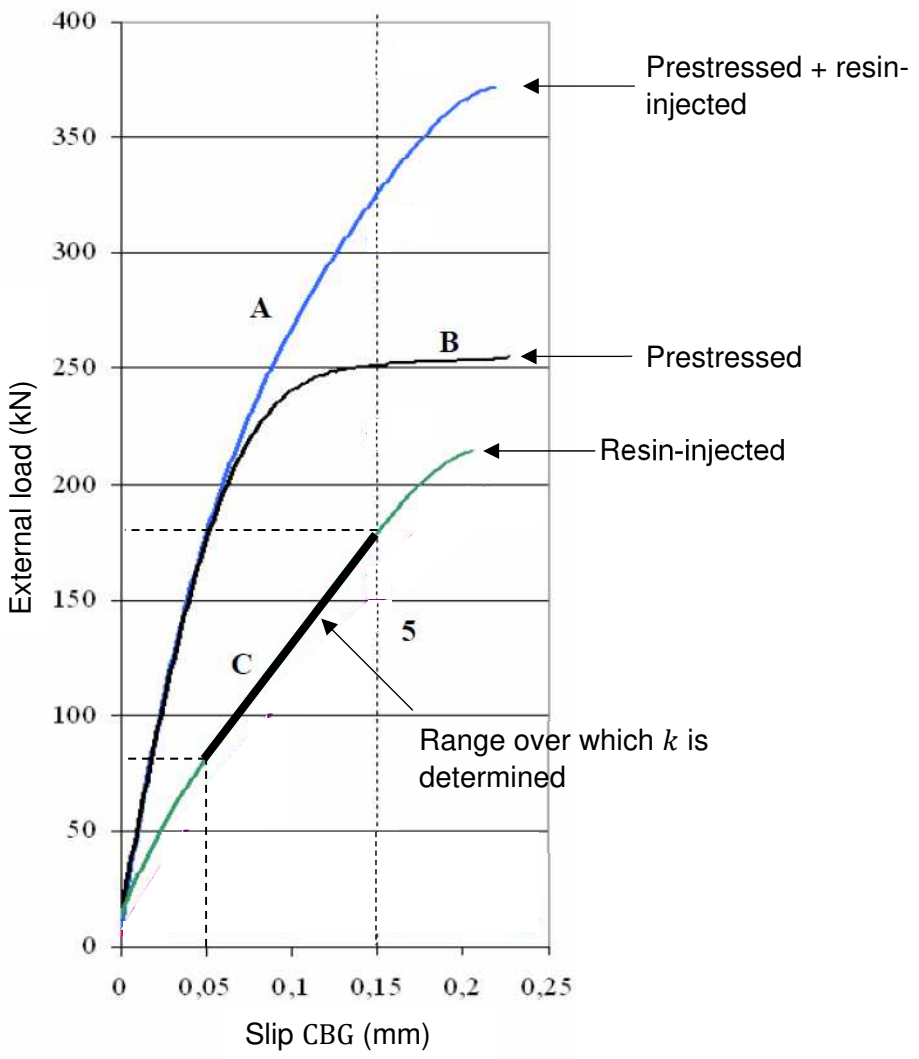

Figure 35 - Force-displacement diagram for various connection types obtained by Rugelj & Beg (2008) [50]. Tests carried out on the test set-up from Annex G of EN 1090-2 using M20 bolts.

3 Methods

This section discusses the different materials and test set-ups used in experiments required for answering the research questions laid down in Section 1.

3.1 Materials

The materials used in the experiments are outlined in this section. In the description of the tests in Section 3.2 , reference is made to the materials defined in this section.

3.1.1 Steel

Steel is used for all plate and fastener material. Figure 36 illustrates all steel components. The material properties of the different components are tabulated in Table 5.

Table 5 - Steel grade per component used in the experimental programme

Component	Steel Grade	Nominal Yield Strength (MPa)	Nominal Tensile Strength (MPa)
Bolt	10.9	900	1000
Nut	10.9	900	1000
Cover Plate	S355	355	510
Centre Plate	S355	355	510

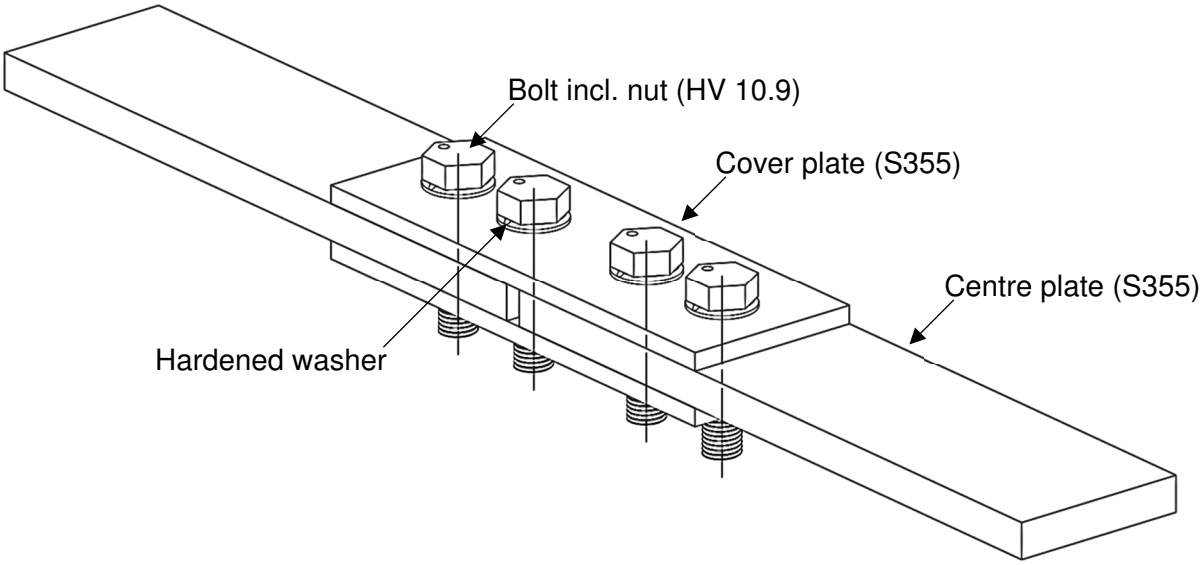

Figure 36 - Steel components including their steel grades used in the experimental programme

Both the cover and centre plates have an epoxy coating on the side of plate-to-plate contact. Such epoxy coatings provide excellent protection against corrosion but have a very low slip factor μ. The low slip factor is beneficial for the experiments since it reduces the influences of friction on the test results.

The bolts are manufactured by FRIEDBERG and have a hole drilled in the head which is used for injection. Apart from this minor adjustment, the bolts can be considered to be conventional HV 10.9 bolts. The washers are special washers suitable for injection with dimensions conform EN 1090-2 [4] (see Section 2.1.1). An overview of the complete fastener system is given in Figure 37.

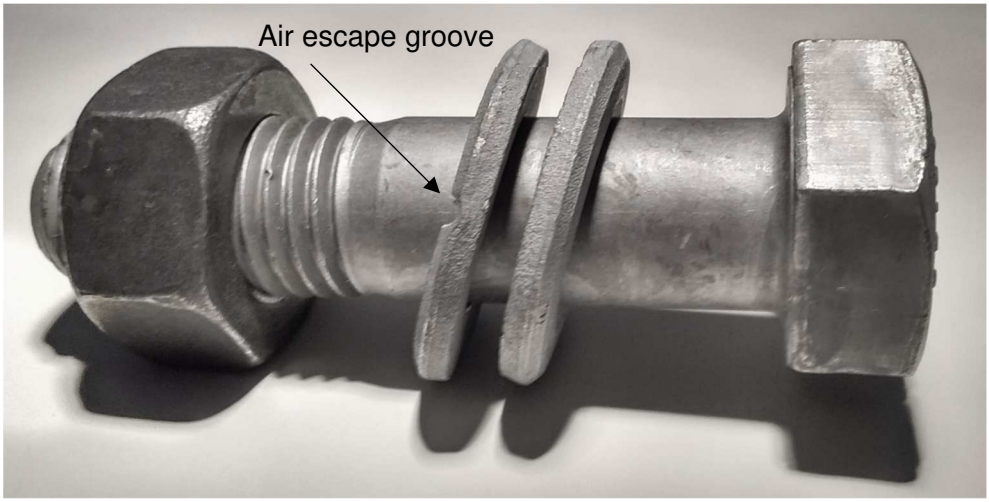

Figure 37 - Fastener system used in the experimental programme, composed of FRIEDBERG HV 10.9 bolt, special washers and HV 10.9 nut

3.1.2 Resin: Araldite/RenGel SW 404 + HY 2404

The resin considered in the experiments is the two-component epoxy resin Araldite/RenGel SW 404 + HY 2404, since this resin is used exclusively in practice. The resin has a characteristic blue colour, and has a compressive strength of $110 - 125$ MPa [12] and a Young's Modulus between $9 - 9{,}5$ GPa. The components are mixed in a mass ratio of $10:1$ (SW 404 : HY 2404) before injection at room temperature. The costs of mixed Araldite/RenGel SW 404 + HY 2404 are about € 22/kg or € 39/l when bought in large cans of 10 and 1 kg respectively (price 25/01/2017; VIBA.nl). Figure 38 shows the unmixed resin components, as well as the hardened/cured epoxy resin material. The product sheet of Araldite/RenGel SW 404 + HY 2404 is included in Appendix A.

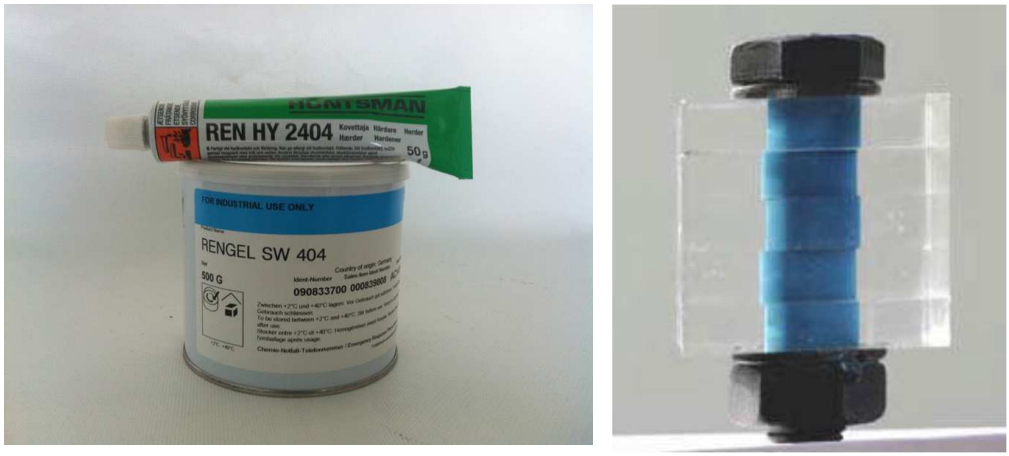

Figure 38 - Left: resin components Araldite/RenGel SW 404 and hardener Araldite/RenGel HY 2404 in small packages of 500g and 50g, respectively [70]. Right: hardened/cured resin in a transparent epoxy mould [69]

3.1.3 Grout: PAGEL V1-0HF

One type of grout, PAGEL V1-0HF, is considered in the experimental programme. The choice for the grout is made based on comparing product sheet data of different grouts, mainly looking at favourable characteristics such as high stiffness, high early and final strength, as well as workability and flowability. The product sheet of PAGEL V1-0HF is included in the Appendix.

V1-HF is an injection mortar from the German manufacturer PAGEL, and is used for diverse applications, ranging from casting joints between high-strength concrete members to embedding train rails [51]. V1-HF is available in three different versions, which differ in the maximum (filler) diameter present in the dry mix. In the experimental programme, V1-0HF is be used, which has a largest particle diameter in the dry mix of 0,15 mm. The injection mortar can be hand-pumped. The effects of chemical/hardening shrinkage are compensated for given a net volume increase after hydration. PAGEL V1-0HF is CE-marked as well as certified by the Dutch KOMO institution. PAGEL V1-0HF is only supplied in bags of 20 kg and costs €3,6/kg or €7,2/l (price 25/01/2017, personal communication with Dutch supplier Verwaard BV).

The properties of PAGEL V1-0HF are listed in Table 6. Figure 39 illustrates the packaging of the injection mortar.

Table 6 - Properties of PAGEL V1-0HF [51]

Grain size		0 mm
Amount of water		20 %
Consumption (dry mortar)		1,84 kg/l
Working time at 20 °C		60 minutes
Expansion after 24 hrs		≥ +0,3 Vol%
Compressive strength	24 hrs	≥ 60 MPa
	7 days	≥ 85 MPa
	28 days	≥ 100 MPa

Figure 39 - PAGEL V1-0HF Injection mortar, as supplied with by Verwaard BV

3.1.4 Release Agents

Release agents prevent adhesion between different components, such that components can be easily separated from each other. The different release agents used in the experimental programme are listed in Table 7.

Table 7 - Release agents used in the experimental programme

Brand / Name	Active Substance	Way of applying/Phase	Volume (ml)	Retail Price (€, approx..)
ACMOS 82-2405	Wax	Spray	400	10
Kelfort Silicon Spray	Silicon	Spray	400	5
De Hazelaar Losmiddelvloeistof PVA	Polyvinyl alcohol (PVA)	Liquid	500	10
*: The price of Teflon is in the same range as that of ACMOS 82-2405. However, Teflon was not considered in the experimental programme				

Figure 40 - Release agents used in the experimental programme, respectively wax, silicon and PVA-based.

3.1.5 Tools

Injection

The injection material is mixed/prepared to the specifications of the manufacturer. Hereafter, the mixed material is transferred to a caulk tube. The injection materials are injected using a hand-operated caulking gun, as exemplified in Figure 41.

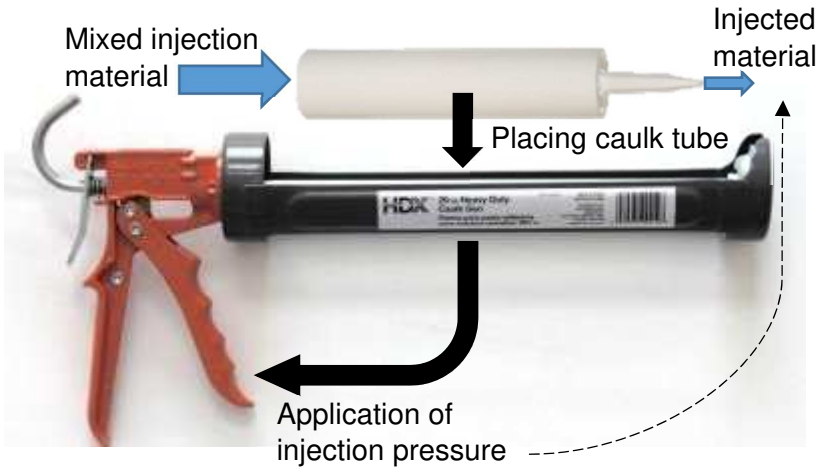

Figure 41 - Hand-operated caulking gun with a caulk tube containing the mixed injection material [71]

3.2 Tests

3.2.1 Injectability Tests

Injectability tests are carried out on specimen injected with either resin or grout. The goal of the injectability tests is to see whether or not a material is suitable to be injected. For the resin under consideration (Araldite/RenGel SW 404 + HY 2404) the suitability for injection does not need to be proven since it has been injected numerous times by other authors. However, no information is known about whether the entire free volume can be filled if there is risk of air inclusions within this volume.

In order to investigate the injectability of the resin and grout materials, a transparent Perspex assembly is used. The Perspex assembly consists of three plates: the outer plates are $10\ \mathrm{mm}$ thick and have a hole with a nominal diameter of $22\ \mathrm{mm}$, whereas the centre plate is $20\ \mathrm{mm}$ thick and has a hole with a nominal diameter of $36\ \mathrm{mm}$. The holes in all three plates are positioned concentrically and an M20 fastener system cf. Section 3.1.1 is (randomly) inserted. Figure 42 illustrates the final test set-up.

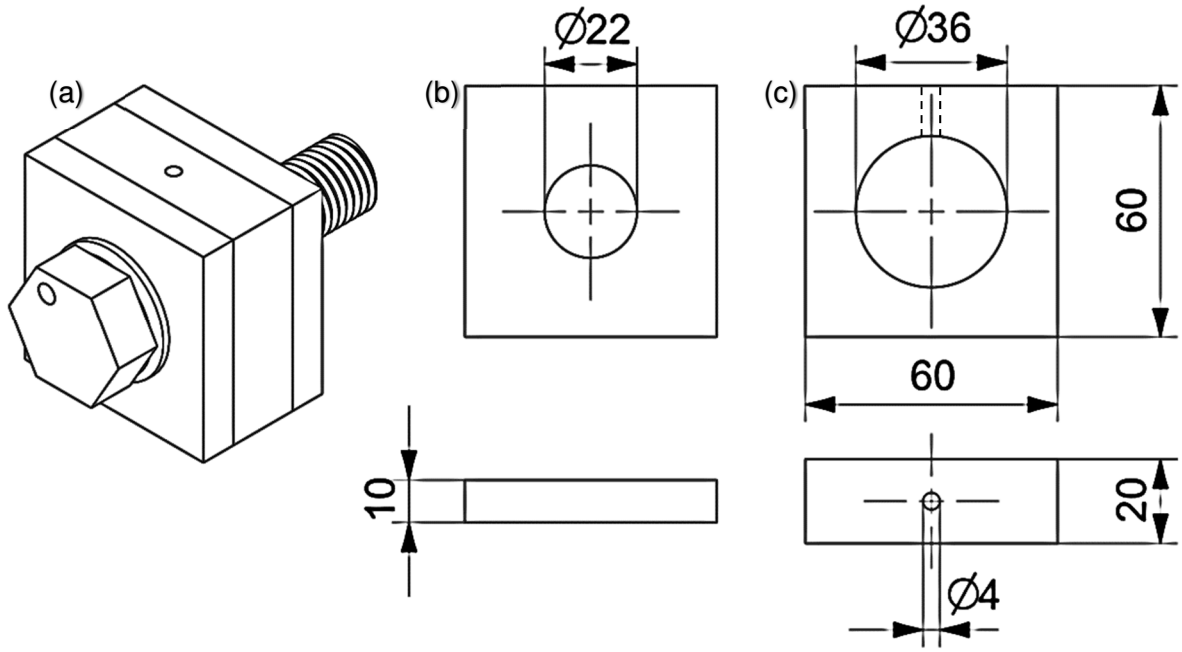

Figure 42 - Injectability test set-up, (a) final assembly, (b) cover plate and (c) centre plate with air escape channel. Fastener system cf. Section 3.1.1. All dimensions in mm.

Figure 42 indicates an air escape channel in the centre plate. This air escape channel is used to make sure the entire volume is filled with injection material and no air inclusions exists within the specimen. The need of an air escape channel is further exemplified in Figure 43. Also experiments proving the need for such an air channel will be included in the experimental programme.

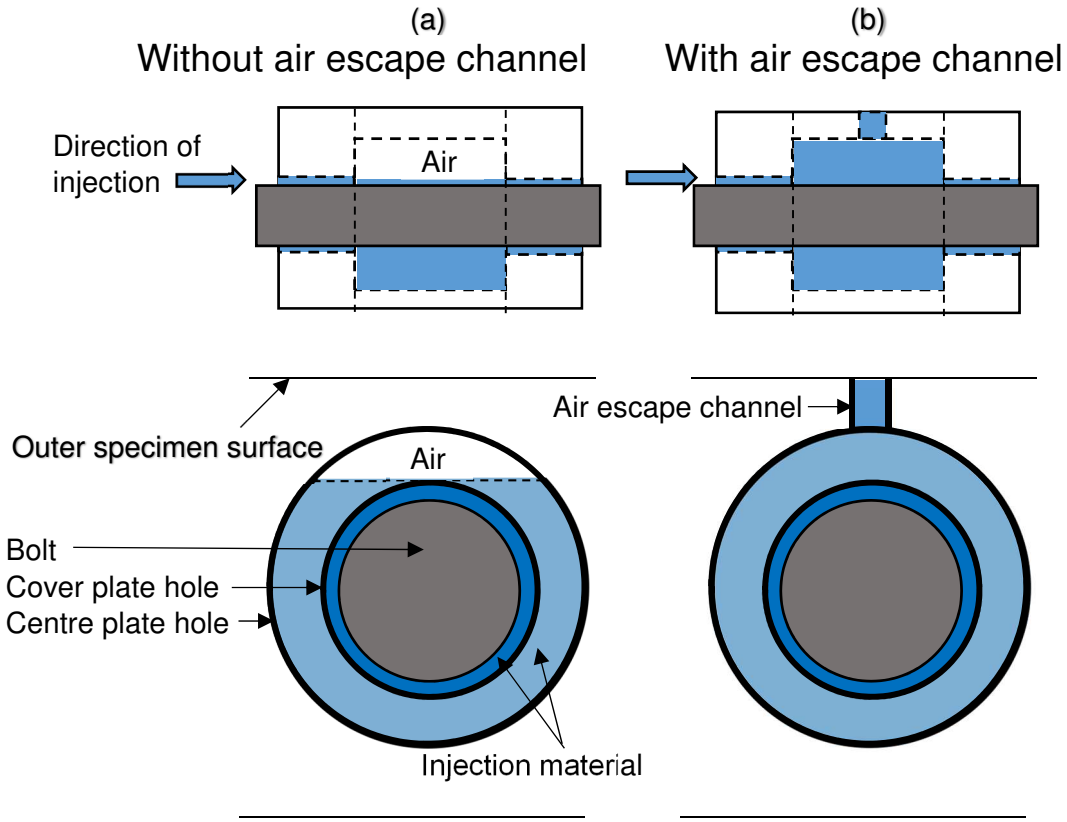

Figure 43 – (a) Possible consequence of air inclusion on the quality of the injection, (b) prevention of air inclusion due to the presence of an air escape channel. Not to scale.

3.2.2 Demountability Tests

Demountability tests are carried out on specimen that have undergone a treatment with release agents, as specified in Section 3.1.4. The goal of the demountability tests is to investigate whether or not connections that have been treated with release agents are capable to be taken apart without excessive use of force.

In order to determine what type of release agent shall be used in the double lap shear connections discussed in Section 3.2.3, a preliminary study is conducted using several types of release agents (Wax-, silicon- and PVA-based). The test setup used to determine the demountability of injected connections is illustrated in Figure 44, and consists of two plates bolted/clamped onto each other. The top plate has through holes with a diameter of 26 or 32 mm. The lower plate functions as a bottom, so that a circular compartment with a horizontal bottom is created in the plate package. Pieces of threaded end of metric size $M20$ are vertically inserted in the holes. The empty volume in between the hole and threaded end is then filled with injection material.

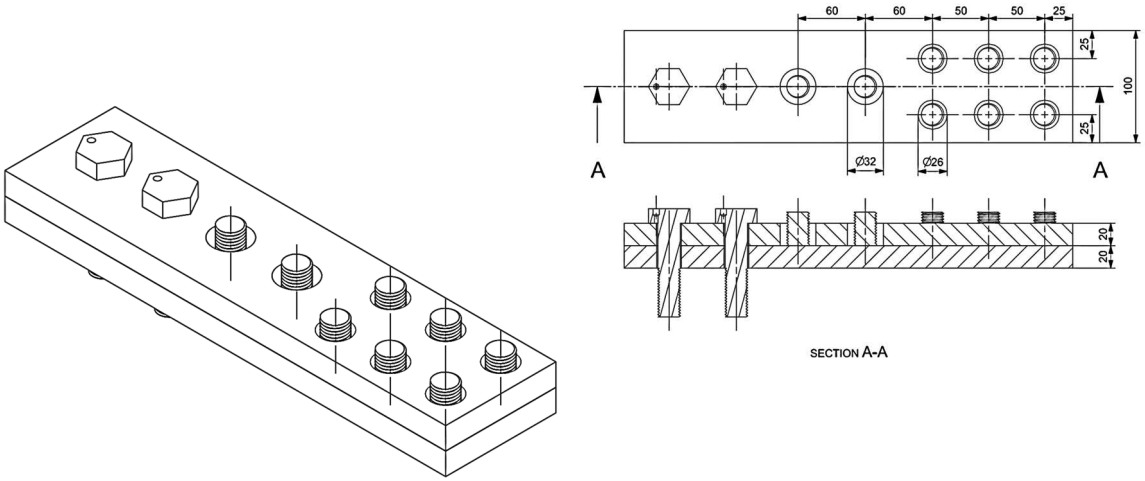

Figure 44 - Test set-up for determining demountability of injected connections

After sufficient curing/hardening time (24 hrs for resin, 7 days for grout), it is attempted to demount the assembly in the following way:

1. Removal of the infill including threaded end by applying a tensile force by hand (tools) to the threaded end;
2. Relative turning by hand tools of the threaded end with respect to the infill;

The first step will show whether or not the injection material is easily separated from the inner surface of the hole. The second step shows whether the adhesion between the threads and infill is prevented in such a way that rotation of the threaded end is still possible with minimum effort. If one or both steps mentioned above cannot lead to demounting of the test assembly, other methods will be looked for to separate the assembly into the original components. If such other methods must be used, this will be extensively documented in the results section (Section 4.2).

After conducting the abovementioned test, a choice will be made on the type of release agent used in the double lap shear connections. After the experiment on the double lap shear connection has been carried out, it will be attempted to dismantle the connection using hand tools.

3.2.3 Double Lap Shear Tests

Double lap shear tests are carried out on several types of injected double lap shear connections. The specimen vary in the degree of oversizing of the hole in the centre plate and the type of injection material (resin or grout). The test set-up used is located in the Stevin II laboratory of the TU Delft, and is illustrated in Figure 45. The specimen are fixed within the machine using hydraulic wedges. The testing rig can deliver a maximum tensile force of $500\ \mathrm{kN}$ (wedge resistance).

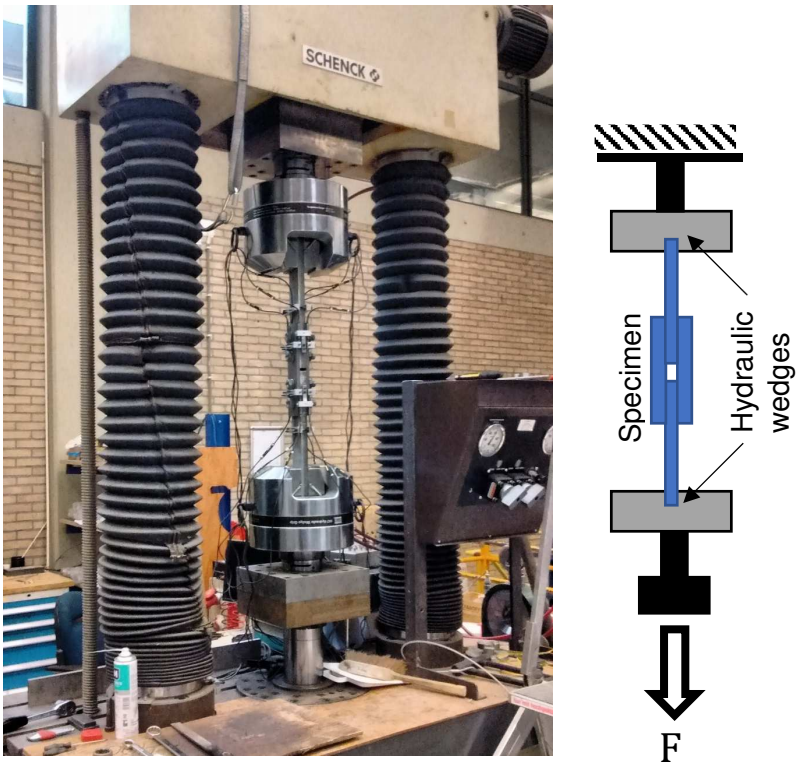

Figure 45 – Left: test machine used in the experimental programme, right: schematization

Before presenting the exact dimensions of the test specimen used in the experimental programme, Figure 46 illustrates a general overview of the type of connection that is made.

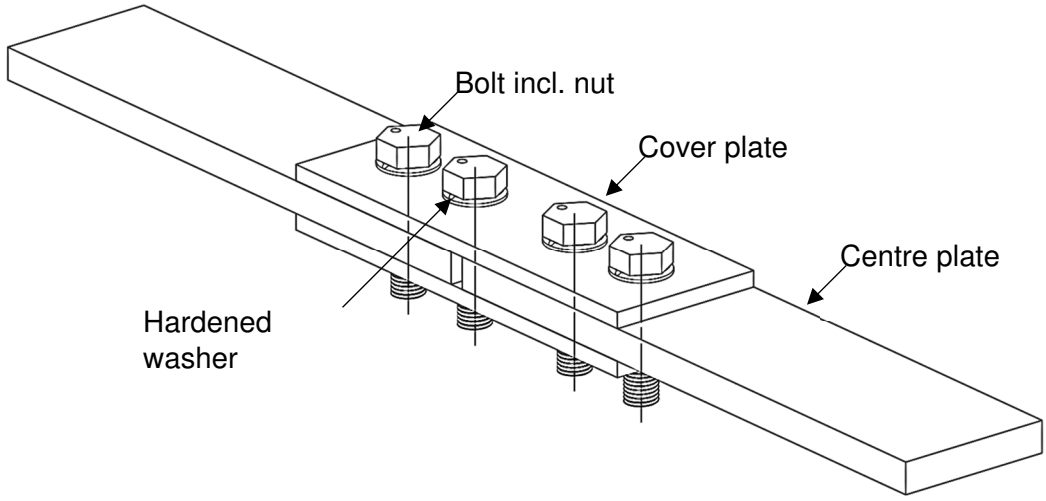

Figure 46 – Three dimensional general overview of double lap connection under consideration

Table 8 shows an overview of the different types of specimen that have been tested in the experimental programme. The specimen with oversize round holes have been fabricated from specimen that originally had dimensions according to Annex G of EN 1090-2 [4]. Figure 47 illustrates an example of a centre plate with Ø36 mm holes, whereas Figure 48 depicts the (constant) dimensions of the cover plates.

Table 8 - Specimen used in double lap shear tests

Specimen ID		Ø cover plate (mm)	Ø centre plate (mm)	Injection Material	Type of test	Release Agent*
R22-ST		22	22	Araldite SW 404 + HY 2404	Short	Wax
R22-LT		22	22	Araldite SW 404 + HY 2404	Creep	Wax
G22-ST		22	22	PAGEL V1-0HF	Short	-
R26-ST		26	22	Araldite SW 404 + HY 2404	Short	Wax
R26-LT		26	22	Araldite SW 404 + HY 2404	Creep	Wax
G26-ST		26	22	PAGEL V1-0HF	Short	-
R32-ST		32	22	Araldite SW 404 + HY 2404	Short	Wax
R32-LT		32	22	Araldite SW 404 + HY 2404	Creep	Wax
G32-ST		32	22	PAGEL V1-0HF	Short	-
R36-ST		36	22	Araldite SW 404 + HY 2404	Short	Wax
R36-ST		36	22	Araldite SW 404 + HY 2404	Creep	Wax
G36-ST		36	22	PAGEL V1-0HF	Short	-
*: see Section 4.2 for motivation						

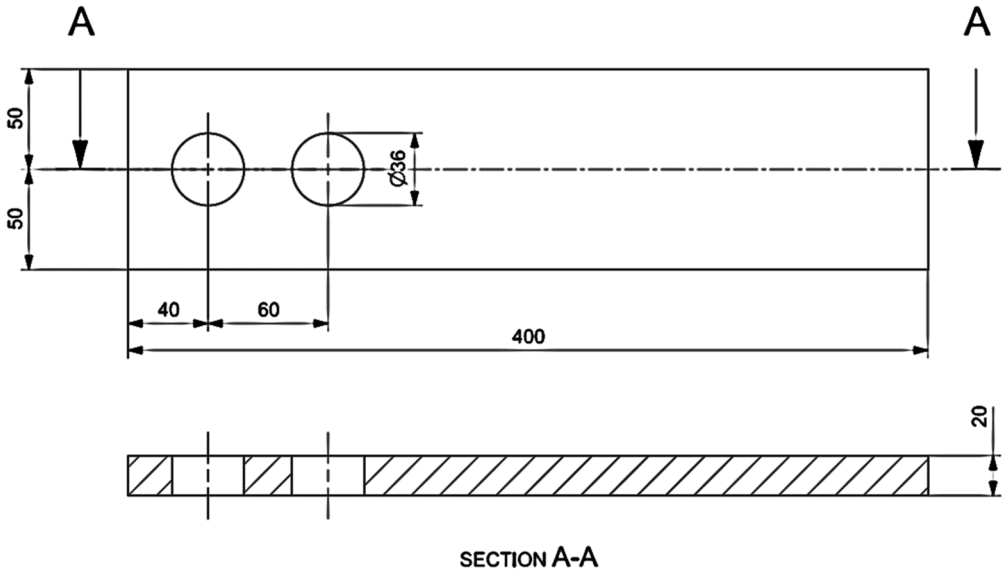

Figure 47 - Example of a centre plate with oversize holes Ø36mm, as used in the experimental programme

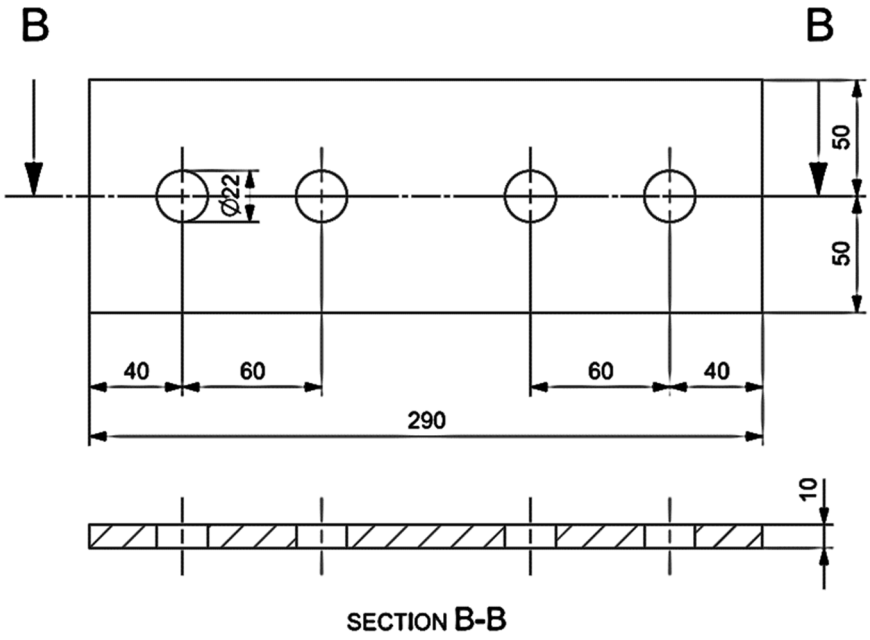

Figure 48 - Dimensions of cover plates used in the experimental programme

The plates are placed such that the holes in the cover and centre plates are concentric. To ensure the alignment of the holes is maintained during further preparation, a steel bar with a width of $10\ \mathrm{mm}$ is used as a spacer between the two centre plates. Hereafter, the bolts are positioned such that they are directly bearing to the steel cover plates. Hence, the bolt is not only eccentrically with respect to the cover plate holes, but also eccentrically to the centre plate holes. A cross section of the final assembly without injection material is illustrated in Figure 51.

In order to allow for the air to escape during injection, air escape holes are drilled into the sides of the centre plates. These air escape holes are positioned upward during the injection to facilitate the injection process.

Two types of test are carried out: short-term and long-term tests. The short-term test is a load controlled test in which the specimen will be loaded up to either the maximum capacity of the test rig or failure. The force at which a connection slip of $0{,}15\ \mathrm{mm}$ is reached is taken as an input for the long-term tests, during which the specimen will be loaded to 90% of the short-term force for obtaining $0{,}15\ \mathrm{mm}$ slip. Figure 49 illustrates the testing sequence.

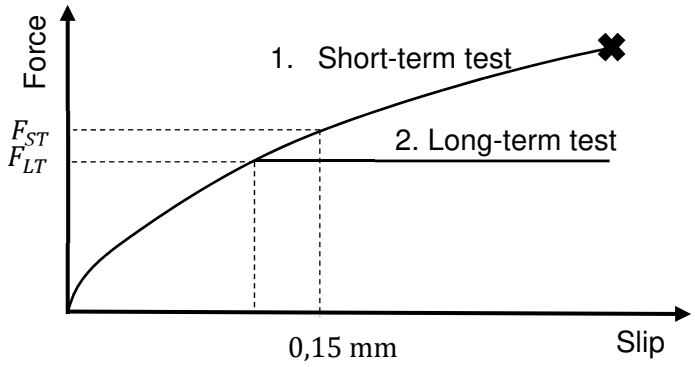

Figure 49 - Testing sequence, F_{LT} is 90% of F_{ST}

The long-term tests last for $72\ \mathrm{hrs}$, which is hopefully enough to show that the extrapolated slip after 50 years is not more than $0{,}3\ \mathrm{mm}$. Such extrapolation is carried out by plotting a slip-log(time) diagram, as exemplified in Figure 50. It is not possible to continue the long-term tests for longer than $72\ \mathrm{hrs}$, given the limited time frame available for the experiments.

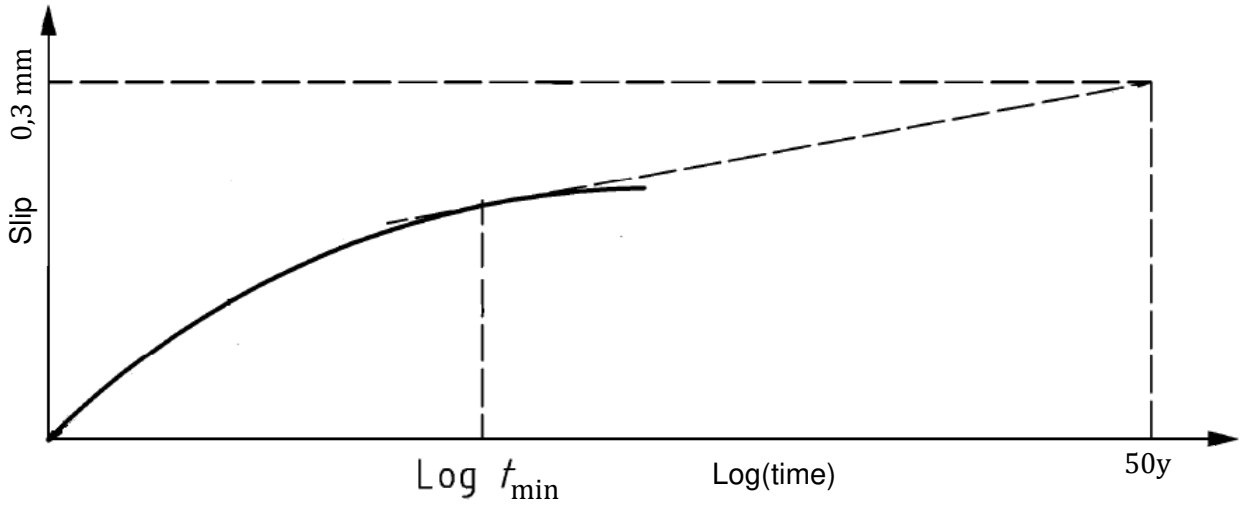

Figure 50 - Determination of minimum duration of long-term tests by extrapolating the slip in a slip-log(time) diagram. Slip after 50 years may not be more than 0,3 mm. Adapted after EN 1090-2 [4]

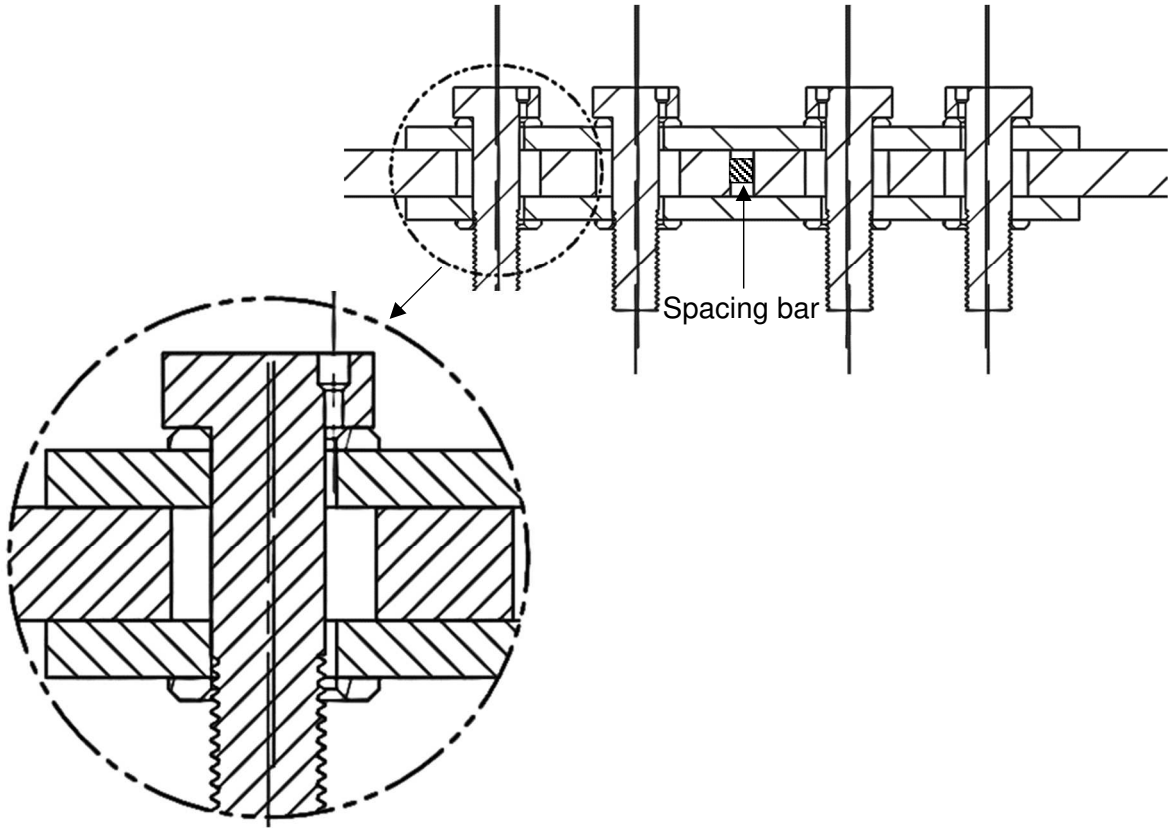

Figure 51 – Cross-section of assembly with holes Ø36 mm in centre plates. Detail indicating that the bolts are bearing directly on the steel cover plates. Nuts are not shown.

The relative displacement between the cover and centre plates is measured using LVDTs. An overview of measuring locations is given in Figure 52. The LVDTs have a range of up to 2,0 mm and are always installed such that they measure at the same location per specimen.

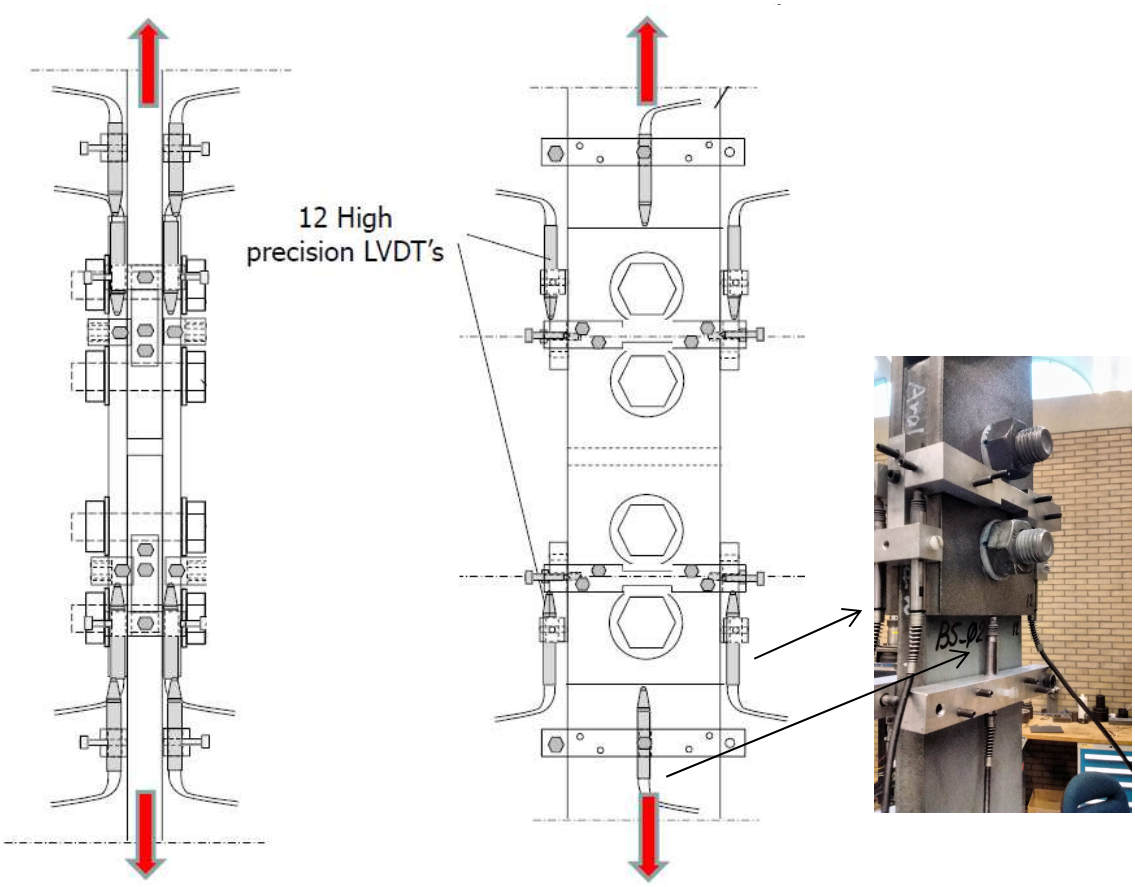

Figure 52 - Locations of LVDTs used to measure slip at CBG and PE [69]

3.2.4 Ultimate Failure Tests

Several tests are conducted on resin-injected specimen in order to determine the behaviour of double lap shear connections at ultimate failure (i.e. the state at which no additional force can be resisted). In order to reach ultimate failure, the same test set-up is used as discussed in Section 3.2.3. However, given the maximum load capacity of the test rig of $500\ \mathrm{kN}$, only one bolt is installed in the end-hole of the centre plate. Connections with hole diameters in the centre plate of 36 and $22\ \mathrm{mm}$ are loaded up to failure using a displacement-controlled regime. The test assembly is illustrated in Figure 53.

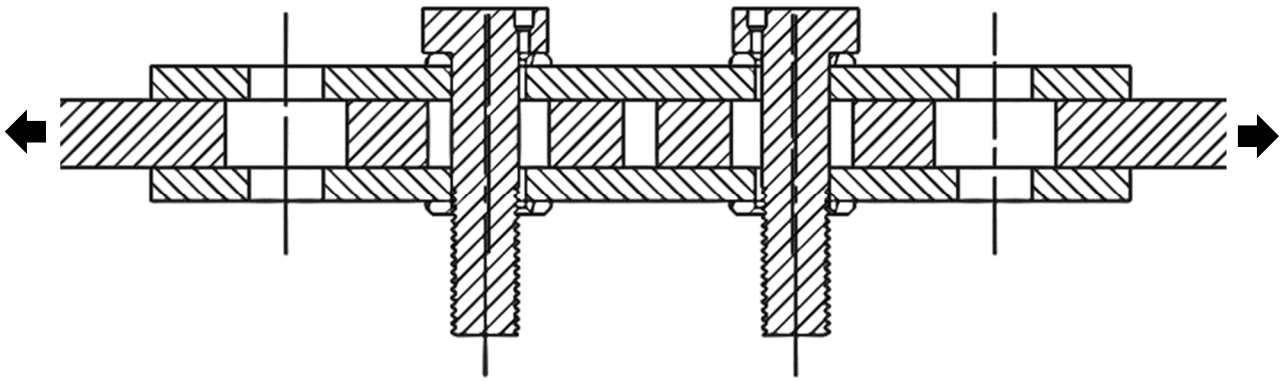

Figure 53 - Assembly used to determine the behaviour of resin-injected double lap connection at ultimate failure, example given for $Ø_{centre}$ = 36 mm

4 Results

4.1 Injectability of Injection Materials

Figure 54 shows a cross section of an injected double lap connection with and without an air escape channel, as defined in Section 3.2.1 (Figure 43). The cover plates have a nominal hole diameter of $22\ \mathrm{mm}$, whereas this is $32\ \mathrm{mm}$ for the centre plate. From Figure 54, it can be seen that an air pocket remains within the centre plate cavity if no precautions are taken to prevent this.

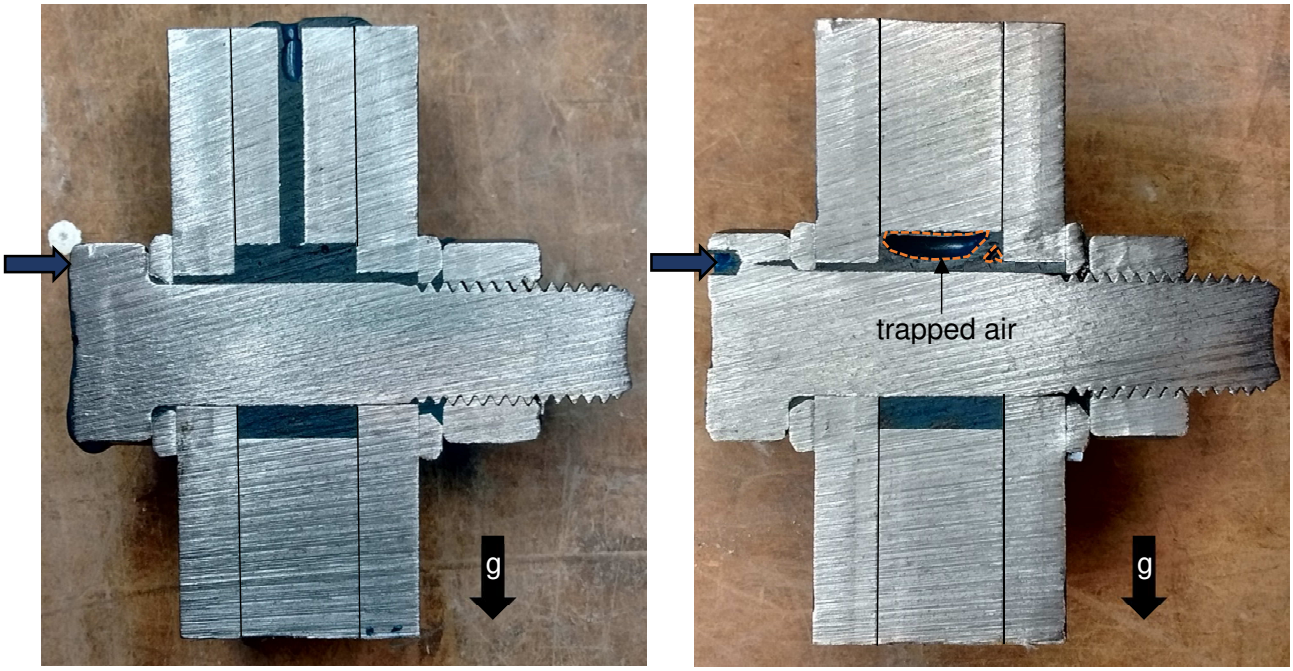

Figure 54 – Cross-section of a resin-injected double lap shear connection with (left) and without (right) air escape channel. Bolts are M20, diameter of cover plate hole 22 mm and centre plate hole 32 mm.

The injectability of the grout has been assessed using a Perspex cylinder, which was successfully injected using a manual caulking gun, as can be seen from Figure 55. Only the area where the bolt and the Perspex specimen are in direct contact is not covered with grout, but further all cavities are filled and no air inclusions are visible with the naked eye.

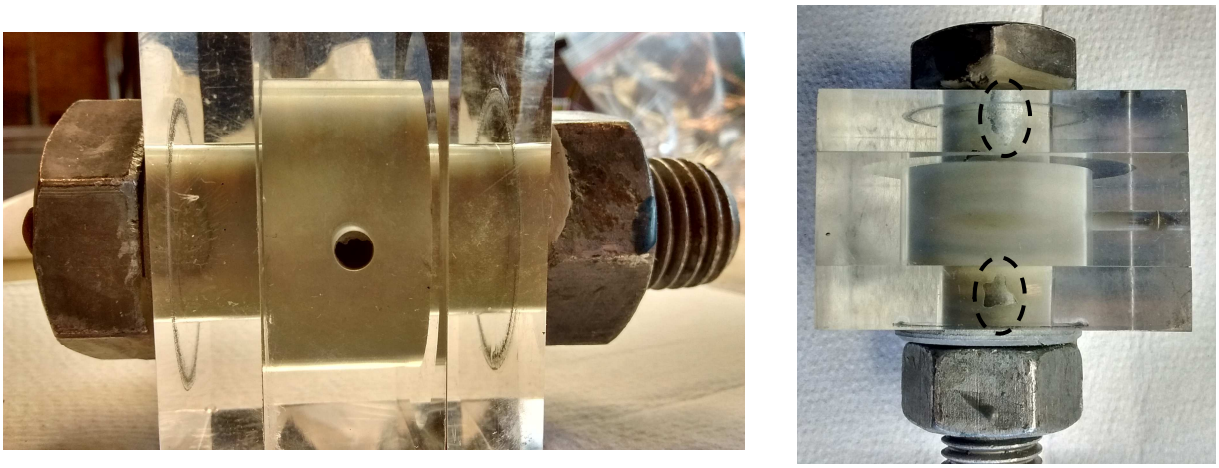

Figure 55 - Perspex specimen injected with grout. In the areas within the dashed lines the bolt is in direct contact with the Perspex.

During the injection of the specimen for the double lap shear tests, it was observed that it was not in all cases possible to inject the grout through the bolt head. The main limiting factor seems to be the position of the washer with respect to the bolt hole. During injection, this problem has been overcome by injecting through the air escape hole rather than through the bolt head. Such an air escape channel was not available for the specimen with normal clearance holes, which has influenced the test results (see Section 4.3).

4.2 Demountability of Injected Connections

4.2.1 Test to Determine Suitable Release Agents

Wax spray

Figure 56 illustrates a piece of threaded end that has been cast in resin. Prior to injection of the resin, both the mould and the threaded end have been treated with a wax-based release agent. After allowing for 24 hours of hardening, it was possible to separate the specimen from the mould by hand by pulling. Hereafter, the threaded end has been fixed in the work bench and the resin infill could be separated by screwing using water pump pliers.

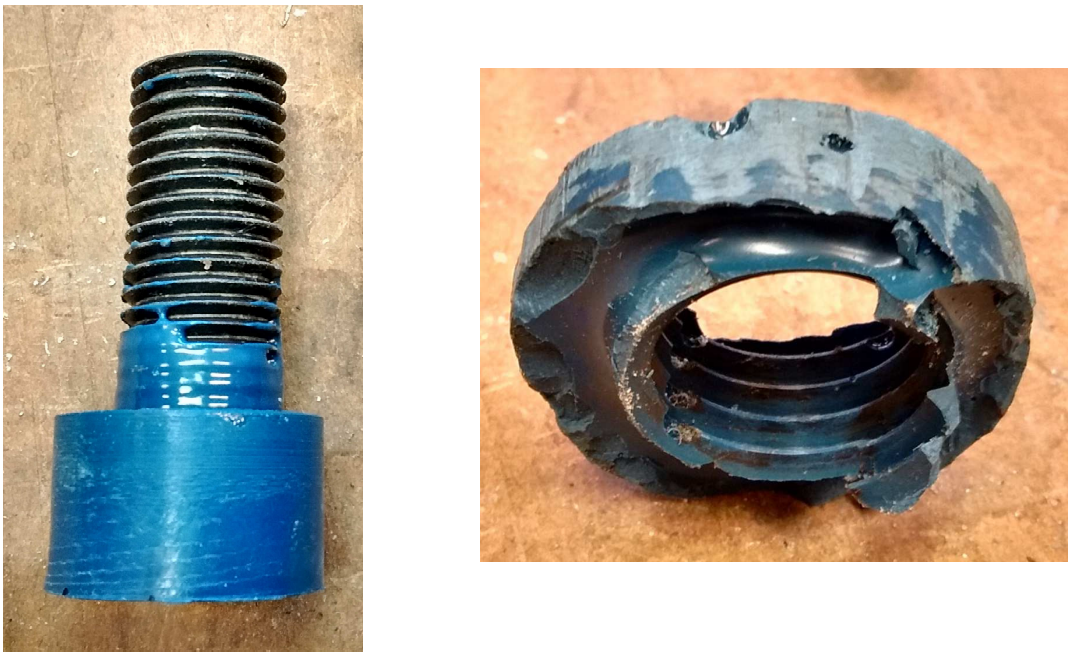

Figure 56 - Left: threaded end including resin released from a mould treated with a wax-based release agent. Right: Formation of threads in the resin: due to application of a waxy release agent the threaded end could be removed by unscrewing

Silicon spray

In addition to the stubs of threaded end, also the threaded part of a bolt has been cast into resin after undergoing a treatment with silicon-based release agent. After allowing 24 hours for hardening, the bolt could be easily removed from the resin using a wrench, as is illustrated in Figure 57. The resin did not adhere to either the bolt or the steel mould.

Figure 57 – Left: Unscrewing a bolt from resin infill using a wrench. Right (top): disassembled components. Right (bottom): cross section of resin infill showing the bolt threads cast into the resin.

PVA (Polyvinyl alcohol)

Similar to the wax and silicon spray, the PVA-solution (polyvinyl alcohol) successfully prevented adhesion between the steel and resin, as can be seen from Figure 58. After unscrewing the threaded end from the resin infill by hand, the PVA-film that prevented adhesion was clearly visible and detached.

Figure 59 illustrates the structure of the resin at a location where PVA-solution was able to accumulate, although all (visible) excess PVA was removed before injection took place. At this location, the resin is rather porous. Also, it appears that the PVA-solution disappears between the clamped plates (Figure 59, right).

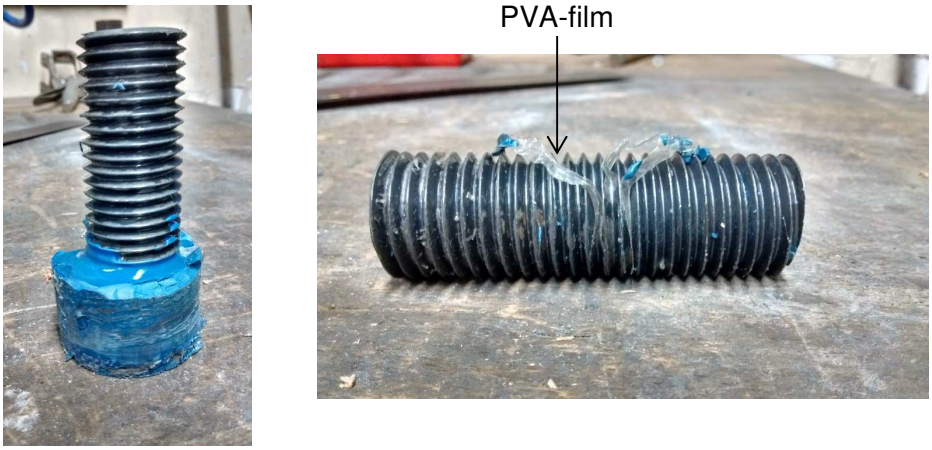

Figure 58 - Left: threaded end including resin released from a mould treated with polyvinyl alcohol as a release agent. Right: Polyvinyl alcohol film detaches after unscrewing of resin infill.

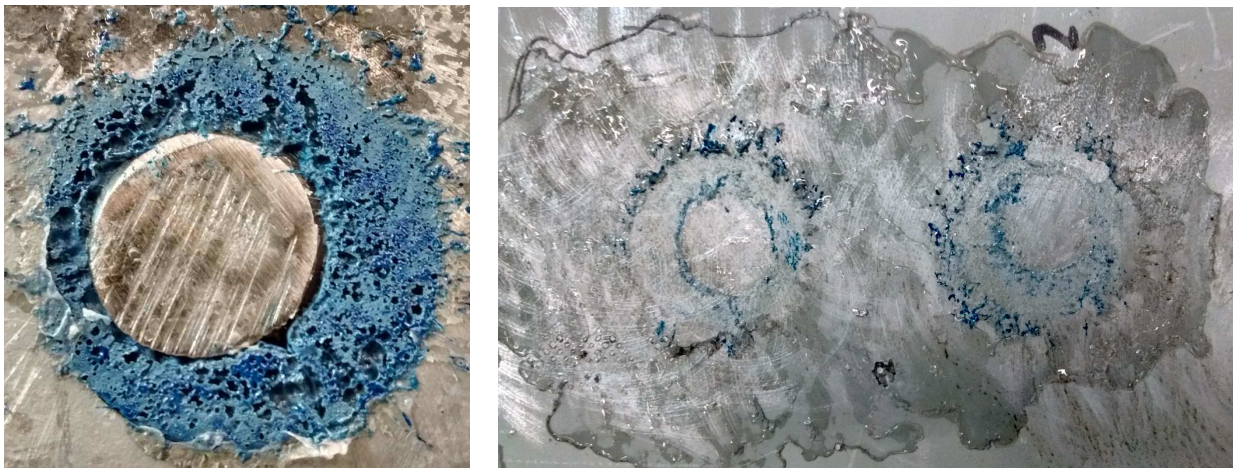

Figure 59 - Left: porous resin as a result of PVA-accumulation, right: PVA-solution spreads between the clamped plates.

4.2.2 Choice of Release Agent in Double Lap Shear Tests

Based on the preliminary results discussed in Section 4.2.1, it is chosen to use wax-based spray as a release agent within the rest of the experimental programme related to resin-injected connections. Although the performance of silicon spray is similar to that of wax spray, silicon is not chosen since the presence of silicon may degrade the material properties of the resin. In case of grout-injected connections, no release agent is used, due to the negligible adhesive bond between smooth steel and grout.

4.3 Stiffness and Strenght of Injected Double Lap Shear Connections

4.3.1 Short-term Double Lap Shear Connection Tests

Resin

Figure 60 presents the results obtained from the short-term tests on resin-injected specimen (curing time 24 hrs). The results focusing on the deformation below $0{,}15$ mm slip are given in Figure 61, whereas a summary of the results is laid down in Table 9. The spread within the initial connection stiffness is lower than $3{,}9\%$.

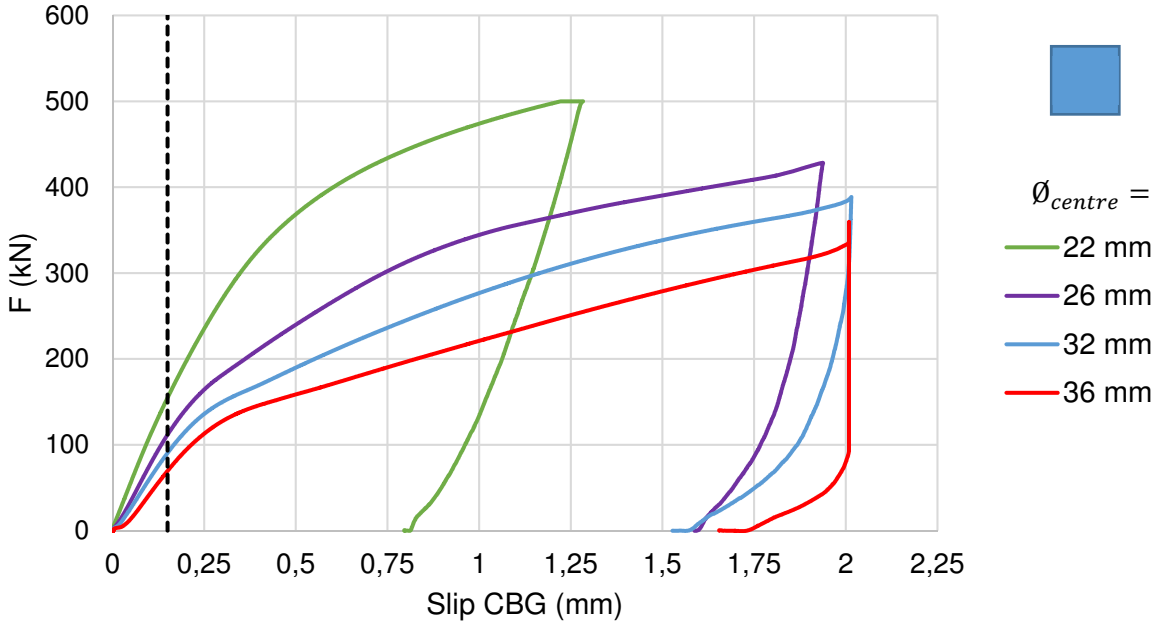

Figure 60 - Relationship between external load and connection slip measured at CBG for short-term tests on resin-injected specimen (averaged)

Table 9 – Average results of short-term test on resin-injected specimen

	$Ø_{centre}$ (mm)				Units
	22 mm	26 mm	32 mm	36 mm	
External load at 0,15 mm slip	154,8	111,5	90,4	69,2	kN
Initial stiffness* k_{ini}	$9{,}8 \cdot 10^2$	$7{,}7 \cdot 10^2$	$6{,}4 \cdot 10^2$	$5{,}6 \cdot 10^2$	kN/mm
Spread k_{ini} (2 tests)	$\pm 0{,}4\%$	$\pm 3{,}9\%$	$\pm 3{,}8\%$	$\pm 1{,}7\%$	–
Max. observed external load	500	428,3	388,6	335	kN
Slip at max. observed external load	1,243	1,938	2,0	2,0	mm
*: Measured over the interval $0{,}05 - 0{,}15$ mm slip at CBG.					

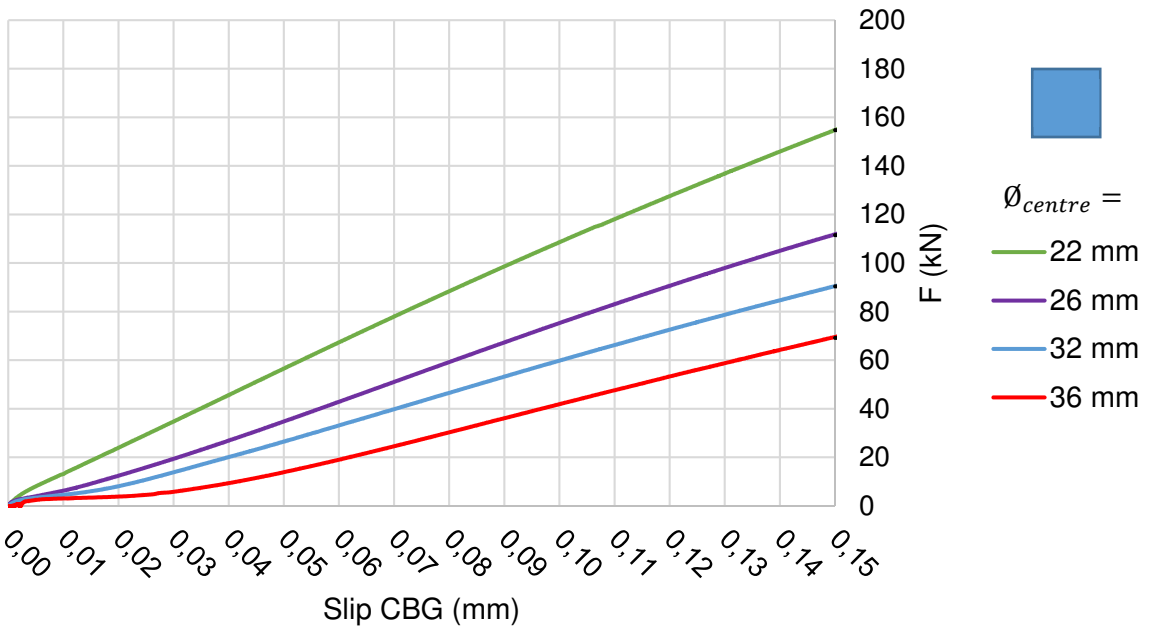

Figure 61 - Relationship between external load and connection slip measured at CBG for short-term tests on resin-injected specimen, zoomed in on the range of 0-0,15 mm slip (averaged)

After loading, the specimen have been demounted by first unscrewing the nuts and subsequently removing the bolts using a hammer. The condition of the resin in the centre plate bolt hole is shown in Figure 62. It must be noted that when removing the bolt from holes with a diameter of $22\ \mathrm{mm}$, also the resin is completely removed. After removal of the bolt, the resin infill could easily be removed as well, as exemplified through Figure 62 (bottom).

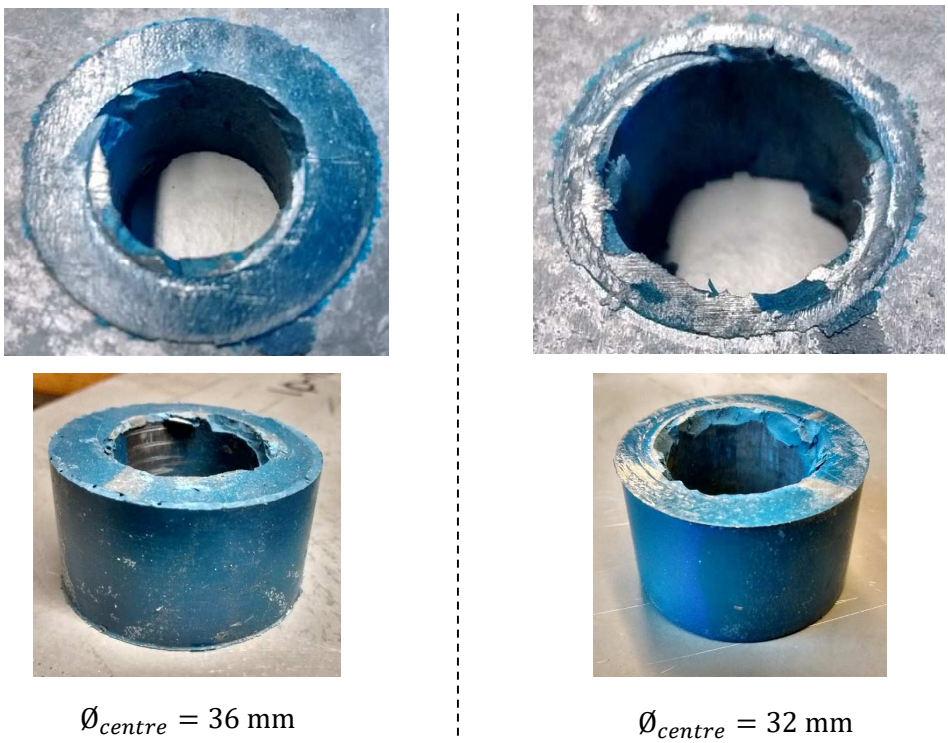

Figure 62 – Top: centre plate bolt holes of resin-injected specimen after loading, bottom: resin infill after removal from centre plates by hand using a hammer

Based on the short-term test the load level for the long-term test is determined using the initial stiffness, which yields the load levels listed in Table 10. It is deliberately chosen to use the initial stiffness (defined between $0{,}05$-$0{,}15\ \mathrm{mm}$ of CBG slip) as an input for the long-term tests rather than the force measured at $0{,}15\ \mathrm{mm}$ slip, given that within the mentioned slip range the behaviour is more constant and thus more reliable.

Table 10 - F_{ST} and F_{LT} for resin-injected specimen

$\emptyset_{centre}\ (\mathbf{mm})$	$F_{ST} = 0{,}15\ \mathbf{mm} \cdot k_{ini}\ (\mathbf{kN})$	$F_{LT} = 0{,}9 \cdot F_{ST}\ (\mathbf{kN})$
22	147,4	132,7
26	115,6	104,0
32	96,1	86,5
36	83,5	75,2

In order to have an estimate of the resin strength at the age of testing $(24\mathrm{hrs})$, a cylindrical resin sample with $\emptyset = 50\ \mathrm{mm}$ was used to determine the resin compressive strength. Figure 63 illustrates the condition of the small-scale resin sample before and after testing. The compressive failure load of the sample was $809{,}4\ \mathrm{kN}$, which leads to a compressive strength of $412\ \mathrm{MPa}$. It should be noted that this is not the uniaxial compressive strength, given that the specimen is rather thin and thus confinement resulting from the steel plates in the compression machine is obtained in the entire sample. However, given that the material application (e.g. a double lap shear connection) also presents confinement, the result is still meaningful.

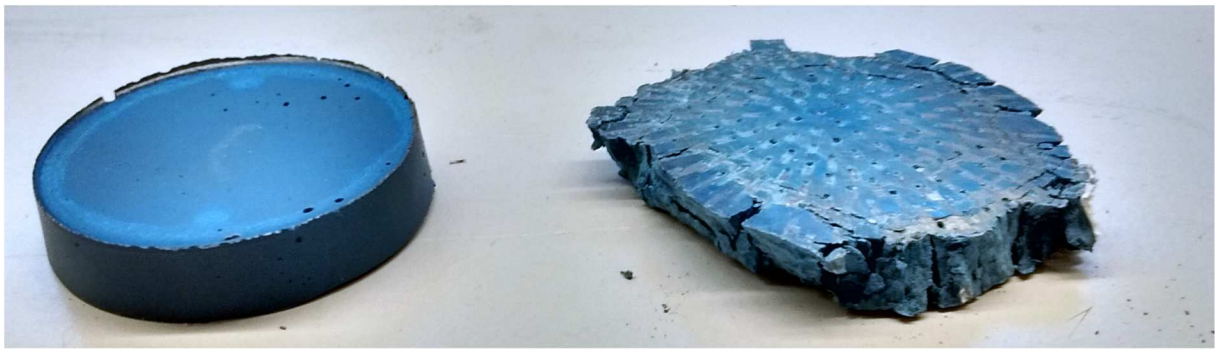

Figure 63 - Small-scale resin sample used to determine the compressive strength, before (left) and after (right) loading in a compression machine.

Grout

The results of the short-term tests on grout-injected specimen (curing time 48hrs) are illustrated in Figure 64. The results focusing on the deformation below $0{,}15\ \text{mm}$ slip are given in Figure 65, whereas a summary of the results is laid down in Table 11. The spread within the results is lower than $3{,}7\%$. It should be noted that the specimen with normal clearance holes could not be properly injected, hence the results are different from the expectations.

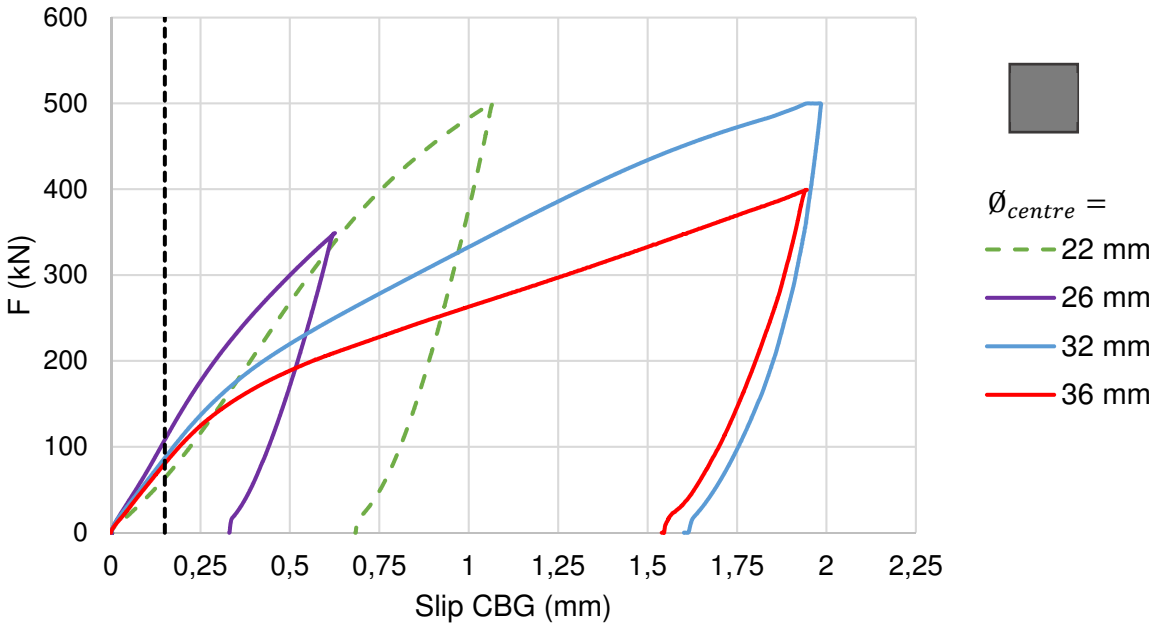

Figure 64 - Relationship between external load and connection slip measured at CBG for short-term tests on grout-injected specimen (averaged)

Table 11 - Results of short-term test on grout-injected specimen

	$Ø_{centre}$ (mm)				Units
	22 mm**	26 mm***	32 mm	36 mm	
External load at 0,15 mm slip	NA	107,5	86,3	79,9	kN
Initial stiffness* k_{ini}	NA	$7{,}1 \cdot 10^2$	$5{,}4 \cdot 10^2$	$5{,}0 \cdot 10^2$	kN/mm
Spread k_{ini} (2 tests)	NA	NA	±3,7%	±2,8%	–
Max. observed external load	NA	343,6	500	399,3	kN
Slip at max. observed external load	NA	0,626	1,89	1,945	mm
*: Measured over the interval $0{,}05 - 0{,}15\ \text{mm}$ slip at CBG. **: Both connections within the specimen could not be fully injected					

***: The load level has not been further increased due to unsuccessful injection in one of the two connections. Only the properly injected connection is considered.

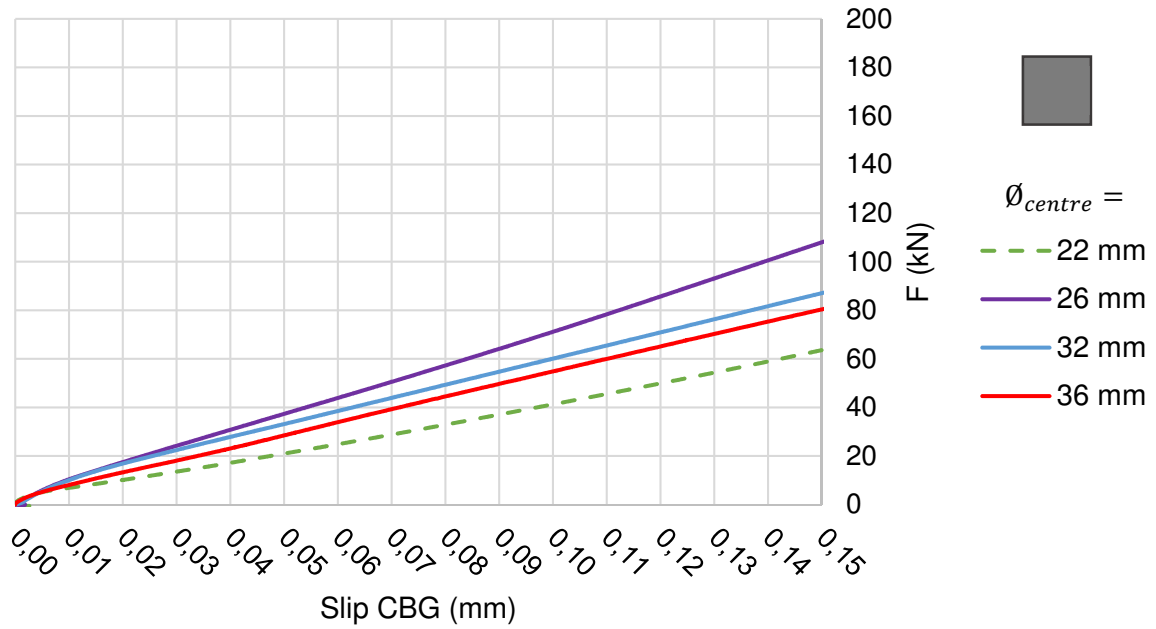

Figure 65 - Relationship between external load and connection slip measured at CBG for short-term tests on grout-injected specimen, zoomed in on the range of 0-0,15 mm slip (averaged)

After loading, the specimen have been demounted by first unscrewing the nuts and subsequently removing the bolts using a hammer. The condition of the grout in the centre plate bolt hole is shown in Figure 66. It must be noted that when removing the bolt from holes with a diameter of 26 mm and 22 mm, also the grout is completely removed. When attempting to remove the grout infill from the holes in one piece, the grout shatters.

$Ø_{centre} = 36$ mm $\qquad$ $Ø_{centre} = 32$ mm

Figure 66 - Centre plate bolt holes of grout-injected specimen after loading

In order to have an estimate of the grout strength at the age of testing (48hrs), a cylindrical grout sample with $\text{Ø} = 50\ \text{mm}$ was used to determine the resin compressive strength. Figure 63 illustrates the condition of the small-scale grout sample before and after testing. The compressive failure load of the sample was $139{,}1\ \text{kN}$, which leads to a compressive strength of $71\ \text{MPa}$. The compressive strength after $48\ \text{hrs}$ $(71\ \text{MPa})$ is within bounds of the supplier's product sheet (Appendix B).

Figure 67 - Small-scale grout sample used to determine the compressive strength, before (left) and after (right) loading in a compression machine.

4.3.2 Long-term Tests

Resin

Figure 68 presents the averaged results obtained from the creep tests on resin-injected specimen (curing time 24 hrs). The spread in the results seem to increase for larger values of $Ø_{centre}$. Moreover, for increasing $Ø_{centre}$, the slip rate on a log(time)-scale appears to increase in time, whereas the slip rate more or less stabilises for connections with normal clearance holes. Based on the results, it is evident that the 72hrs period is not in all cases sufficient to determine whether or not the slip criterion $(0{,}30\ \text{mm})$ after 50yrs is violated.

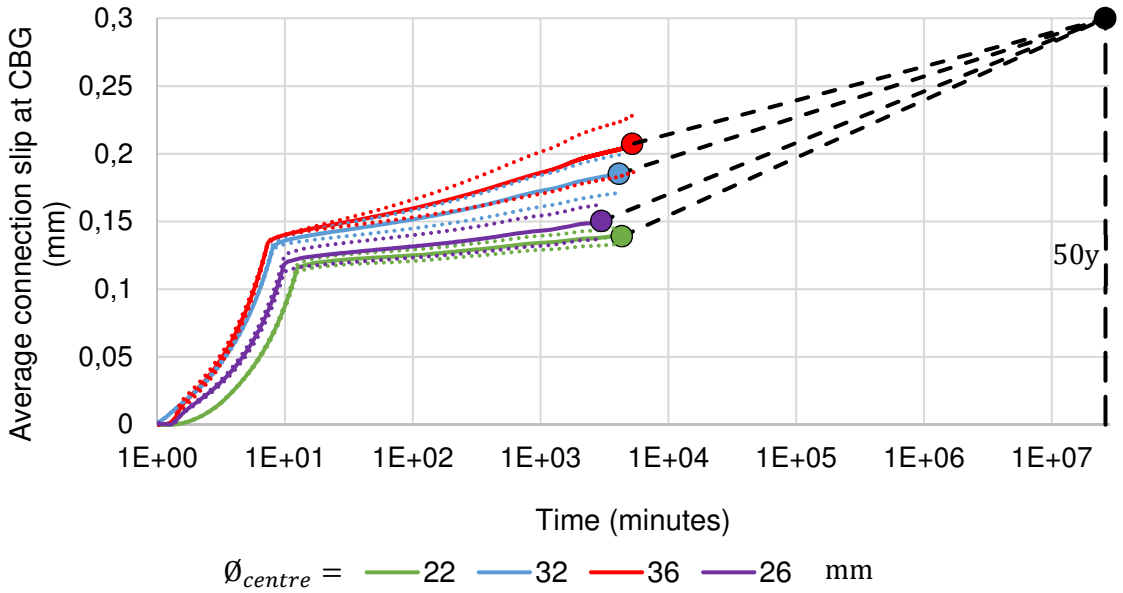

Figure 68 - Connection slip vs. time, indicating the creep deformation of resin-injected specimen

4.3.3 Ultimate Failure of Resin-Injected Specimen

Figure 69 shows the load-displacement diagrams of a double lap shear connections with one bolt for connections with hole diameters of 22 and $36\ \mathrm{mm}$ in the centre plate. It should be noted that in Figure 69, the displacement is that of the jack, and not the slip. The reason that the connection slip cannot be plotted is due to the limited range over which the LVDTs can measure $(2\ \mathrm{mm})$.

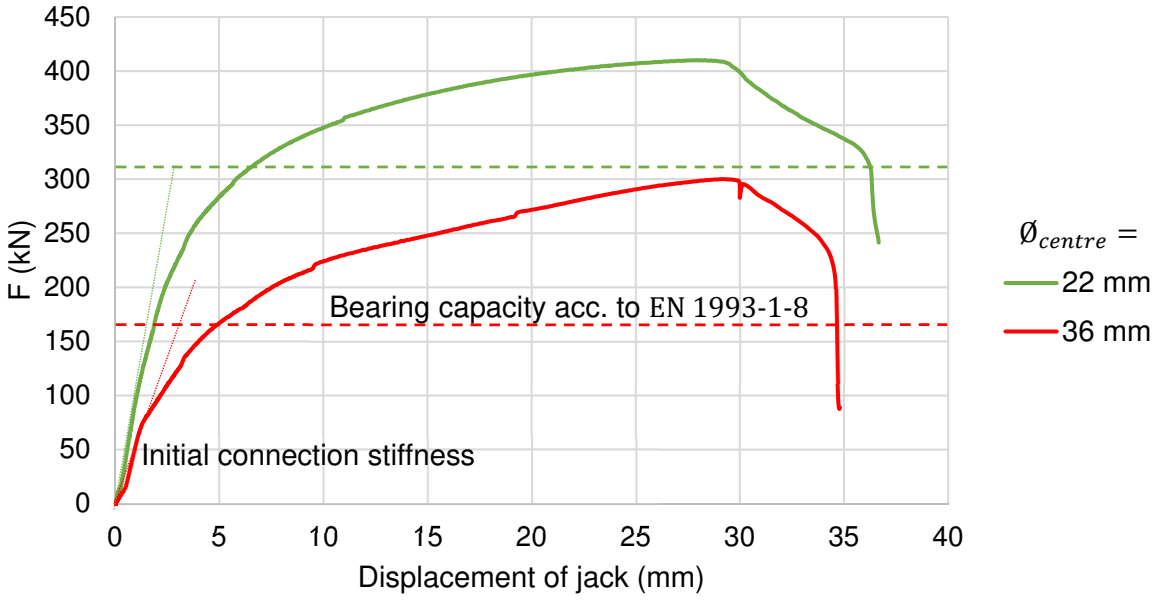

Figure 69 - Load-displacement curve of specimen loaded up to ultimate failure (note: the bearing resistance for the 36 mm is officially not defined by EN 1993-1-8 [3]).

Figure 70 illustrates the condition after ultimate failure of the specimen with a hole diameter of $36\ \mathrm{mm}$ in the centre plate. The connection failed at the moment the resistance of the plate was reached. At one side of the specimen, a small reduction in plate thickness at the net-section was visible. However, this was due to the air escape channel being located at this side of the connection.

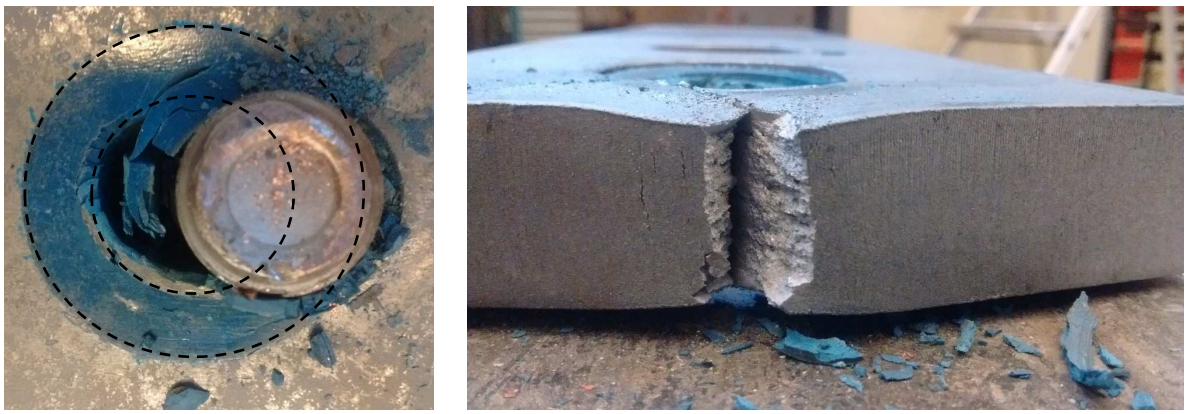

Figure 70 - Condition of centre plate with $Ø_{centre}$ = 36 mm after being loaded to ultimate failure

Figure 71 illustrates the condition after ultimate failure of the specimen with a hole diameter of $22\ \mathrm{mm}$ in the centre plate. Also this connection failed at the moment the resistance of the plate was reached. Moreover, the bolts underwent significant plastic deformation. Another difference is that this specimen clearly has a pile-up of material in front of the bolt, which was not present in the $36\ \mathrm{mm}$ -specimen

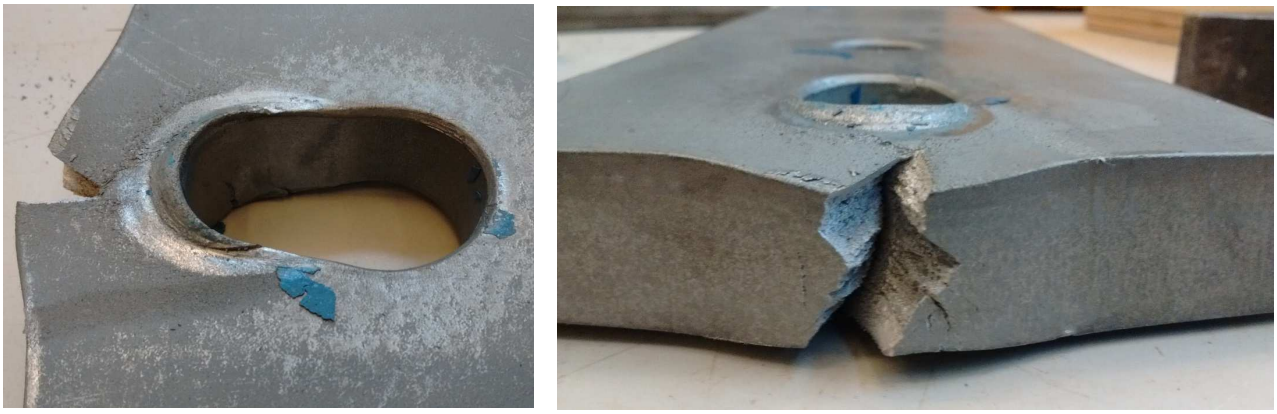

Figure 71 - Condition of centre plate with $Ø_{centre}$ = 22 mm after being loaded to ultimate failure

5 Modelling of Double Lap Shear Connection

5.1 Numerical

5.1.1 Derivation of Finite Element Model

The experimental test set-up of the injected double lap shear connection has been modelled in three dimensions using the finite-element package ABAQUS. Figure 72 shows a fully detailed impression of one connection (half a specimen).

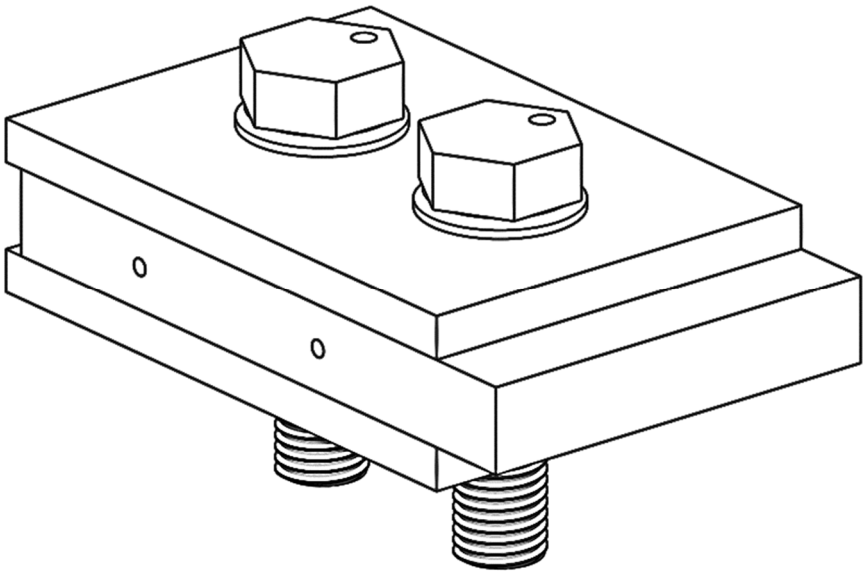

Figure 72 – Fully-detailed impression of a half specimen

The components of the connection are not modelled using the exact geometry of the specimen used in the experiments (i.e. not cf. Figure 72). Table 12 lists an overview of geometrical simplifications Such simplifications are made since their influence during the experiments is only marginal, e.g. the shape of the bolt head does not influence the way the load is transferred through the injection material.

Table 12 - Geometrical simplifications in numerical experiments

Component	Experimental geometry	Numerical simplified geometry
Fastener system	Separate bolt, nut and two special washers.	Integral part containing bolt, bolt head and washer. Bolt does not have a threaded part or hole in head. Bolt head is round.
Centre plate	Plate with two bolt holes and two air escape holes	No air escape holes
Cover plate	Plate with two bolt holes	-
Injection Material	Injected through bolt head, may be small voids within the material	Homogeneous component attached to the bolt

The symmetry of the connection is utilized to reduce the required computational resources. Figure 73 illustrates the different simplified connection components in the numerical model. Together, the components form $1/8\text{th}$ of a connection or $1/16\text{th}$ of a complete specimen. The injection material is assumed to be fixed to the bolt, since this ensures proper convergence of the analysis.

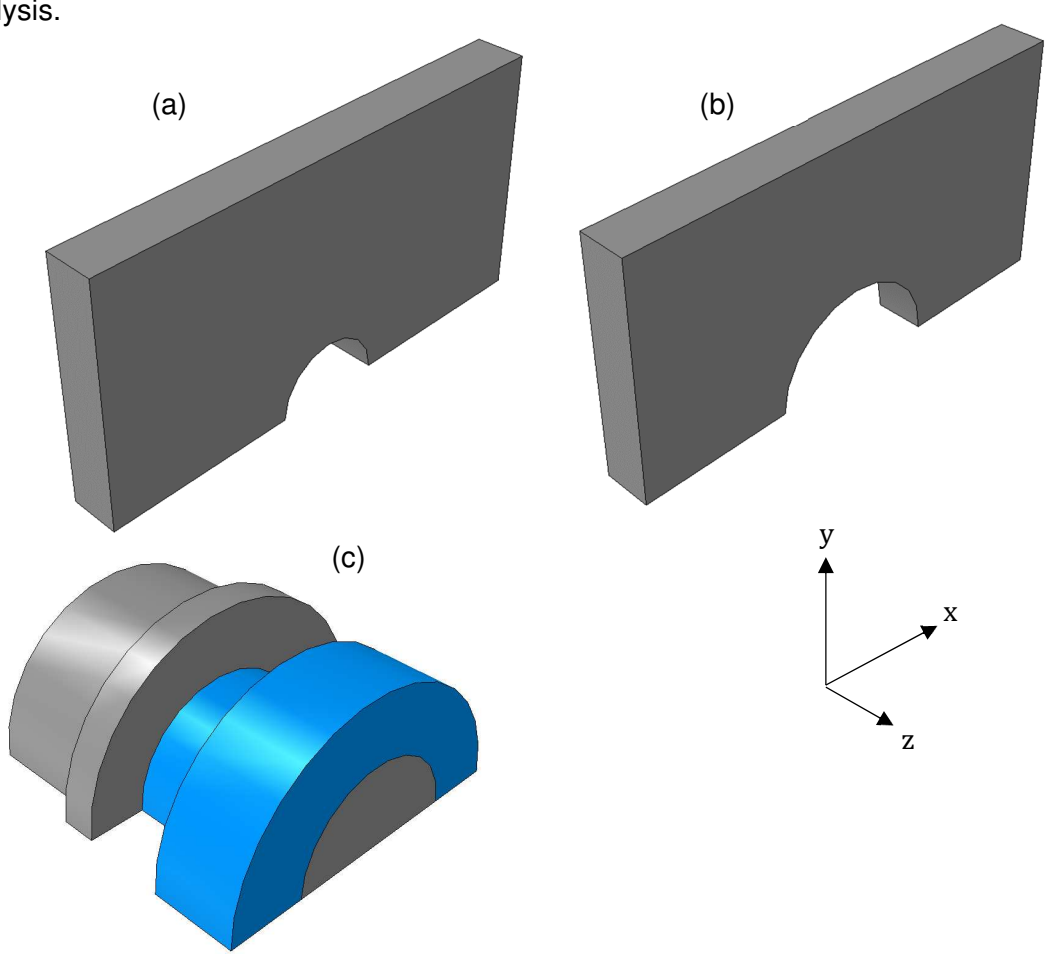

Figure 73 - Components used in the numerical analysis, example given for $Ø_{centre}$ = 36 mm. (a) cover plate, (b) centre plate and (c) bolt with attached injection material (blue)

The symmetry of the connection is represented using the built-in boundary conditions of ABAQUS. All boundary conditions are listed in Table 13 and illustrated in Figure 74. Moreover, Figure 74 illustrates the external loading which is schematized as uniformly distributed.

Table 13 - Boundary conditions prescribed at the faces of symmetry

	x-y plane			y-z plane			z-x plane		
	x =	y =	z =	x =	y =	z =	x =	y =	z =
Cover plate (a)	-	0	0	0	0	0	-	0	0
Centre plate (b)	-	-	-	-	0	0	-	0	0
Bolt incl. injection (c)	-	0	0	-	-	-	-	0	0

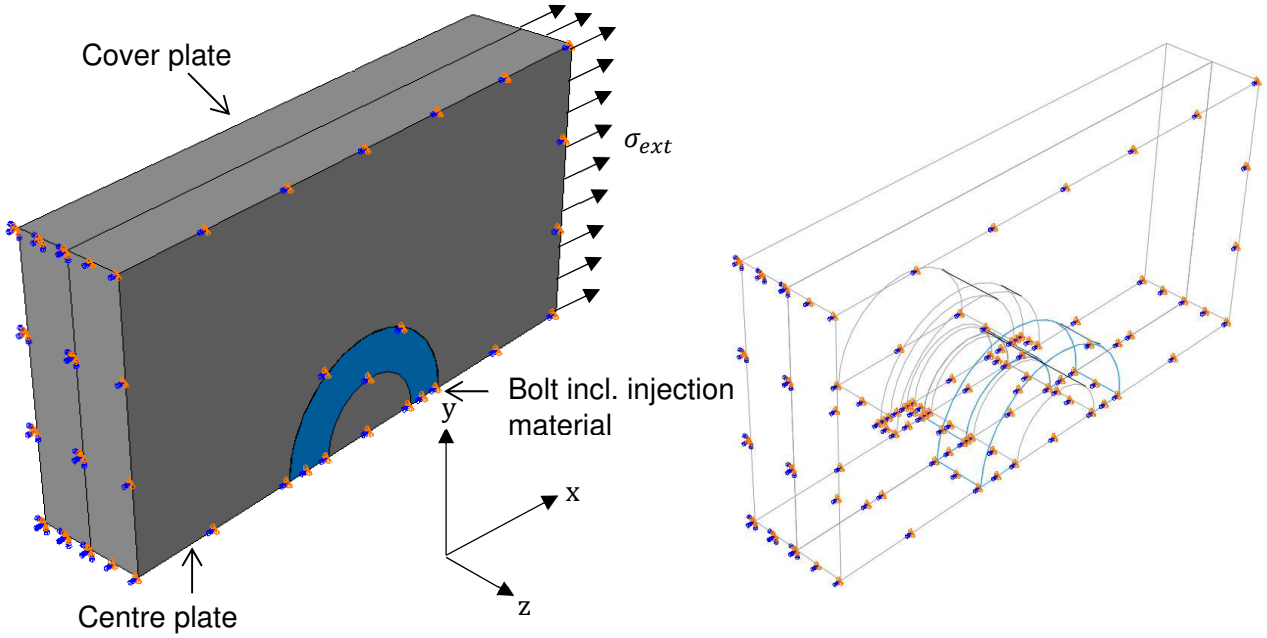

Figure 74 – Assembly with boundary conditions at faces of symmetry (see also Table 13) and uniformly distributed applied load.

Based on the experimental results, it is suggested to use linear-elastic material properties. For steel, the conventional values of $E = 210\ \text{GPa}$ and $\upsilon = 0{,}3$ are adopted. For the resin, the Young's Modulus is to be fitted to the experimental results, assuming a common value $\nu_{resin} = 0{,}3$ [52]. The material properties are summarized in Table 14.

Table 14 - Material properties in FE-analysis

		Young's Modulus (E) (MPa)	Poisson Ratio (υ) (-)
Cover plate (a)	-	210000	0,3
Centre plate (b)	-	210000	0,3
Bolt incl. injection (c)	Bolt	210000	0,3
	Resin	to be fitted	0,3 [52]*
	Grout	to be fitted	0,2*
*: Assumption			

The cover and centre plates are meshed with 8-node linear brick elements, known in ABAQUS as C3D8-elements. The bolt and the injection material are meshed using quadratic triangular prism elements in order to allow for a proper mesh in the regions where the volume of injection material is low. Such quadratic triangular prism elements are also referred to as C3D15-elements. Figure 75 illustrates both types of elements used in the finite element model.

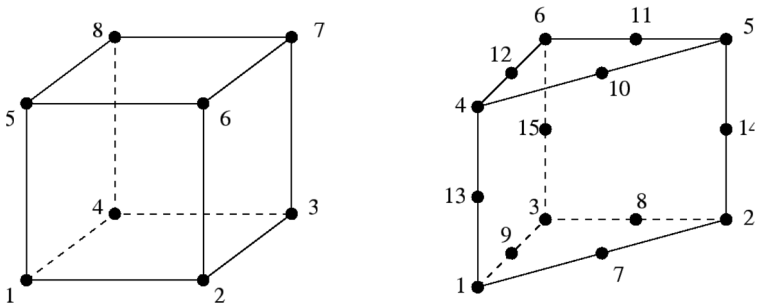

Figure 75 - C3D8R (left) and C3D15 (right) elements used in finite element analysis [72]

The powerful GENERAL CONTACT option of ABAQUS has been used to define the contact behaviour between the different members. Perpendicular to surfaces, 'hard-contact' is defined, whereas tangential to surfaces an absence of friction is assumed.

5.1.2 Validation of Finite Element Model

Finite element models were created for all types of double lap shear connections tested in the experimental programme. The Young's Modulus needed to fit the numerical model to experimental data was obtained by carrying out FE-analysis by assuming several different Young's Moduli and iterating towards the best fit. The stiffness of a complete double lap shear connection is 8 times the stiffness of the numerical model, given that symmetry has been used to reduce the problem to 1/8th of a connection. The connection stiffness is calculated using Eq. 22 and Eq. 23.

$$k_{1,FEA} = \frac{F}{u_{FEA}} \qquad \text{Eq. 22}$$

$$k_{ini,FEA} = 8 \cdot k_{1,FEA} = 8 \cdot \frac{F}{u_{FEA}} \qquad \text{Eq. 23}$$

With:

$k_{1,FEA}$	Stiffness of 1/8th of the double shear connection
F	Summation of external uniformly distributed load σ_{ext} in finite element model
u_{FEA}	Slip in finite element-model (see Figure 76)
$k_{ini,FEA}$	Total stiffness of full double lap shear connection

The slip in the numerical model is defined as the relative displacement of the cover and centre plate at the centre of the bolt, as exemplified in Figure 76.

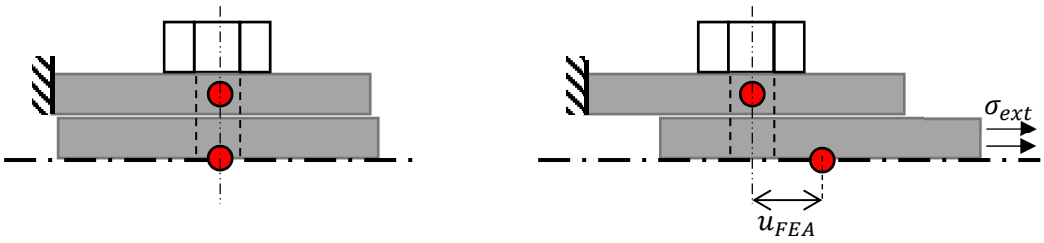

Figure 76 - Top view of FE-model indicating the definition of the slip u_{FEA}

The best fit for the resin is $E = 4{,}25\ \text{GPa}$. Figure 77 shows the comparison between the numerical and experimental results. An overview of the relative and absolute difference between the experimental and numerical results is given in Table 15.

Table 15 – Absolute and relative comparison between experimental results and numerical model for resin-injected specimen, for *E* = 4,25 GPa

$\emptyset_{centre}$ (mm)	Experimental k_{ini} (kN/mm)	Numerical $k_{ini,FEA}$ (kN/mm)	Absolute Difference(kN/mm)	Relative Difference
22	$9{,}8 \cdot 10^2$	$9{,}8 \cdot 10^2$	$-1{,}3$	$-0{,}1\%$
26	$7{,}7 \cdot 10^2$	$7{,}9 \cdot 10^2$	$+18{,}9$	$+2{,}5\%$
32	$6{,}4 \cdot 10^2$	$6{,}0 \cdot 10^2$	$-35{,}7$	$-5{,}6\%$
36	$5{,}6 \cdot 10^2$	$5{,}4 \cdot 10^2$	$-16{,}9$	$-3{,}0\%$

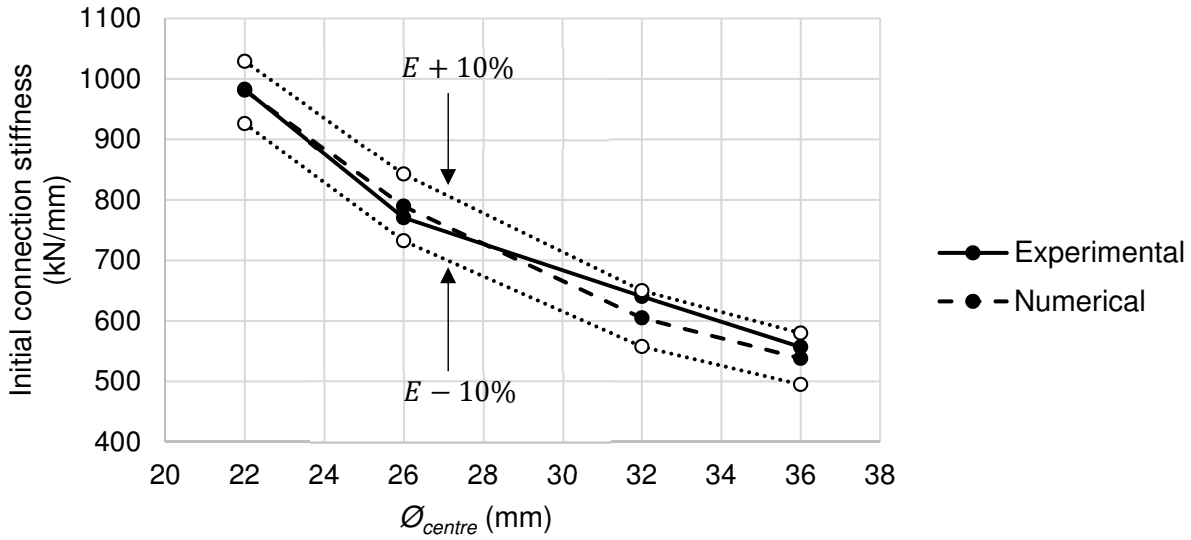

Figure 77 - Comparison between experimental data and numerical model for resin-injected specimen, for *E* = 4,25 GPa, including sensitivity of ±10% change in *E*

In order to increase the degree of credibility of the finite element model, an additional test has been carried out on a resin-injected double lap shear connection. In this connection, the bolts are positioned at their most unfavourable positions (i.e. cf. Annex G of EN 1993-1-8 [4]). The difference between this test set-up and the test set-up in the rest of the experimental programme lays in the position of the bolt with respect to the cover plate. The bolts used are M20 and the centre plate has a nominal clearance hole ($Ø_{centre} = 22$ mm). For this case, the numerical prediction for the initial connection stiffness is $k_{ini,FEA} = 7{,}7 \cdot 10^2$ kN/mm, whereas the established experimental connection stiffness is $k_{ini} = 8{,}2 \cdot 10^2$ kN/mm, which is a difference of $-6{,}0\%$.

The best fit for the grout is $E = 4{,}45$ GPa. The result for the specimen with $Ø_{centre} = 22$ mm is not considered in the verification, given that injection of this specimen was not possible. Figure 78 shows the comparison between the numerical and experimental results. An overview of the relative and absolute difference between the experimental and numerical results is given in Table 16.

Table 16 – Absolute and relative comparison between experimental results and numerical model for grout-injected specimen, for *E* = 4,45 GPa

$Ø_{centre}$ (mm)	Experimental k_{ini} (kN/mm)	Numerical $k_{ini,FEA}$ (kN/mm)	Absolute Difference (kN/mm)	Relative Difference
22	-	$9{,}0 \cdot 10^2$	-	-
26	$7{,}1 \cdot 10^2$	$7{,}0 \cdot 10^2$	-1,8	-0,3%
32	$5{,}4 \cdot 10^2$	$5{,}4 \cdot 10^2$	+0,3	+0,1%
36	$5{,}0 \cdot 10^2$	$4{,}8 \cdot 10^2$	-18,7	-3,7%

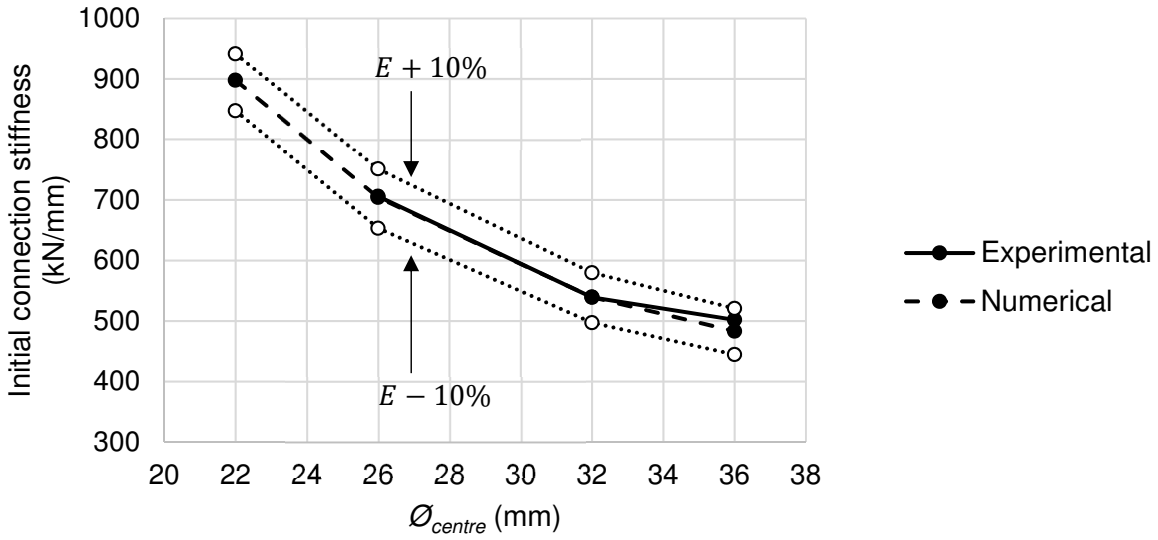

Figure 78 - Comparison between experimental data and numerical model for grout-injected specimen, for *E* = 4,45 GPa, including sensitivity of ±10% change in *E*

5.1.3 Parametric Study on Resin-Injected Connections

Based on the validated numerical model for resin-injected connections, a parameter study is conducted in order to find the influence of several factors. Such factors include the deformation (bending and shear) of the bolt, as well as the influence of type of hole. The parametric study will be started by looking at the initial connection stiffness for bolts placed in their most negative position with respect to connection slip.

Most negative placement of bolt in holes

If the bolt is positioned within a connection with an oversize hole at its most negative location with respect to connection slip (i.e. cf. Figure 79), the initial connection stiffness can be estimated through Figure 80. The results are computed using the verified numerical model.

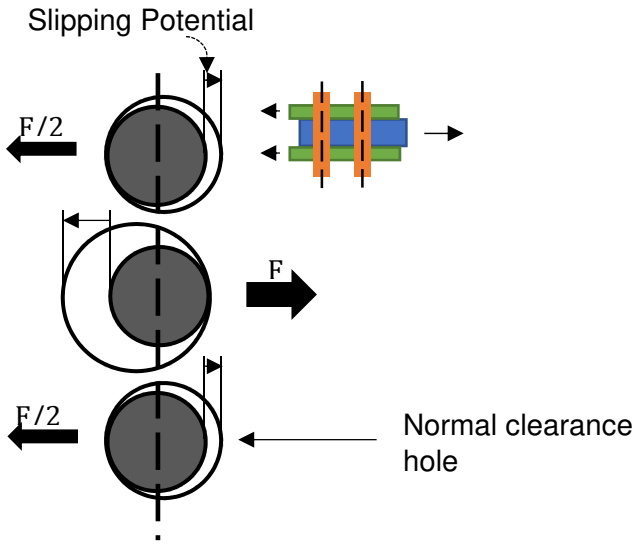

Figure 79 – Eccentric position of the bolt (grey) with respect to the bolt hole, causing the greatest potential of connection slip

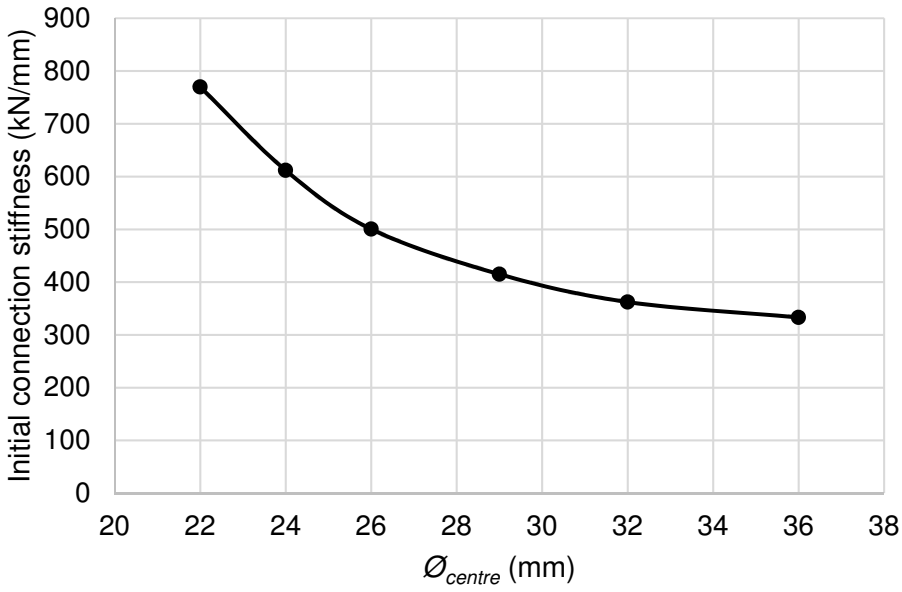

Figure 80 - Initial connection stiffness of resin-injected connections as a function of the hole size in the centre plate for an M20 bolt, assuming most negative placement of bolts with respect to potential connection slip

Figure 80 clearly shows that the connection stiffness decreases rapidly when opting for a larger hole diameter in the centre plate compared to a normal hole clearance. The results presented in Figure 80 are compared to the numerical results for the test set-up as in the experimental programme in Table 17.

Table 17 - Comparison of the initial connection stiffness depending on bolt position within holes

$Ø_{centre}$ (mm)	Initial connection stiffness (kN/mm) for bolt placement (numerical)		Difference
	As in experiments	Eccentrical	
22	$9{,}8 \cdot 10^2$	$7{,}7 \cdot 10^2$	-22%
26	$7{,}9 \cdot 10^2$	$5{,}0 \cdot 10^2$	-37%
32	$6{,}0 \cdot 10^2$	$3{,}6 \cdot 10^2$	-40%
36	$5{,}4 \cdot 10^2$	$3{,}3 \cdot 10^2$	-38%

By plotting the reciprocal of the initial connection stiffness (the connection compliance) versus the hole diameter in the centre plate (Figure 81), it becomes evident that the amount of slip per unit of force decreases for increasing values of $Ø_{centre}$. This effect can be attributed to the spreading of the bearing stress in lateral direction with respect to the direction of the force, as illustrated in Figure 82. as a result of this effect, it is expected that for very large hole diameters the connection stiffness will not significantly differ (as can also be seen from Figure 80). The connection compliance at point A gives an indication of the amount of slip caused by factors such as bolt deformation.

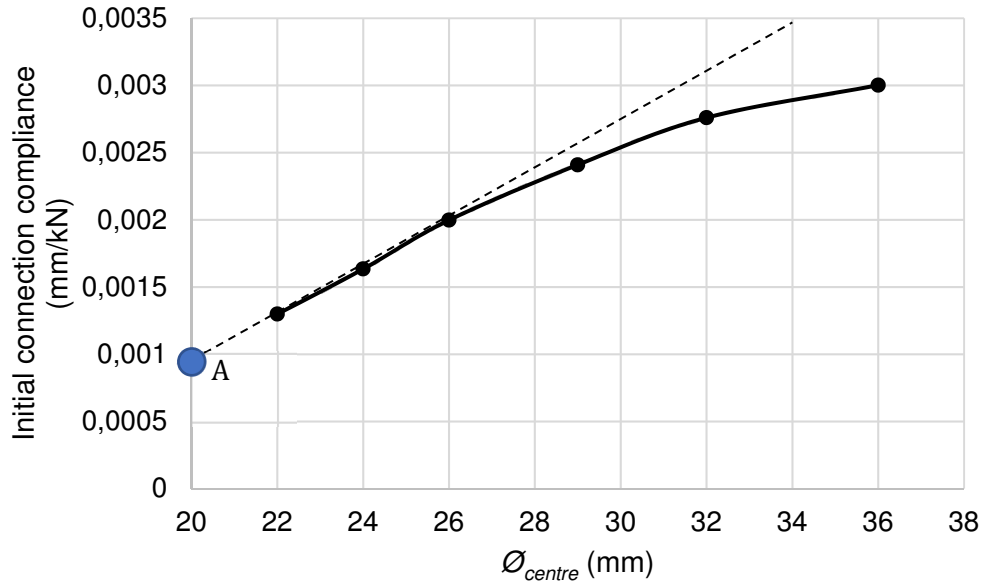

Figure 81 - Initial connection compliance as a function of the hole size in the centre plate for an M20 bolt, assuming most negative placement of bolts with respect to potential connection slip

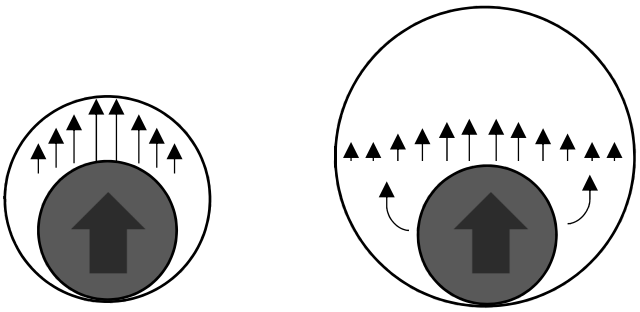

Figure 82 - Schematic bearing stress distribution, left: small hole clearance with relatively high bearing stresses, right: large hole clearance with relatively low bearing stresses

Bolt deformation

The influence of the shear and bending deformation of the bolt on the connection stiffness is first assessed by looking at numerical results with $E_{bolt} = 210\ \mathrm{GPa}$ and $E_{bolt} \to \infty$. Figure 83 illustrates the initial connection stiffness k_{ini} for both bolt stiffness cases.

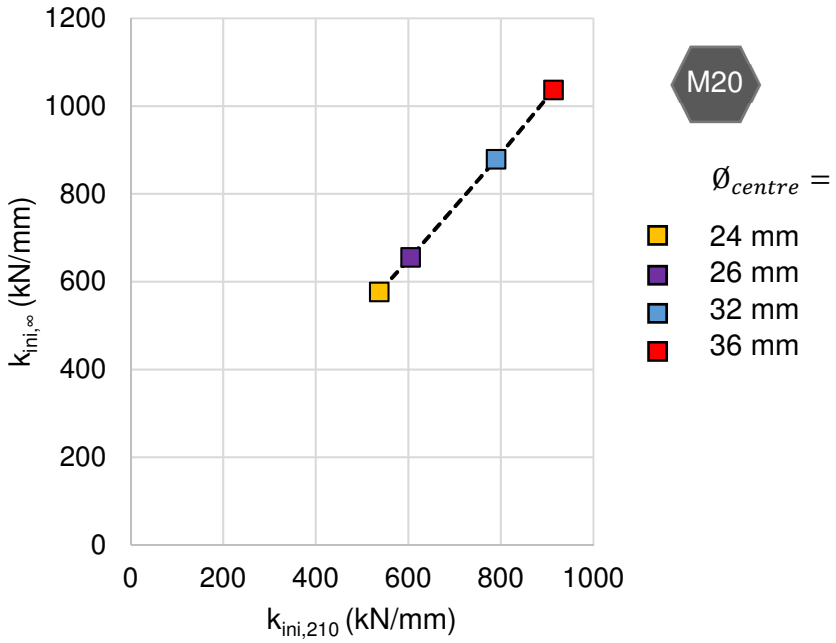

Figure 83 - Comparison between initial connection stiffness with deformable ($k_{ini,210}$) and infinitely stiff bolt ($k_{ini,\infty}$). Position of bolts as in experiments.

As can be seen from Figure 83, all points lay on a single line, indicating that there is no difference in bolt deformation as a result of oversizing of the centre plate hole. Considering metric M20 bolts, the total connection slip due to bolt deformation is roughly $1{,}3 \cdot 10^{-4}\ \mathrm{mm/kN}$ for the plate thicknesses $t_2 = \frac{1}{2} \cdot t_1 = 10\ \mathrm{mm}$. For this specific case, the deformation pattern of the bolt is exemplified in Figure 84.

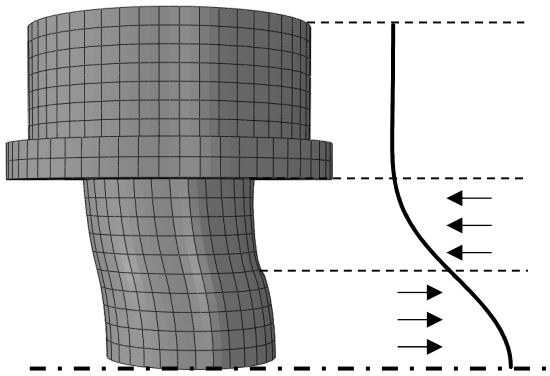

Figure 84 - Deformation pattern of bolt for $t_2 = 0{,}5t_1$

Ratio of bolt length over bolt diameter

Currently, EN 1993-1-8 limits the effective width of the resin to $3d$, assuming the plate dimensions are not governing. In order to investigate the validity of this prescription, finite element calculations are carried out for various l/d ratios with a constant ratio t_2/t_1. The length l is defined as the bolt length within the entire clamping package. All numerical specimen are loaded such that they have an identical nominal bearing stress σ_b. Apart from the differences mentioned, the test set-up is equal to the set-up used in the numerical validation.

Figure 85 presents the results of this numerical investigation, clearly indicating the effects of the l/d ratio on the relative slip at equal nominal bearing stress.

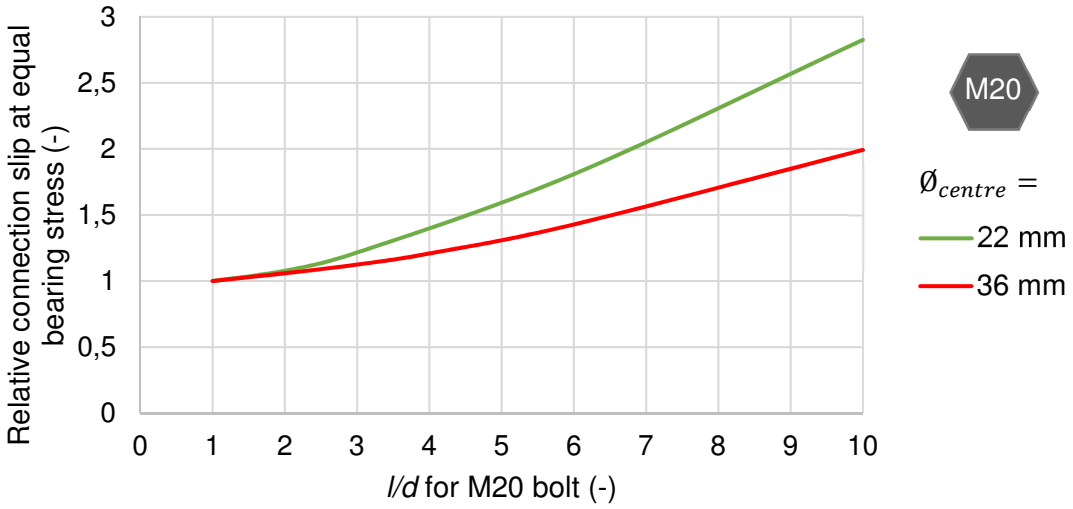

Figure 85 - Relative connection slip as a function of the ratio between bolt length and diameter, under the assumption of equal nominal bearing stress

As can be seen from Figure 85, the connection slip increases with an increase in the ratio l/d. This is the case for connections with and without oversize holes. Especially above $l/d \approx 3-4$ the connection slip increases significantly. The main reason for the rapid increase in connection slip is deformation of the bolt, as can be seen from Figure 86. For $l/d \geq 6-7$, the short-term connection slip consists of bolt deformation for more than 50% for $\emptyset_{centre} = 22\ \mathrm{mm}$ and for more than 33% for $\emptyset_{centre} = 36\ \mathrm{mm}$.

The deformation of the bolt has a direct influence on the bearing stress distribution along the length of the bolt, as can be seen from Figure 87. A large difference exists for the bearing stress distribution for normal clearance and oversize holes, the latter being more favourable, which can be explained by the fact that the bolt is relatively stiffer compared to the injection material. For $\emptyset_{centre} = 36\ \mathrm{mm}$ and $l/d \geq 3-4$, the bearing stress distribution can no longer be schematized as being constant along the bolt length, whereas this is the case at slightly lower l/d ratios for $\emptyset_{centre} = 22\ \mathrm{mm}$

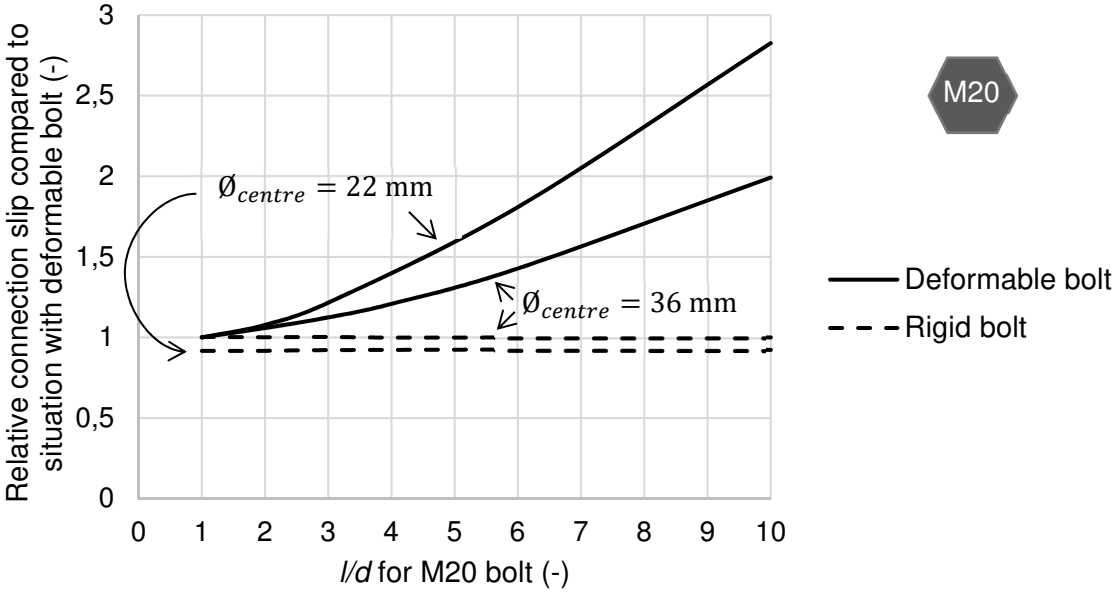

Figure 86 - Relative connection slip as a function of the ratio between bolt length and diameter, for connections with deformable and rigid bolts.

For several l/d ratios, the numerical results have been compared to the analytical model developed by Koper (2017) [15]. Figure 88 illustrates the bearing stress distribution for several l/d ratios for both models. Although the differences in stress distribution are quite substantial, especially for higher l/d ratios, the deformations shape of both models matches for all l/d ratios. It should be noted that the model of Koper predicts a region of zero bearing stress, which the stress may tend to, but never reach.

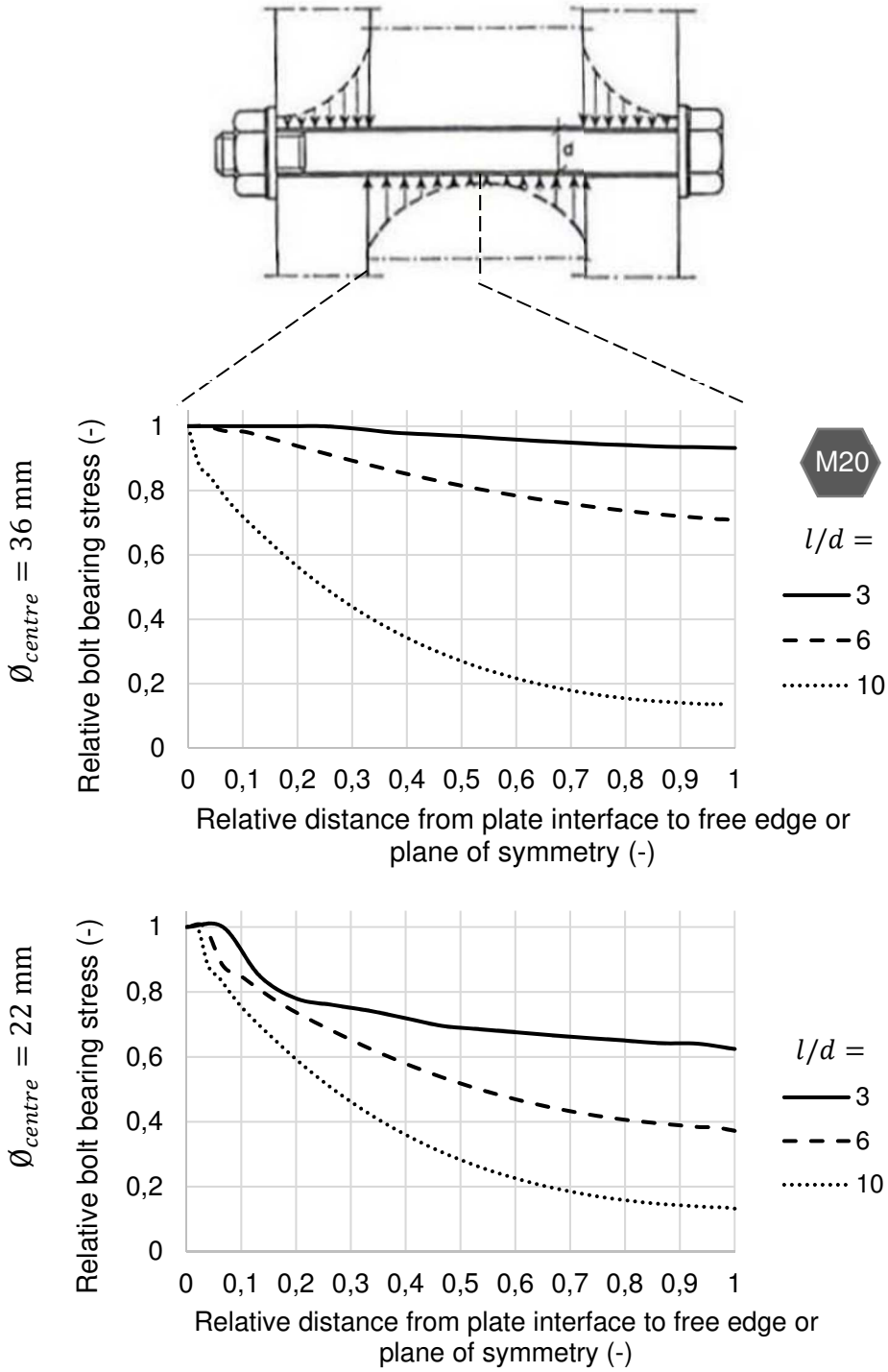

Figure 87 –Middle/Bottom: Distribution of bearing stress along the length of the bolt as a function of *l/d* for $Ø_{centre}$ = 22 and 36 mm. Top: stress distribution as presented in EN 1993-1-8 [3].

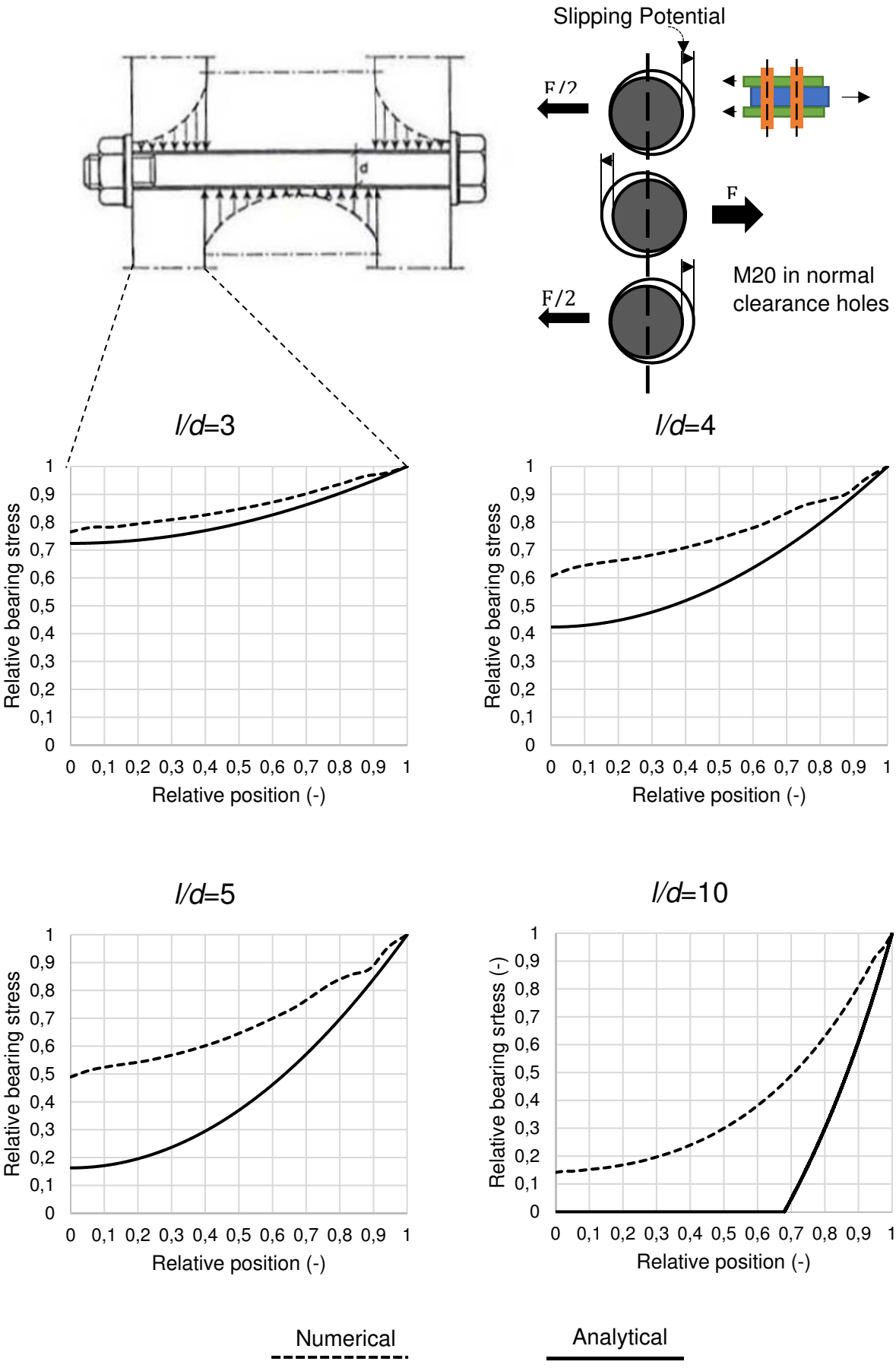

Figure 88 - Relative bearing stress along bolt according to analytical (Koper, 2017) [15] and numerical model for varying *l/d* ratios

5.1.4 Stiffness of Connections with Slotted Holes

In this section, the numerical solution for the initial connection stiffness of double lap shear connections with slotted holes in the centre plates are analysed. It is assumed that the bolts are placed in the most negative location with respect to slip potential (cf. Figure 89). The total slot length is denoted as L, in transverse direction the bolts have a normal nominal clearance of $2\ \mathrm{mm}$ (cf. Figure 24, p. 26). The plate thickness ($2t_2 = t_1 = 20\ \mathrm{mm}$) and the bolt diameter ($d_b = 20\ \mathrm{mm}$) as well as all other geometric parameters are equal to those used in the experimental programme and verified numerical model.

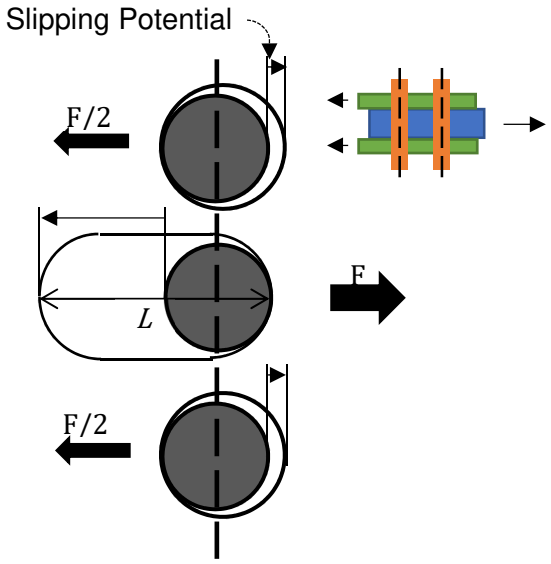

Figure 89 – Eccentric position of the bolt (grey) with respect to the bolt hole (cover plate) and slot (centre plate), causing the highest slipping

Figure 90 illustrates the initial connection stiffness as a function of the slot length L.

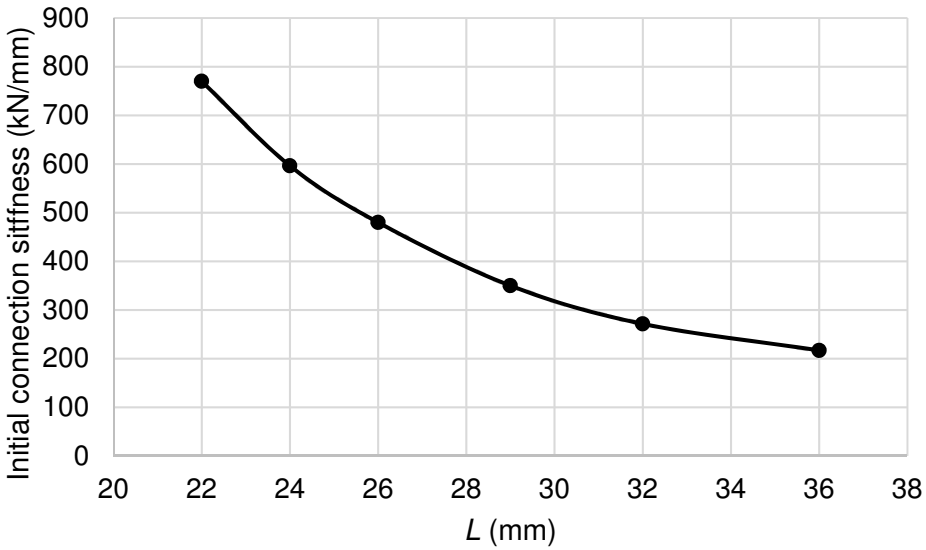

Figure 90 - Initial connection stiffness for double lap shear connection as a function of slot length *L* within the centre plate

5.2 Analytical Framework

In this section, an analytical framework is developed that can be used to assess the initial connection stiffness of injected bolted connections. The framework is meant as an aid for other authors. No specific expressions are given to determine the stiffness of injected connections of arbitrary dimensions. No time-dependent behaviour is included within this framework.

5.2.1 Derivation

The initial connection slip consists of two main components: slip as a result of compression of the injection material, and slip as a result of other factors, such as bolt deformation.

An analytical model that predicts the connection stiffness of a demountable connection can be linked to the amount of injection material that is present in the load bearing direction. This is due to the fact that the injection material has little to no adhesion to the surrounding surfaces, meaning that only forces in compression can be transferred, as is illustrated in Figure 91

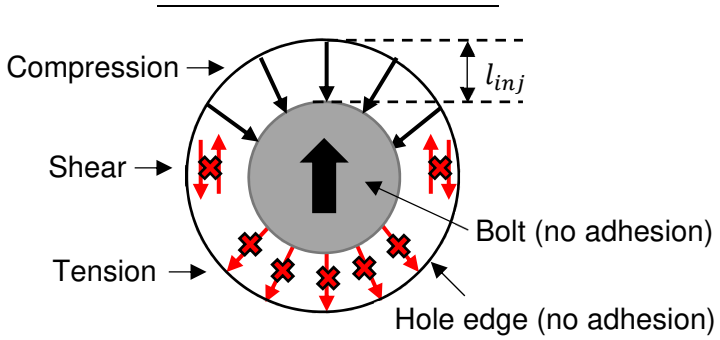

Figure 91 - Release agents prevent adhesion between injection material and surrounding surfaces, only allowing for force transfer in compression

In order to find an analytical expression capable of prediction the connection stiffness, the connection slip at unity load is plotted versus l_{inj} (Figure 91) in the centre plate, as done in Figure 92. The continuous line can be extrapolated to $l_{inj} = 0$. The value of u_{ini} at $l_{inj} = 0$ is then a measure for the slip per unit of force that is due to effects such as bolt bending, and is denoted as C_1. The steepness of the curve, denoted as C_2, is a measure of the effect of the injection layer thickness l_{inj}. The decrease of C_2 for increasing l_{inj} could be incorporated through a yet unknown factor $c_0 = \mathrm{f}\,(d_b, \emptyset_{centre}, x)$, but ignoring this beneficial factor will lead to a somewhat conservative approximation of the initial connection stiffness, as is currently done in this model.

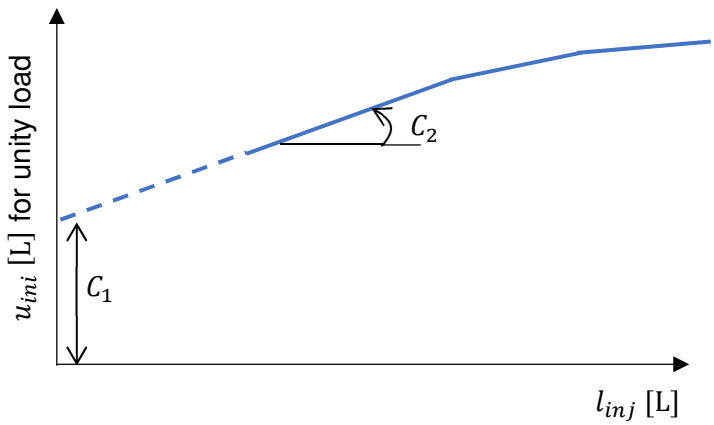

Figure 92 - Schematization of analytical model

The suggested expression is given by Eq. 24 and Eq. 25. It should be noted that in C_1 depends on several factors, e.g. the bolt diameter and length, whereas C_2 is principally a material property (given the same conditions, e.g. confinement).

$$u_{ini,unity} = C_1 + C_2 \cdot l_{inj} \quad \text{Eq. 24}$$

$$k_{ini} = \frac{1}{u_{ini,unity}} = \frac{1}{C_1 + C_2 \cdot l_{inj}} \quad \text{Eq. 25}$$

5.2.2 Validation

Figure 93 shows the diagram suggested in Section 5.2.1 (Figure 92) containing the numerical results for bolt placement cf. the experimental programme and bolt placement in the most negative location regarding connection slip. It is found that $C_1 = 9{,}44 \cdot 10^{-4}$ mm/kN and $C_2 = 1{,}75 \cdot 10^{-4}$ 1/kN. Table 18 lists the difference between the stiffness according to the numerical and analytical model, clearly showing the conservativeness for large hole diameters by ignoring the unknown factor $c_0 = \mathrm{f}\,(d_b, \emptyset_{centre}, x)$.

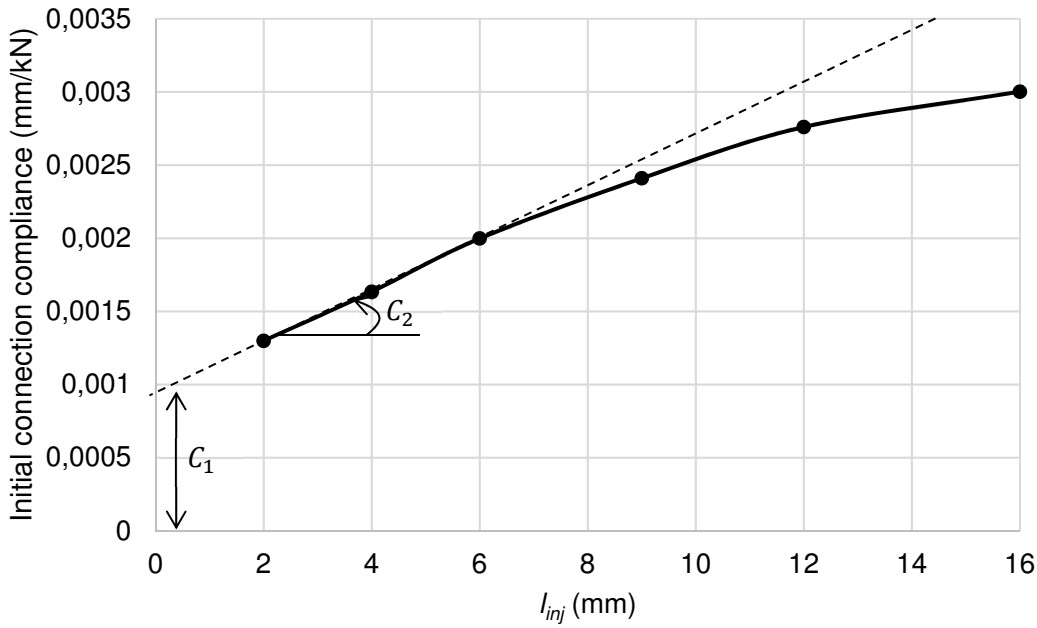

Figure 93 - Validation of analytical model based on numerical results for resin-injected connections positioned at most negative location regarding potential connection slip. Dimensions of connection members as in experimental programme.

Table 18 - Comparison between numerical and analytical model for initial connection stiffness

$\emptyset_{centre}$ (mm)	l_{inj} (mm)	$k_{ini,FEA}$ (kN/mm)	$k_{ini,ana}$ (kN/mm)	Difference
22	2	$7{,}7 \cdot 10^2$	$7{,}7 \cdot 10^2$	+0,4%
24	4	$6{,}1 \cdot 10^2$	$6{,}1 \cdot 10^2$	-0,6%
26	6	$5{,}0 \cdot 10^2$	$5{,}0 \cdot 10^2$	+0,2%
29	9	$4{,}2 \cdot 10^2$	$4{,}0 \cdot 10^2$	-4,3%
32	12	$3{,}6 \cdot 10^2$	$3{,}3 \cdot 10^2$	-9,3%
36	16	$3{,}3 \cdot 10^2$	$2{,}7 \cdot 10^2$	-19,8%

6 Development: Reinforced Resin-Injected Connections

Based on the observations from the experiments carried out on double lap shear connections so far, an attempt is made to create a demountable connection with a higher (initial) stiffness and less creep deformation. For this investigation, the plates used in the earlier experiments have been re-used, and all details regarding the set-up and execution of the experiments are the same as discussed in Chapter 3, unless stated otherwise.

6.1 Concept

To increase the initial connection stiffness and decrease the creep deformation of resin-injected connections with oversize holes, small, strong and stiff particles ('reinforcement') are added to the free volume within the connection prior to injection of the resin takes place. The small particles are in direct contact with each other and fill most of the volume within the connection, as indicated in Figure 94.

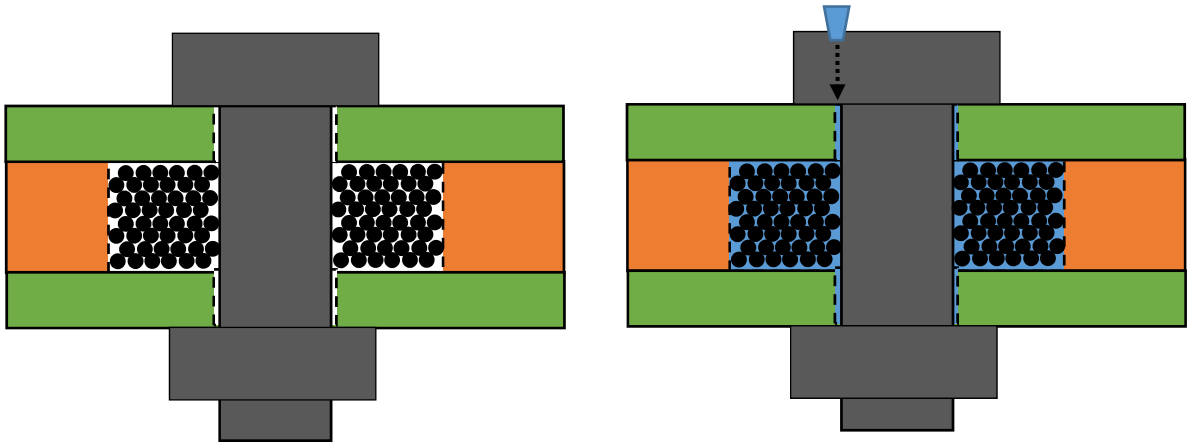

Figure 94 - Concept of reinforced resin-injected connection, left: situation before injection, right: situation after injection (blue)

The small reinforcing particles form a continuous skeleton throughout the free volume within the connection, and hereby form a load bearing path. The resin acts more as a filler and bonding material. Table 19 lists the functions of the particles and resin.

Table 19 - Functions of Particles and Resin within a reinforced resin-injected connection

Function of Particles	Function of Resin
Transfers load through direct particle-to-particle contact	Fills the (residual) free volume
Reduces the required resin volume (economic benefit)	Prevents any sudden free body movement of the particles
	Provides initial stiffness in case particles are not in direct contact with the fastener or hole surface
	Protects particles from degradation due to environmental influences (e.g. corrosion)

The concept of reinforced resin-injected connections is comparable to the concept of Stone Mastic Asphalt (SMA, Figure 95), which is used in pavement engineering. In SMA, the stones are used to create a stiff load path, and are kept in place using a binder (mastic, bitumen). The stiff load-carrying stone-skeleton reduces time-dependent deformation (creep) of the pavement surface, such as rutting.

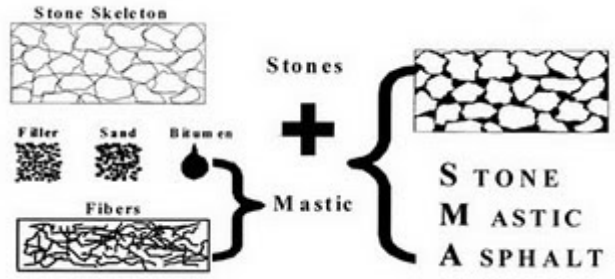

Figure 95 - Stone Mastic Asphalt (SMA) as used in pavement engineering. The load is borne through the stone skeleton, whereas the mastic (binder) keeps the stones together [73]

6.2 Feasibility Study

In order to assess the potential of reinforced resin-injected connections, a similar test on double lap shear connections is carried out as on the non-reinforced resin-injected connections. The resin is the same as the resin used all other experiments (Araldite RenGel SW 404 + HY 2404), but the curing time is reduced from 24 to 6 hours.

The reinforcing particles used are so called steel shot particles, which are frequently used in shot peening, a process to remove residual welding-induced tensile stresses. Also, shot is used as an abrasive in blast cleaning. An alternative to shot is grit: the latter has an irregular shape, whereas the former is spherical. The main reason to choose for spherical particles is their easy workability and short-term deliverability. Shot is available in many different size, ranging from $\text{Ø} = 0{,}3 - 2{,}4$ mm. As a first attempt, shot of size class S330 is used, which has a nominal diameter of 1 mm (Figure 96).

Figure 96 - Steel shot of size class S330 (nominal diameter 1 mm) as used in the experiments

To establish an idea whether or not the suggested connection type has any potential, a test specimen with $\emptyset_{centre} = 32\ \mathrm{mm}$ is prepared. As opposed to all other specimen, the specimen for this test has been assembled in the most negative position for connection slip in the centre plate, as indicated in Figure 97. The bolt is directly bearing to the cover plates. Also, all other geometrical parameters are as discussed as in Section 3.2.3.

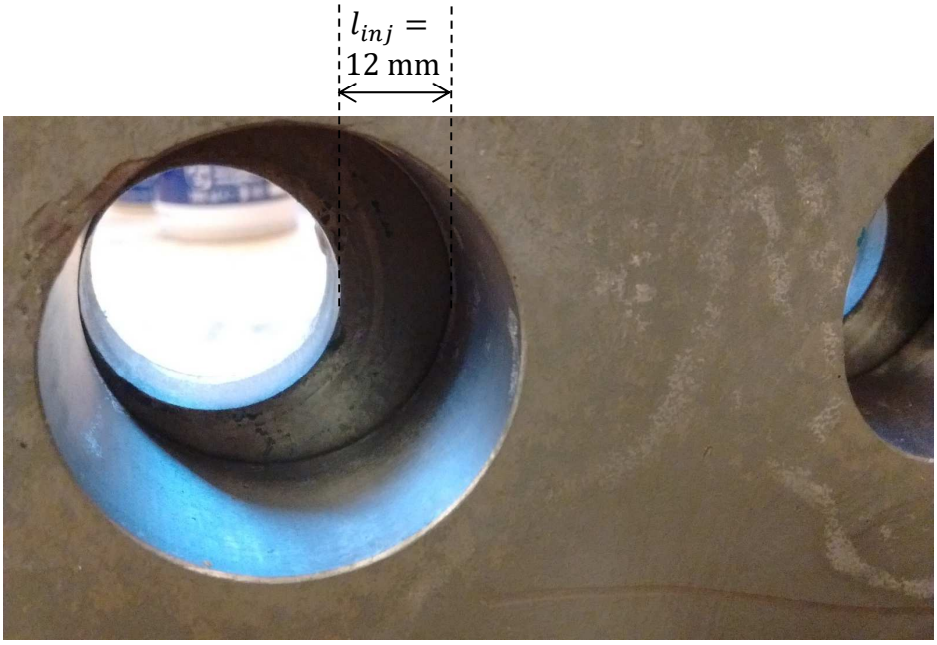

Figure 97 – Connection build-up used in initial test to determine potential for shot-reinforced resin-injected connections

The connection build-up presented in Figure 97 has $l_{inj} = 12\ \mathrm{mm}$, which is $3\ \mathrm{mm}\ (+33\%)$ more than the specimen with $\emptyset_{centre} = 36\ \mathrm{mm}$ as tested in the experimental programme for non-reinforced resin-injected connections with oversize holes. The specimen is loaded to a load level belonging to $0{,}15 - 0{,}20\ \mathrm{mm}$ slip at CBG, and the load is kept constant in order to determine the creep sensitivity of the shot-reinforced resin-injected connection.

6.2.1 Proof of Concept

To see if the suggested concept can be realized in practice, a transparent sample connection is made using Perspex plate elements (for dimensions see Section 3.2.1, Figure 42, p.39). The shot is inserted through the air escape channel in the centre plate. Simultaneously, the shot within the connection is compacted by vibrating the specimen using a hammer and more shot is added until the specimen is completely filled. The result of this step is illustrated in Figure 98.

Figure 98 - Perspex specimen filled with S330-shot

After filling the specimen with shot, the specimen is injected with resin through the hole in the bolt head. Although the voids in between the shot particles is relatively small, no additional effort for the injection process is necessary and all voids are filled with resin. Figure 99 illustrates the completed shot-reinforced resin-injected specimen.

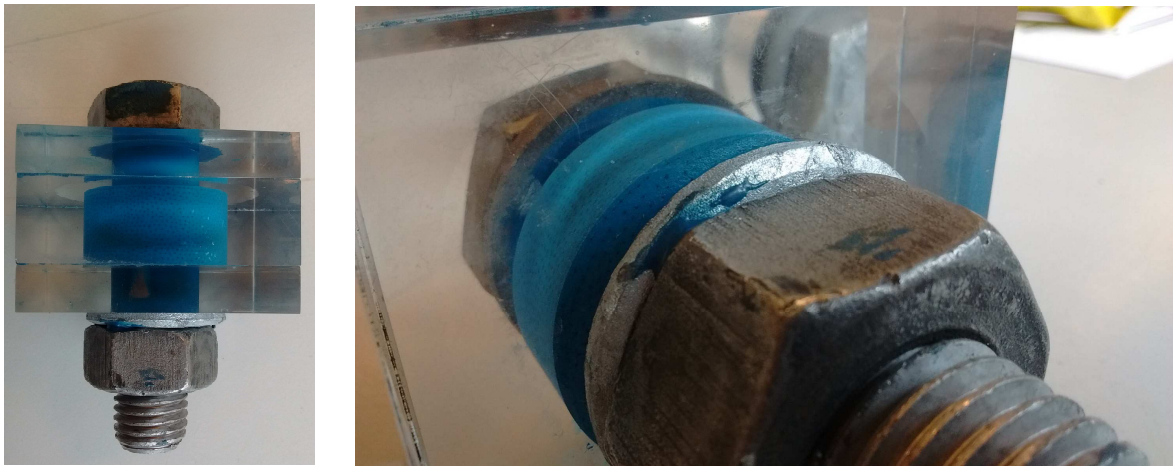

Figure 99 - Completed shot-reinforced resin-injected specimen

6.2.2 Results & Discussion

Results

The test results from the shot-reinforced resin-injected connection with geometry as discussed in Section 3.2 and 6.2 are presented in Figure 100 and Figure 101. Figure 100 illustrates the load-displacement diagram obtained during loading the specimen to a load belonging to an initial average slip at CBG of 0,19 mm (159 kN), whereas Figure 101 shows the subsequent creep behaviour. It should be noted that two of the eight LVDTs used to determine the slip at (the lower) CBG produced strange, inexplicable results, and are thus not considered in the diagrams.

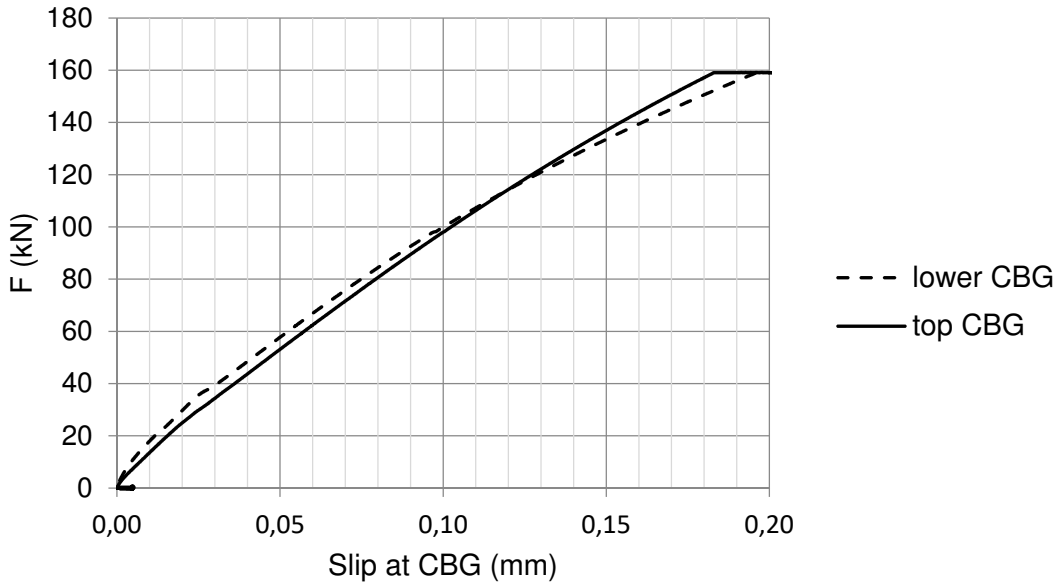

Figure 100 - Load-displacement diagram of shot-reinforced resin-injected connection with $Ø_{centre}$ = 32 mm and bolts positioned at most negative position in centre plate hole.

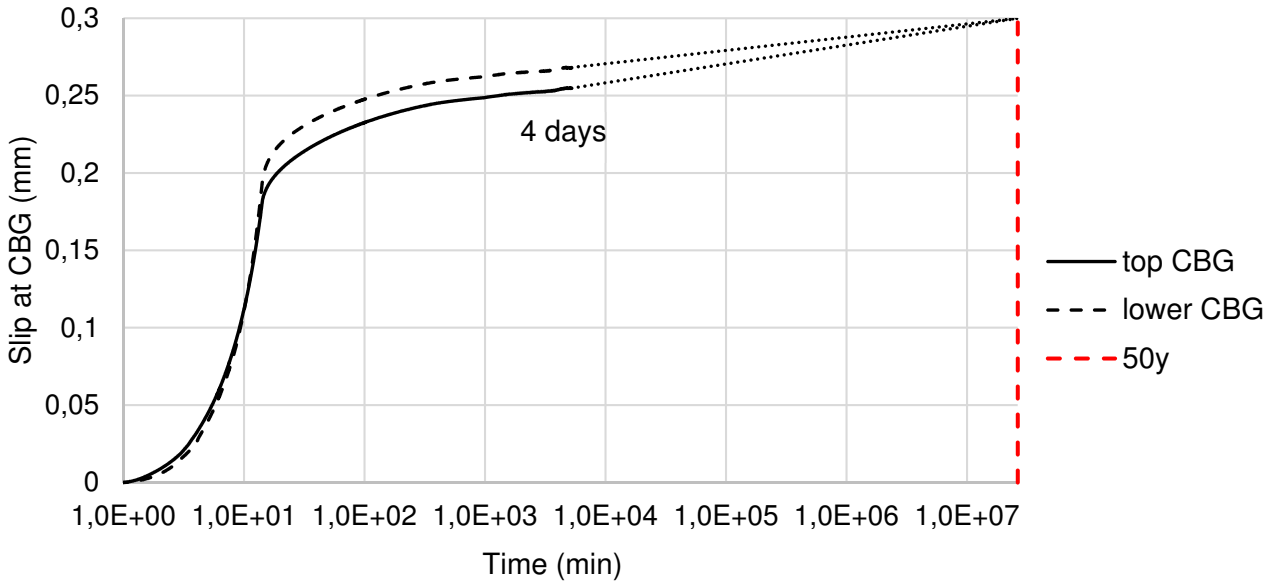

Figure 101 - Connection slip at CBG vs. time, indicating the creep deformation of shot-reinforced resin-injected specimen used in feasibility test

The initial connection stiffness (defined between $0{,}05$ and $0{,}15\ \mathrm{mm}$ connection slip) is $k_{ini} = 8{,}0 \cdot 10^2\ \mathrm{kN/mm}$, with a spread of $\pm 5\%$. The average spread in the creep-phase is 3%.

Figure 102 illustrates a cross sectional view of the shot-reinforced resin after removal from the specimen. Not only the oversize hole in the centre plate was filled with shot, but also the small volume between the bolt and hole in the cover plate was saturated.

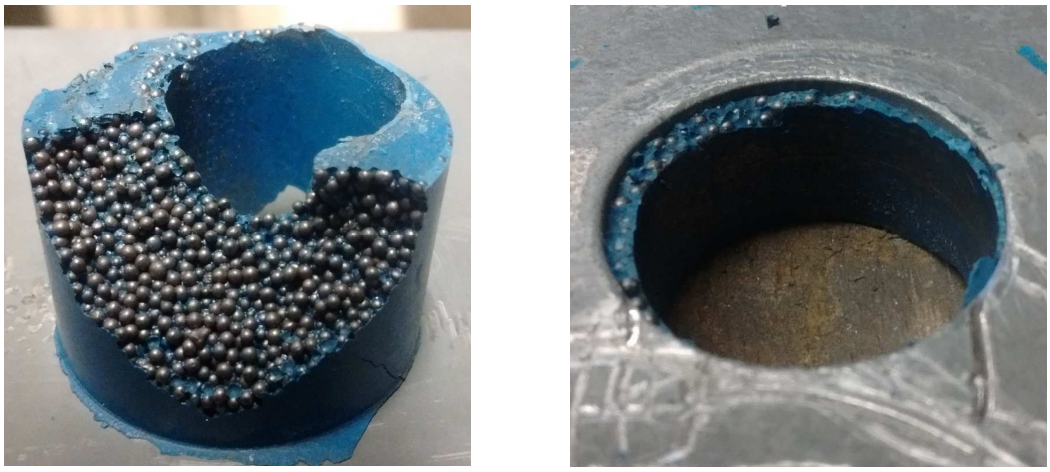

Figure 102 - Shot-reinforced resin after dismantling of the specimen, left: cross sectional view of infill from centre plate, right: infill within cover plate

Discussion

The experimental initial connection stiffness k_{ini} for the shot-reinforced resin-injected connection is double ($\approx 200\%$) that of the numerically obtained initial connection stiffness for the non-reinforced connection. The load level during the creep test was $159\ \mathrm{kN}$, which leads to a nominal bearing stress of $\sigma_b = 199\ \mathrm{MPa}$. The slip after 50 years is not expected to be larger than $0{,}30\ \mathrm{mm}$, given that the tangent of the slip curve is smaller than that is needed to reach the coordinate $[50\ \mathrm{y}, 0{,}30\ \mathrm{mm}]$. This conclusion could already be drawn after roughly 10^3 minutes ($17\ \mathrm{h}$), but the experiment was continued for several days to see the development of creep deformation in time.

The use of shot-reinforced resin-injected connections with oversize holes seems promising. In the case of the shot-reinforced connection, a nominal bearing stress $\sigma_b = 199\ \mathrm{MPa}$ is rather high compared to the bearing stress of non-injected connections ($\sigma_b = 94\ \mathrm{MPa}$ for non-reinforced connection with $Ø_{centre} = 36\ \mathrm{mm}$). Moreover, the results of the shot-reinforced connection were obtained using $l_{inj} = 12\ \mathrm{mm}$, whereas this was maximally $l_{inj} = 9\ \mathrm{mm}$ for the non-reinforced connection (for $Ø_{centre} = 36\ \mathrm{mm}$).

Although the amount of connections tested is limited ($\mathrm{n} = 2$), it seems that shot-reinforced resin-injected connections have the potential to reduce creep and increase connection stiffness compared to non-reinforced resin-injected connections. Thus, it is decided to continue with this concept.

6.3 Short-term Behaviour under Repeated Loading

In order to investigate the behaviour of resin-injected connections under repeated short-term loading, a small number of experiments is carried out. One specimen was reinforced using shot and then injected with resin, whereas another specimen was merely injected. Moreover, a specimen with shot was prepared that was not injected. All specimen have $Ø_{centre} = 36\ \mathrm{mm}$ and are built-up as discussed in Section 3.2.3.

The specimen are first loaded up to a load level corresponding to $0{,}10\ \mathrm{mm}$ of average connection slip (at $0{,}01\ \mathrm{mm/s}$ of jack displacement). Hereafter, the load is quickly removed ($-5\ \mathrm{kN/s}$) and the connection is again loaded to $0{,}10\ \mathrm{mm}$ of connection slip. This is repeated for a total of 5 times. Then, the connection slip is increased to $0{,}15\ \mathrm{mm}$ and the same procedure is followed. The same is done for a connection slip of $0{,}25$ and $0{,}40\ \mathrm{mm}$. The test procedure is schematized in Figure 103.

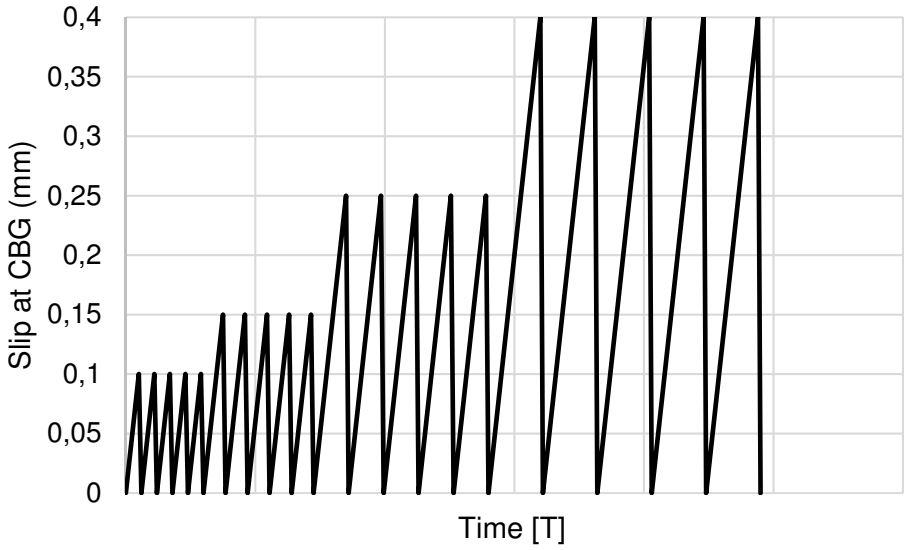

Figure 103 - Schematization of test procedure to determine short-term behaviour under repeated loading

Figure 104 illustrates the load-slip diagram obtained for the reinforced resin-injected specimen, whereas the force belonging a certain slip level is plotted in Figure 105 as a function of the amount of load iterations. The same diagrams are plotted in Figure 106 and Figure 107, respectively, for non-reinforced resin-injected connections.

A clear hysteresis is present in both load-slip diagrams, however the hysteresis loops are rather narrow, especially after a number of slip repetitions. Also, in both cases, every first application of a certain slip level leads to a permanent deformation. All other iterations of that same slip level also lead to incremental permanent deformation, but to a lesser extent. The force belonging to a certain slip level decreases for increasing amount of iterations, and this decrease is more pronounced for larger slip levels. After a few iterations, the load level that can be reached at a certain slip level stabilizes. The relative decrease in load capacity at a slip level is largest for shot-reinforced connections, although it should be noted that in this case the force is more than twice as high as for non-reinforced connections.

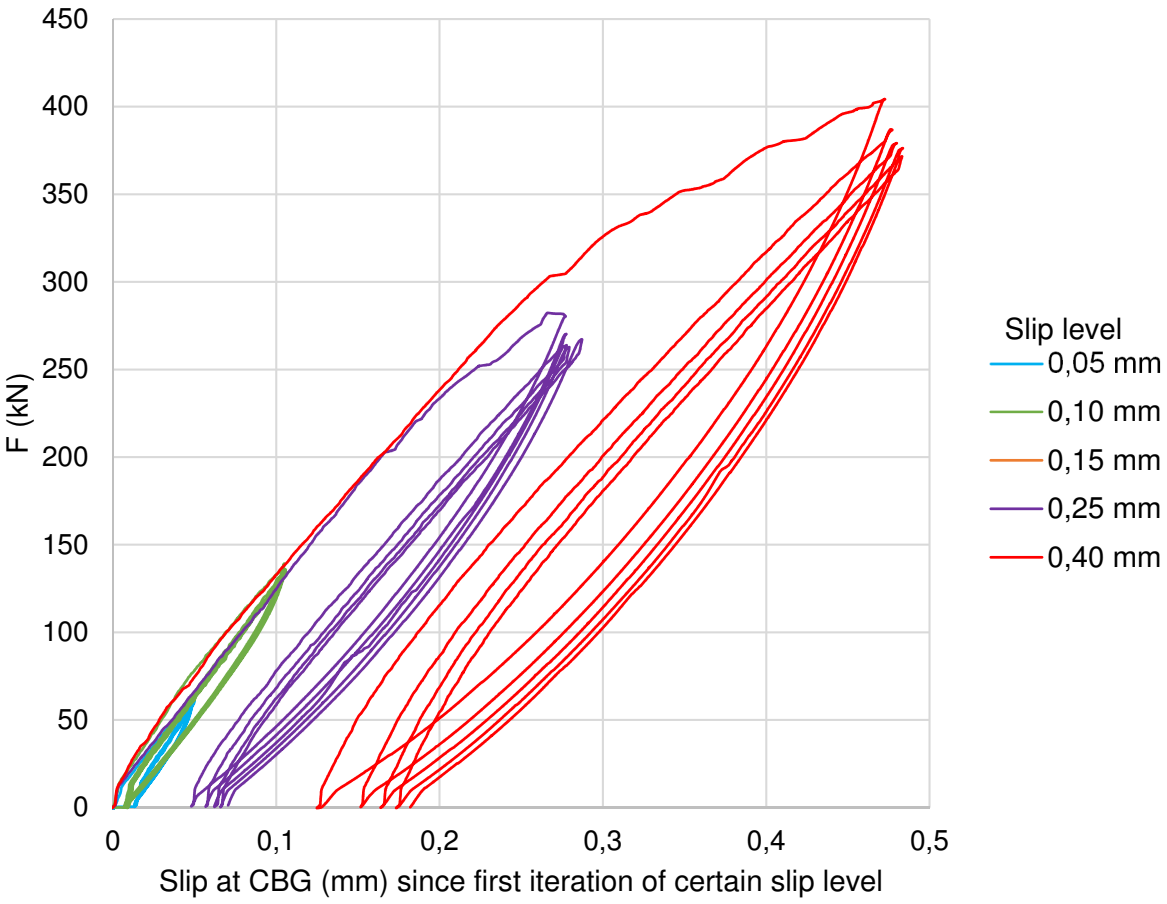

Figure 104 - Load-displacement diagram showing several loading and unloading cycles for a shot-reinforced resin-injected specimen ($Ø_{centre}$ = 36 mm) (averaged)

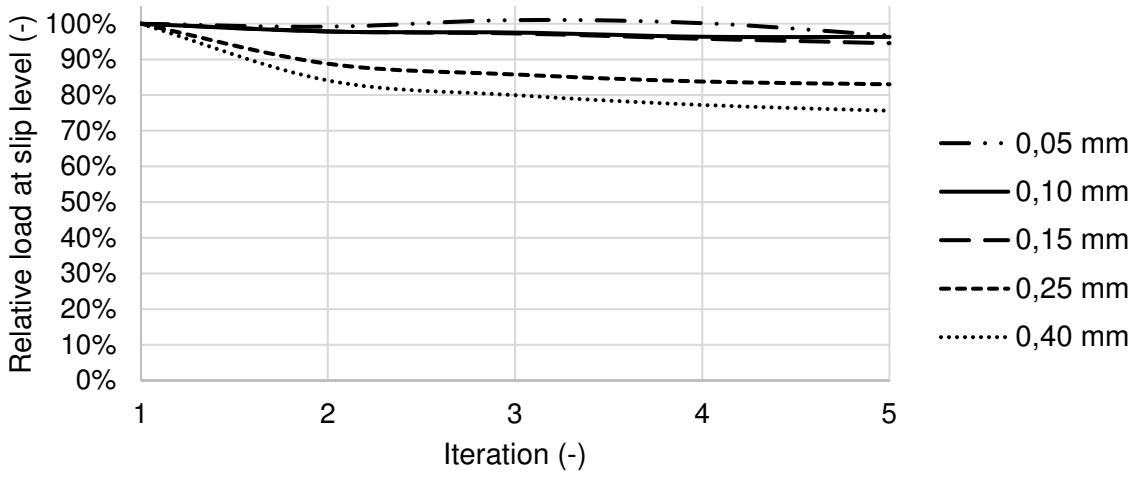

Figure 105 - Stabilization of load capacity at a given slip level after a number of iterations for shot-reinforced resin-injected specimen (averaged)

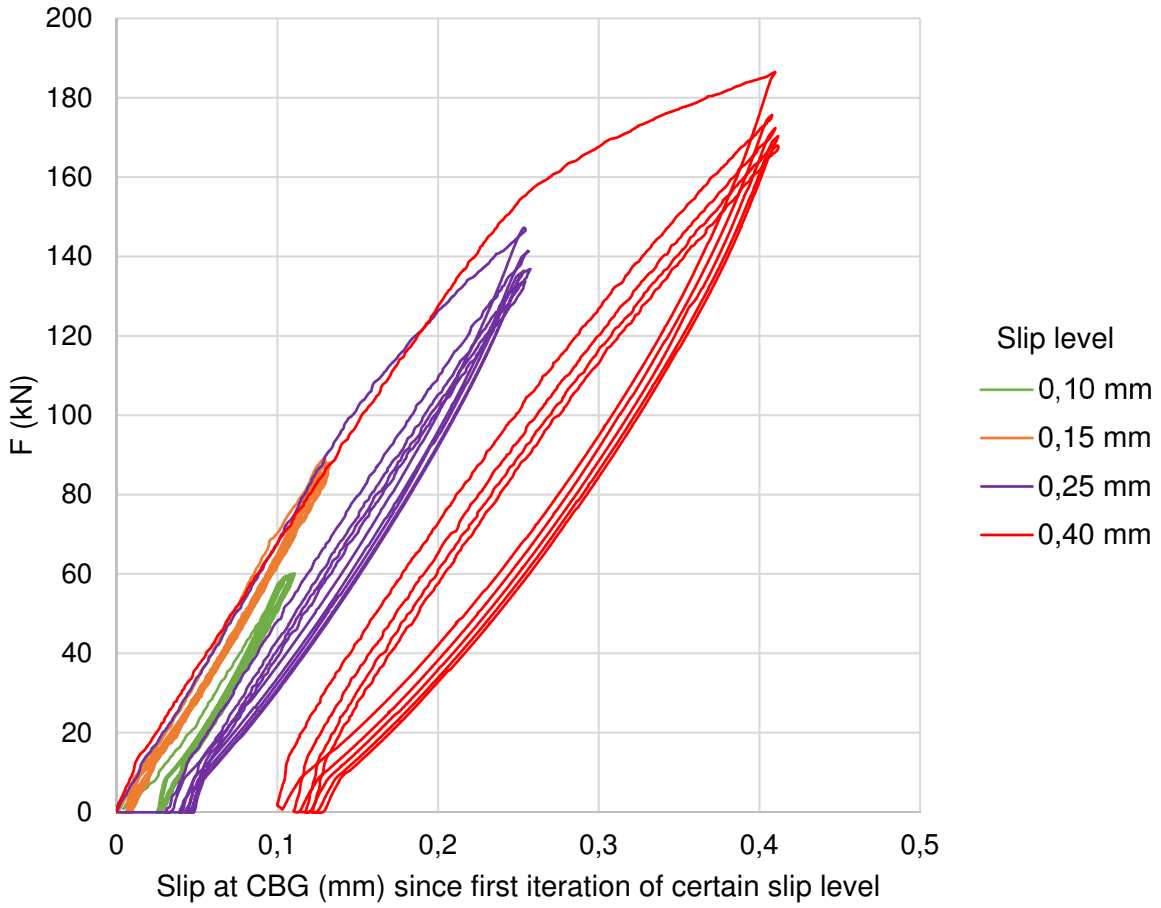

Figure 106 - Load-displacement diagram showing several loading and unloading cycles for a non-reinforced resin-injected specimen ($Ø_{centre}$ = 36 mm) (averaged)

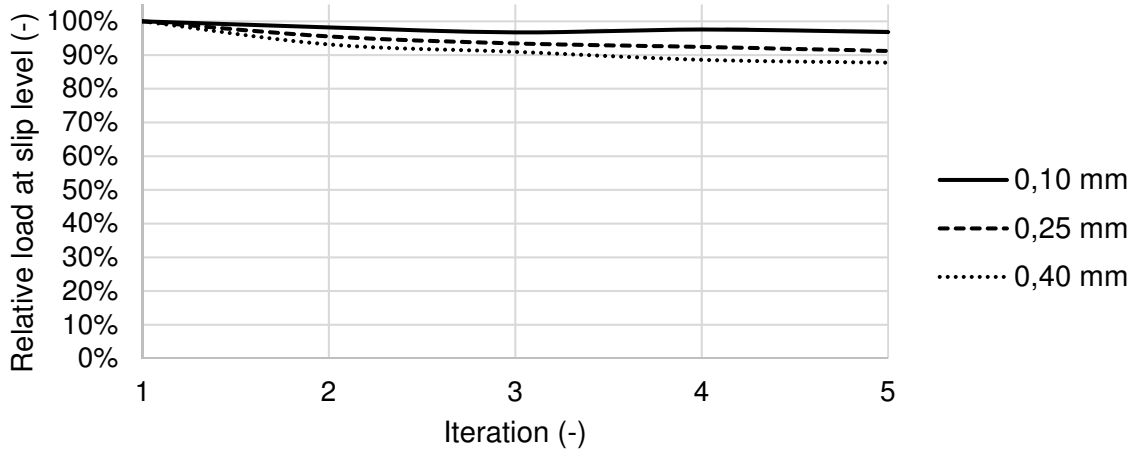

Figure 107 - Stabilization of load capacity at a given slip level after a number of iterations for non-reinforced resin-injected specimen (averaged)

Figure 108 illustrates the force-displacement diagram for a connection filled with shot, which has not been injected. Figure 108 clearly illustrates that without the resin, the connection stiffness is rather low and increases for increasing slip. It was not possible to repeat the slip pattern suggested in Figure 103, since there was nearly no slip recovery upon unloading. The hardness of the shot is so large compared to that of the steel member, that indentation was clearly visible, as exemplified through Figure 109.

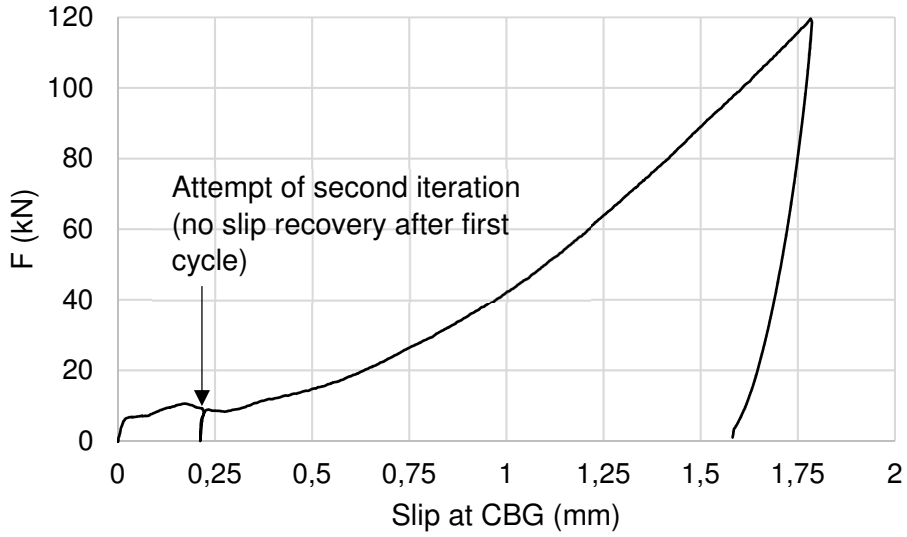

Figure 108 - Relationship between force and slip for a connection filled with only shot (averaged)

Figure 109 - Indentation of shot in bolt (top) and plate surface (bottom)

6.4 Long-term Behaviour

In this section it is attempted to determine the long-term (creep) behaviour of shot-reinforced resin-injected connections. In order to see the difference in initial and time-dependent behaviour, a shot-reinforced resin-injected specimen with $Ø_{centre} = 36\ \mathrm{mm}$ is prepared under the same conditions (i.e. position of the bolt with respect to the holes) as done for the non-reinforced resin-injected specimen (also $Ø_{centre} = 36\ \mathrm{mm}$).

The shot-reinforced specimen is loaded using a force-controlled regime $(0{,}2\ \mathrm{kN/s})$ until an average CBG slip of $u_{CBG} = 0{,}135\ \mathrm{mm}$ (90% of the short-term strength based on an $0{,}15\ \mathrm{mm}$ slip criterion). At the moment the average slip of $0{,}135\ \mathrm{mm}$ at CBG is reached, the force is kept constant in time.

Figure 110 and Figure 111 illustrate the results of the shot-reinforced resin-injected specimen. Figure 110 focuses on the short-term behaviour, whereas Figure 111 gives insight in the creep behaviour of both specimen types. A summary of the results is given in Table 23.

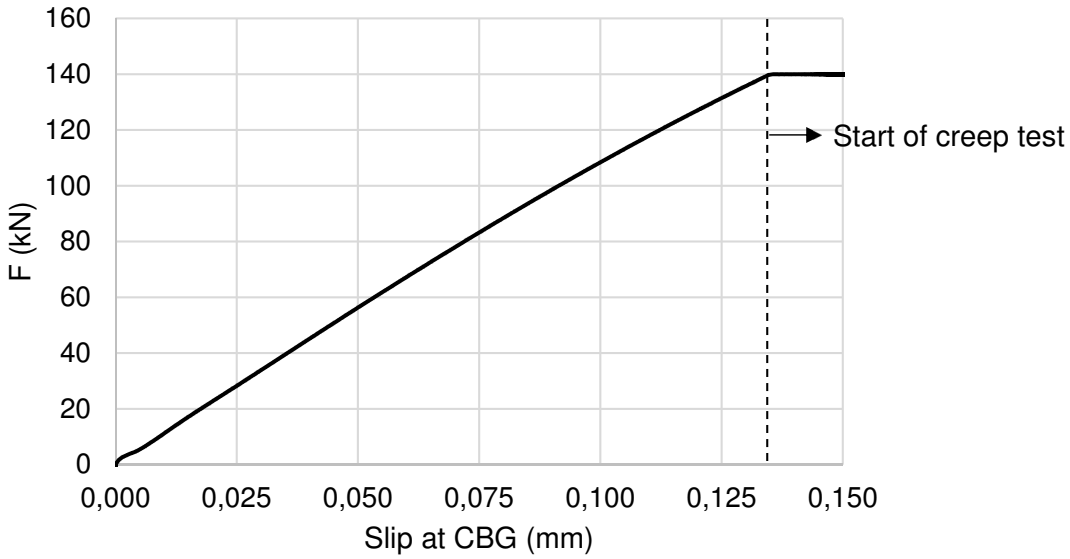

Figure 110 - Force-slip diagram for non-reinforced and shot-reinforced specimen with $Ø_{centre}$ = 36 mm (averaged)

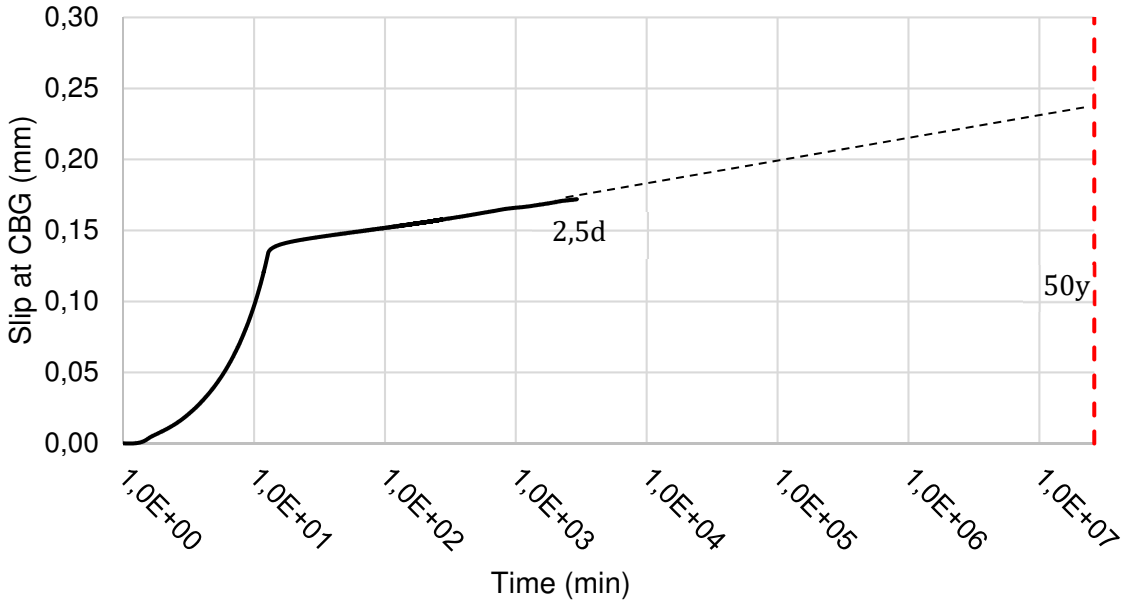

Figure 111 – Slip-time diagram for shot-reinforced specimen with Øcentre = 36 mm (averaged)

After execution of all other tests within the experimental programme, another shot-reinforced resin-injected specimen with $Ø_{centre} = 36\ \mathrm{mm}$ was prepared in order to determine the creep behaviour over multiple weeks. This specimen was (also) loaded up to $140\ \mathrm{kN}$. The results are shown in Figure 112, and clearly indicate that the slip line can be linearly extrapolated on the slip-log(time) axes. A straight line in the slip-log(time) diagram means that the slip as a result of creep can be presented in the form proposed in Eq. 26.

$$u_{CBG} = c_1 \cdot \log(t) + c_2 \qquad \text{Eq. 26}$$

With:

t	Time [T]
c_1, c_2	Constants depending on connection detailing and load level

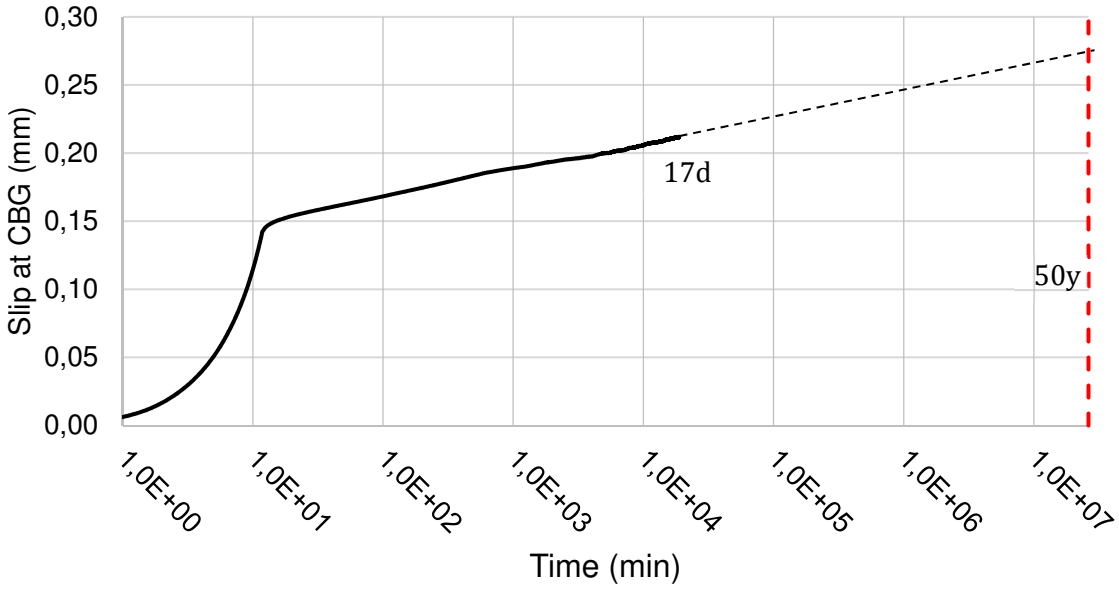

Figure 112 - Slip-time diagram for shot-reinforced specimen with Øcentre = 36 mm (averaged), over multiple weeks (17 days)

6.5 Potential Conceptual Improvements

6.5.1 Increasing Packing Density

An increase in packing density theoretically leads to a higher (connection) stiffness, given that there is less 'soft' resin within the confined volume of the connection and that initial movement of particles is further prevented. So far, in this chapter only resin-injected connections have been discussed that were reinforced using a single diameter of shot. In 1611, Johannes Kepler conjectured that the theoretical maximum packing density of equally sized spheres is 74% (Eq. 27), which is not rejected until present day. Figure 113 illustrates cubic and hexagonal close packing of spheres, which both lead to the maximum packing density suggested by Kepler, as discovered by Gauss (1831) [53]. However, it must be noted that in practice an average packing density of 64% is observed if the spheres are positioned randomly (Scott & Kilgour, 1969) [54].

$$\eta_{Kepler} = \frac{\pi}{3\sqrt{2}} \approx 74{,}048\% \qquad \text{Eq. 27}$$

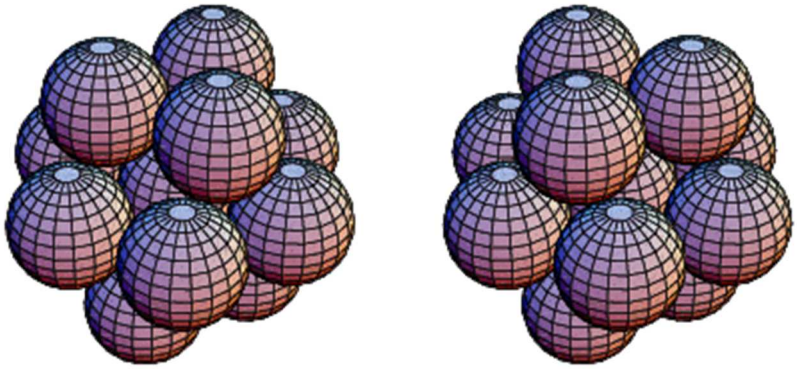

Figure 113 - Cubic (left) and Hexagonal Close Packing of spheres. Both have a maximum packing density of 74% [74]

In order to increase the packing density, smaller spheres can be used to fill the voids (26%-36% in volume) in between the larger spheres. However, the radius of the smaller sphere may not be larger than 41% of the larger sphere diameter. If this limit is exceeded, the smaller spheres do not fit in within the close-packed structure of larger spheres, hereby reducing the overall packing density. Theoretically it is possible to have denser packing when the 41%-limit is exceeded, but this requires a transition to a different stacking of spheres (Marshall & Hudson, 2010) [55]. Although adding spheres of smaller diameter(s) may increase the packing density, it is not possible to exceed a packing density of $93{,}25\%$ (Reis et al., 2012) [56].

6.5.2 Irregularly Shaped Reinforcing Material

Spheres have the characteristic of mobility, i.e. they are easily moved throughout a volume, if not fully dense-packed. Since the optimal fully-dense packing is hard to obtain and control in practice, an option is to use irregularly shaped filler material (Figure 114). Due to their irregular shape, such particles interlock, hereby allowing for less slip as a result of rigid body movement of particles compared to for instance spherical particles.

Figure 114- Particles with different geometrical characteristics. Left: shot (spherical), right: grit (irregularly shaped) (Shanghai Bosun Abrasive Co., Ltd.)

The benefits of using irregularly shaped particles (grit) on the slip as a result of peak stresses and accompanying deformation in particle-to-particle contact are hard to quantify, given that Hertzian contact theory is not applicable to non-spherical particles. If irregularly shaped particles are used as reinforcing material, care should be taken to ensure proper insertion of such particles, especially given their low mobility compared to their spherical counterparts.

6.5.3 Insertion of Reinforcement into Connection

Within the experiments conducted at the Stevin Laboratory, the shot-reinforcement was inserted into the free volume within the connection by the use of a funnel and gravity, as indicated in Figure 115. However, this procedure is not very practical in case the reinforcement must be inserted horizontally or even vertically (upward). A potential solution to such situations can be to insert the reinforcement using pneumatics, as indicated in Figure 115. However care should be taken to not use a too high nozzle velocity given the (potential) abrasive characteristics of the reinforcing material.

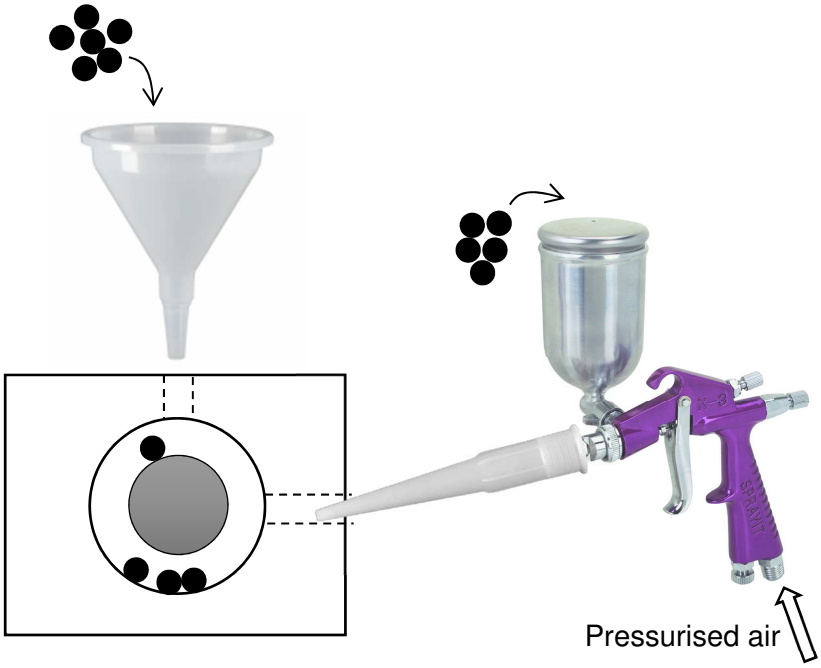

Figure 115 - Insertion of reinforcement as in in the experiments (left) and potential solution for practice (right)

7 Discussion

7.1 Injectability of Injection Materials

Nearly all demounted connections injected with resin show a proper filling of the free volume between the bolt and plate package. Thus, injecting larger volumes of resin than required for a normal clearance hole does not lead to any issues. Whether grout can be successfully injected depends on the position of the washer with respect to the injection bolt, which leaves room for improvements on the washer design, as is for instance done by Qureshi & Mottram (2012) [16]. Investigation has indicated that it is important to allow for the air within the free volume to escape, in order to prevent large air inclusions. As a general rule, it can be stated that there must be an air escape path/channel at each highest point bounded by horizontal restraints, as illustrated in Figure 116. Moreover, for vertical injection (i.e. from above) an additional air escape path must be present apart from the injection channel.

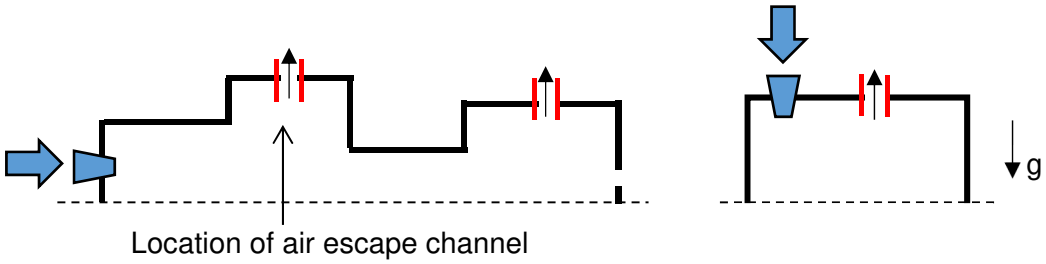

Figure 116 - Air escape channels positioned such to prevent air inclusions within the volume that is injected. Left: horizontal injection, right: vertical injection

The diameter of the air escape channel can be chosen arbitrarily, however it should be noted that the diameter of the air escape channel has an influence on the resistance/capacity of the net cross section. If any reinforcing materials (e.g. shot) shall be inserted into the connection, the minimum diameter of the air escape channel must allow for proper insertion of such materials and any device (e.g. a pin) used for its compaction.

7.2 Suitability of Grout as an Injection Material

As discussed in Section 7.1, the injectability of grout depends on the position of the washer with respect to the bolt. Assuming that injection is done successfully using the current procedure, grout can deliver the same magnitude of initial connection stiffness as non-reinforced resin. However, the nominal Young's Modulus of grout is 3x higher than that of resin, which is not resembled through the results, most likely due to air inclusions within the grout-injected connection. Such air inclusions are present to a smaller extent in plain specimen that were obtained by pouring rather than injection. It is commonly known that super plasticising agents used to increase the workability of cementitious materials can produce small air inclusions. Based on the above, it is suggested that the followed injection procedure is not ideal for grout-like materials, given the higher degree of air inclusions. If air inclusions are averted, the material and thus connection stiffness can increase.

Besides what was investigated in this thesis, also aspects such as long-term (creep) behaviour, fatigue strength and the effects of load reversal must be examined before a final conclusion can be made on the suitability of grout as an injection material.

7.3 Choice of Shape for Bolt Hole

In order to achieve a connection that allows for easy on-site assembly, either slotted or oversize round holes can be used rather than conventional (round) normal clearance holes. In Sections 5.1.2 and 5.1.4 similar connections with both types of holes have been modelled numerically. The results of both models are combined in Figure 117.

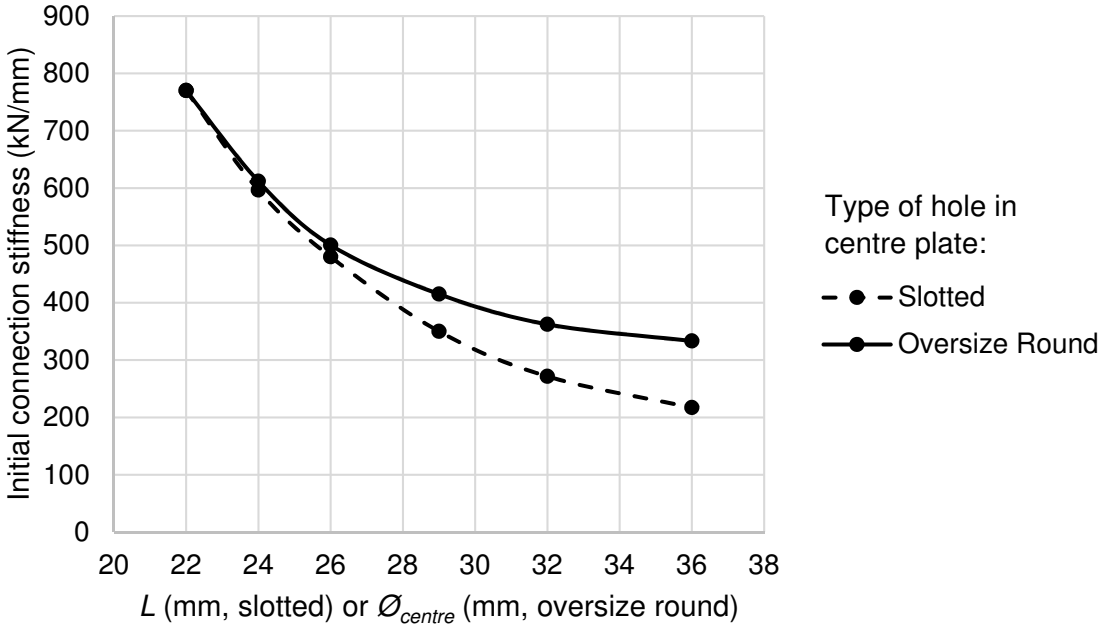

Figure 117 - Comparison between initial connection stiffness for double lap shear connections with slotted and oversize round holes in the centre plate. Bolt (M20) located in most negative position with respect to connection slip.

The results presented in Figure 117 indicate that connections with oversize round holes always lead to a higher initial connection stiffness than connections with slotted holes, and that this effect increases for increasing longitudinal clearance. A potential cause for this effect can be related to load spreading in lateral direction. Based on the numerical models, it is recommended to use oversize round holes (if possible) rather than slotted holes for the following reasons:

- Higher or equal initial connection stiffness.
- Lower or equal average bearing stress, thus hypothetically less creep deformation.
- More favourable executional tolerances in lateral direction for the same longitudinal clearance (see Figure 118).

However, it should be noted that currently EN 1993-1-8 allows higher bearing stresses for slotted holes than for oversize holes. Since the numerical models contradict this prescription, it is suggested to carry out experiments to compare the results of slotted and oversize holes conclusively. In case of reinforced resin-injected connections, a benefit of slotted holes may be observed if the width of the reinforcing material is larger than the lateral holt clearance. In this case, the reinforcing material partially prevents movement of matter past the bolt.

In Section 5.2, the unknown factor $c_0 = \mathrm{f}\,(d_b, Ø_{centre}, x)$ was introduced. Based on the results presented in Figure 117, an estimation for $c_0 = \mathrm{f}\,(20, Ø_{centre}, x = \text{most neg.})$ can be made, as presented in Figure 119. Eq. 28. lists an equation for $c_0 = \mathrm{f}\,(20, Ø_{centre}, x = \text{most neg.})$, which is introduced in Eq. 25 as a multiplier (reduction factor) of C_2. It can be hypothesized that for all other bolt dimensions the expression for c_0 is also bi-linear.

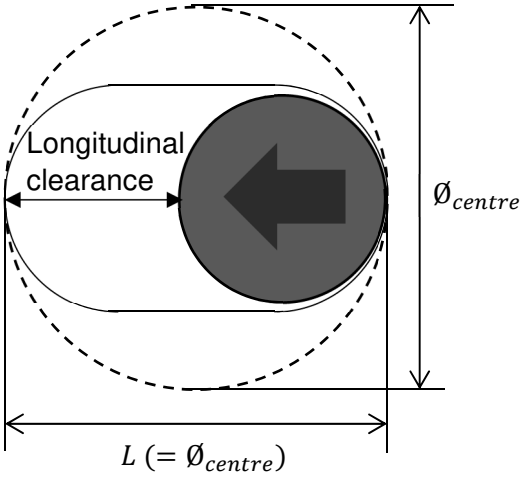

Figure 118 - Slotted and oversize round hole with same longitudinal clearance.

$$c_0 = \mathrm{f}\,(20, Ø_{centre}, x = \text{most neg.}) = \begin{cases} 1, & Ø_{centre} \leq 26\ \text{mm} \\ 1 + 0{,}054 \cdot (Ø_{centre} - 26), & Ø_{centre} \geq 26\ \text{mm} \end{cases} \quad \text{Eq. 28}$$

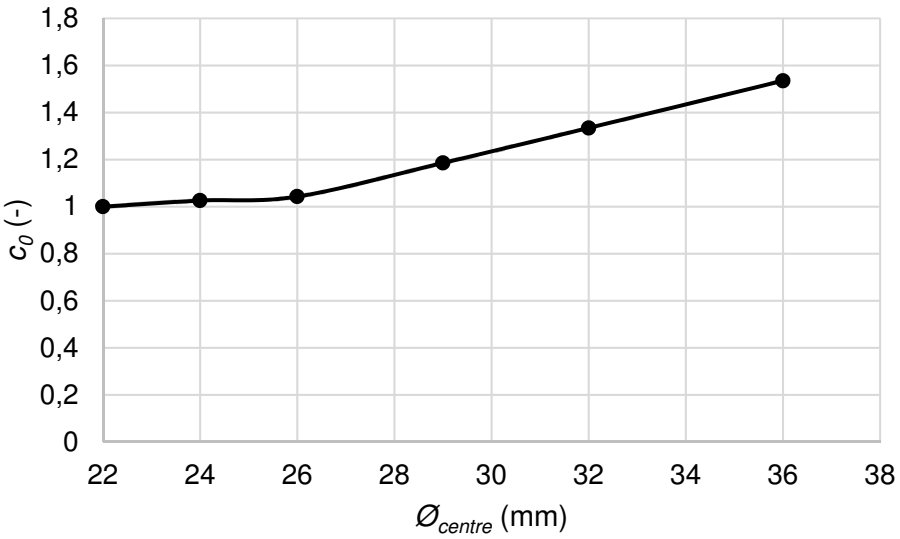

Figure 119 - C_0 as a function of oversize hole in centre plate for an M20 bolt, assuming most negative bolt placement (determined numerically)

7.4 Influence of Release Agent on Connection Stiffness

Figure 120 illustrates the relationship between applied load and connection slip at CBG for resin-injected connections that have and have not been treated with release agent. Both connections have a hole diameter of $22\ \mathrm{mm}$ in all plates in which an $\mathrm{M20}$ bolt is positioned at the most negative location with respect to potential connection slip (i.e. cf. Figure 32, p.32). However, the specimen treated with release agent was compressed using $30\ \mathrm{Nm}$ of torque on the bolt, whereas this was $100\ \mathrm{Nm}$ for the non-treated specimen. The reason for this difference in the amount of torque lays in the fact that the result of the non-treated specimen originates from another author at TU Delft (Koper, 2017) [15], who used rougher plates. Due to the increased friction present in this non-treated specimen, the initial of behaviour of the connection is stiffened

The average initial connection stiffness of the wax-treated connection is $8{,}2 \cdot 10^2\ \mathrm{kN/mm}$, whereas this is $8{,}9 \cdot 10^2\ \mathrm{kN/mm}$ for the non-treated specimen torqued to $30\ \mathrm{Nm}$. This is a difference of 8%, which cannot be said to be significant, given the small amount of specimen. Therefore, it is suggested that the influence of the wax layer is marginal.

The above implies that in connections with and without release agent, only force transfer by compression can take place. Although connections without release agent have a bond between the injection material and steel (bolt, plates), this bond is not strong enough to be utilized to transfer forces in tension. Moreover, there is no indication that the release agent is pushed aside or otherwise deformed (i.e. as suggested in Section 2.6 , Figure 22). Thus, for short-term loading, the presence of release agent does not influence the connection stiffness significantly. For the long-term behaviour, the influence of the release agent was not explicitly determined.

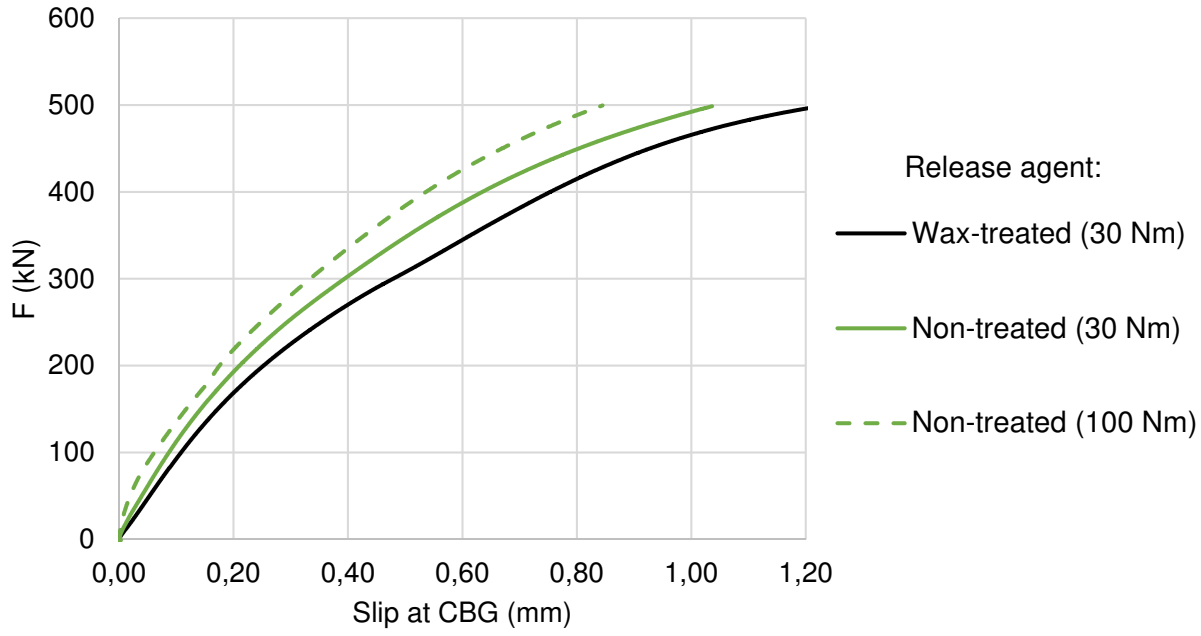

Figure 120 - Relationship between external load and connection slip measured at CBG for specimen treated with and without release agent (wax spray) (averaged) [15]

7.5 Short-term Loading of Injected Bolted Connections

The load at which $0{,}15\ \mathrm{mm}$ slip at CBG occurs decreases with an increase in the oversizing of the hole. This can be proven experimentally and theoretically. Doubling the hole clearance in an injected bolted connection does not reduce the stiffness by 50%, given that there are also deformation mechanisms (e.g. bolt deformation) that are not related to the oversizing of the hole. Also, the beneficial effect of load spreading may be observed for holes that have a diameter that is significantly (say $10\ \mathrm{mm}$) larger than the bolt diameter.

The confinement of the injection material leads to a multiaxial stress state. As a result, the apparent stiffness in longitudinal direction is higher than when there would be no confinement. The same holds for the apparent Young's Modulus in longitudinal direction. Assuming linear material behaviour, the stresses and strains in all three dimensions are described by Eq. 29-Eq. 31. Assuming full confinement by the (significantly stiffer) steel member, the strains in the injection material in both lateral directions are zero, hence $\varepsilon_{yy} = 0$ and $\varepsilon_{zz} = 0$. Inserting these conditions in Eq. 30 and Eq. 31 yields the expressions of Eq. 32 and Eq. 33. Using the principle of substitution, an expression for the apparent Young's Modulus in longitudinal direction can be derived, as presented in Eq. 34 and illustrated in Figure 121.

$$\varepsilon_{xx} = \frac{1}{E}\left(\sigma_{xx} - \upsilon\sigma_{yy} - \upsilon\sigma_{zz}\right) \quad \text{Eq. 29}$$

$$\varepsilon_{yy} = \frac{1}{E}\left(\sigma_{yy} - \upsilon\sigma_{xx} - \upsilon\sigma_{zz}\right) (= 0) \quad \text{Eq. 30}$$

$$\varepsilon_{zz} = \frac{1}{E}\left(\sigma_{zz} - \upsilon\sigma_{yy} - \upsilon\sigma_{xx}\right) (= 0) \quad \text{Eq. 31}$$

$$\sigma_{yy} = \upsilon\sigma_{xx} + \upsilon\sigma_{zz} \quad \text{Eq. 32}$$

$$\sigma_{zz} = \upsilon\sigma_{xx} + \upsilon\sigma_{yy} \quad \text{Eq. 33}$$

$$E_{app,x} = E \cdot \left[\frac{1-\upsilon}{1-\upsilon-2\upsilon^2}\right] \quad \text{Eq. 34}$$

With:

$\varepsilon_{xx,yy,zz}$	The normal strain in x, y and z direction, respectively $[-]$
$\sigma_{xx,yy,zz}$	The normal stress in x, y and z direction, respectively $[-]$
E	Young's Modulus $[\mathrm{F/L^2}]$
$E_{app,x}$	Apparent Young's Modulus in x-direction $[\mathrm{F/L^2}]$

The theoretical longitudinal apparent Young's Modulus $E_{app,x}$ is checked against the apparent numerical Young's Modulus E_x, which is obtained using Eq. 35. Values of σ_{xx} and ε_{xx} are probed using the probe-tool in ABAQUS for several nodes of all connection types (22, 26, 32 and $36\ \mathrm{mm}$ holes).

$$E_x = \frac{\sigma_{xx}}{\varepsilon_{xx}} \quad \text{Eq. 35}$$

All numerical results for resin-injected specimen yield the same value of $E_x \approx 1{,}38 \cdot E$, compared to the theoretical $E_{app,x} = 1{,}35 \cdot E$ $(\upsilon = 0{,}3)$. For grout, the numerically obtained $E_x \approx 1{,}12 \cdot E$ is also rather close to the theoretical $E_{app,x} = 1{,}11 \cdot E$ $(\upsilon = 0{,}2)$. Hence, it can be concluded that (1) the injection material can be assumed to be fully confined and (2) the beneficial effect of confinement on the stiffness is largest for materials with a higher Poisson's Ratio. The latter is directly based on Eq. 34, which is illustrated in Figure 121. Hence, it can be useful to investigate if there are any materials with a high Poisson's Ratio which are suitable for (liquid) injection.

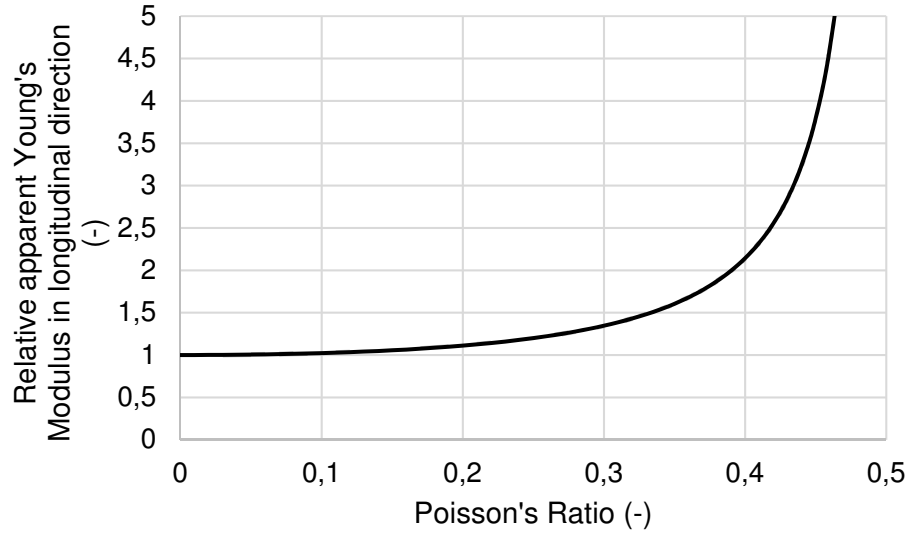

Figure 121 - Graphical representation of Eq. 34, showing the dependency between Poisson's Ratio and relative apparent Young's Modulus in longitudinal direction assuming full lateral confinement

Based on Eq. 29-Eq. 31 and Eq. 34 the effect of the cover plate can be derived. Assuming that in thickness direction the material is unconfined, whereas in lateral (width) direction the material is still confined, hence $\sigma_{zz} = 0$ and $\varepsilon_{yy} = 0$. Substituting these conditions into Eq. 29-Eq. 31 yields Eq. 36. Hence, the effect of the cover plate can be approximated by the difference between the expressions of Eq. 34 and Eq. 36, as expressed through Eq. 37 and Figure 122. For a number of discrete Poisson's Ratios, the effect of the cover plate on the apparent longitudinal Young's Modulus is tabulated in Table 20.

$$E_{app,x,} = E \cdot \left[\frac{1}{1-\upsilon^2}\right] \qquad \text{Eq. 36}$$

$$\Delta E_{app,x,CP} = E \cdot \left[\frac{\upsilon^2}{2\upsilon^3 - \upsilon^2 - 2\upsilon + 1}\right] \qquad \text{Eq. 37}$$

With:

E	Young's Modulus $[\mathrm{F/L^2}]$
υ	Poisson's Ratio $[-]$
$E_{app,x}$	Apparent Young's Modulus in x-direction $[\mathrm{F/L^2}]$

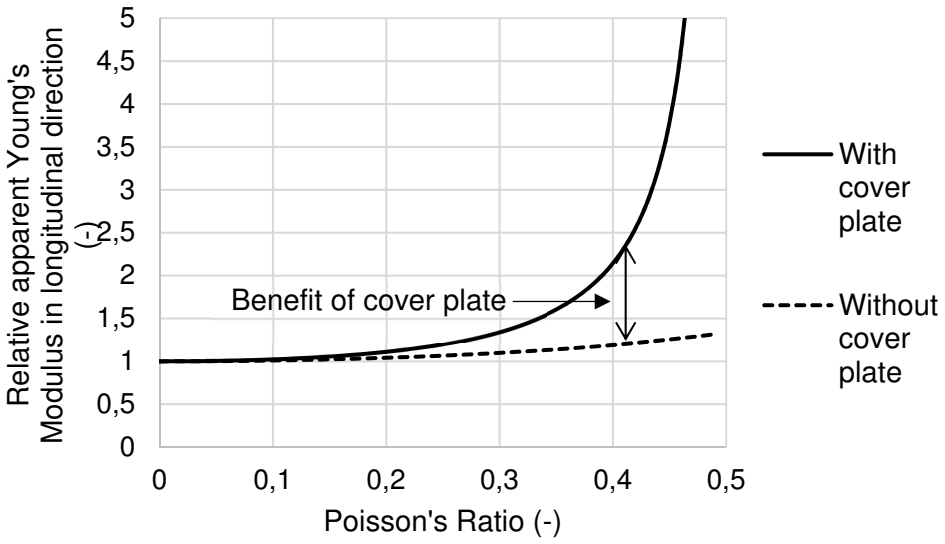

Figure 122 - Graphical representation of Eq. 34 and Eq. 36 , showing the effect of the cover plate (distance between both lines)

Table 20 - Relative beneficial effect of cover plate on the longitudinal stiffness / Young's Modulus

$\boldsymbol{\upsilon}\ (-)$	Gain in longitudinal stiffness as a result of full confinement due to cover plate (%)
0,2	+6%
0,3	+22,5%
0,4	+80%
0,49*	+1200%
*: For $\upsilon = 0{,}5$ the apparent Young's Modulus under the assumption of full confinement goes to infinity	

As a check, the numerical model was adapted to determine the apparent longitudinal Young's Modulus in case no cover plate is present. In this case, $E_x \approx 1{,}11 \cdot E$ compared to the analytical $E_{app,x} = 1{,}1 \cdot E$, indicating the validity of the analytical model.

Using ABAQUS, the relative bearing stress distribution along the perimeter of the bolt is determined and compared to the analytical solution presented in Section 2.8. The results are presented in Figure 123 and clearly indicate that the numerical and analytical model yield the same bearing stress distribution. Since the nominal bearing stress and the true analytical bearing stress distribution are linked analytically (Section 2.8) and that the first is the average of the latter, there is no further use in developing design models based on the true analytical bearing stress distribution. However, for use in creep models, the stress distribution is of utmost importance, given that the creep strain rate does not depend on stress linearly but exponentially.

.

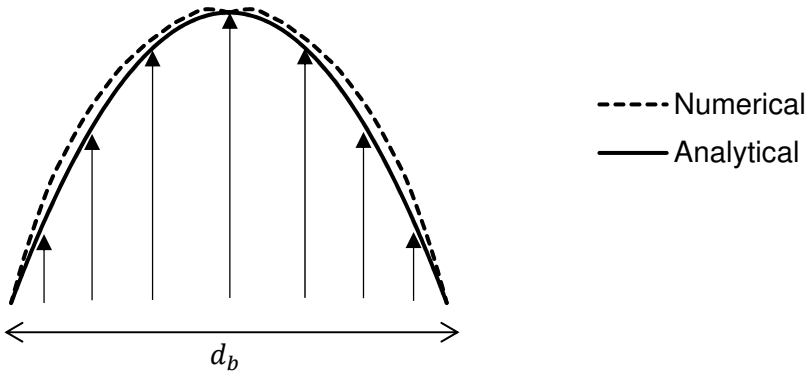

Figure 123 – Relative longitudinal bearing stress distribution according to the numerical and analytical model over the width of the bolt.

Both resin- and grout-injected double lap shear connections can withstand external loads well above the load at which $0{,}15\ \mathrm{mm}$ slip at CBG occurs. Although the connection stiffness decreases for increasing slip levels, sudden slip is prevented for all oversize holes studied. Experiments have shown that the ultimate failure of the connection is caused by failure of the plate, and that until this plate failure initiates the load is able to constantly increase. Hence, it appears that the validity of the conclusion of Gresnigt & Stark (1996) [2] that injection bolts in nominal clearance holes prevent sudden slip can be extended for injection bolts in oversize holes.

Based on the ultimate failure tests, it appears as if the resin ultimately fails internally in shear, allowing for part of the resin to move past the bolt (Figure 124). This happens as a rigid body movement, rather than a flow of material. For the specimen with $Ø_{centre} = 22\ \mathrm{mm}$ the failure occurred as a combination of bearing and cleavage failure, whereas this was mainly cleavage failure for the specimen with $Ø_{centre} = 36\ \mathrm{mm}$. Both types of failure are exemplified through Figure 125

Figure 124 - Rigid body movement (sliding) of parts of resin within centre plate

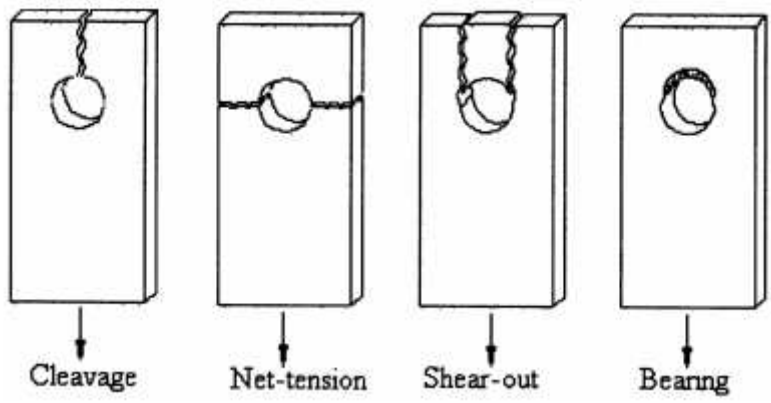

Figure 125 - Failure modes of plates in bolted connections (Pakdil, 2009) [76]

7.6 Long-term Loading of Injected Bolted Connections

The influence of creep deformation on the connection slip increases with increasing oversizing of the hole. Although all specimen were loaded up to 90% of the external load belonging to the short-term deformation criterion ($u_{CBG} = 0{,}15$ mm), a large difference in creep behaviour was observed. This difference can be understood through available creep models. For example, using the power law creep model (see also Section 2.5) expressed through Eq. 38, it can be seen that for a decrease in bearing stress of 50% the creep strain decreases more than 50% given the exponent is always $n > 1$. Using experimental data from other authors at TU Delft [57] the stress exponent can be estimated as $n \approx 1{,}6$ (see Figure 126) using the simplification that $q = \sigma_b$ (hence this is not the true material constant).

$$\varepsilon_{cr} = \frac{A}{m+1} \cdot q^n \cdot t^{m+1} \qquad \text{Eq. 38}$$

With:

A	Material constant $[\mathrm{L}^{2\mathrm{n}}/(\mathrm{F}^{\mathrm{n}} \cdot \mathrm{T}^{1+\mathrm{m}})]$
q	Uniaxial equivalent deviatoric stress (Mises stress) $[\mathrm{F}/\mathrm{L}^2]$
t	Time $[\mathrm{T}]$
m	Time exponent (material property) $[-](-1 < m < 0)$
n	Stress exponent (material property) $[-](n > 1)$

Table 21 provides an explanation for the larger creep deformation as a result of increasing oversizing of the hole. As can be seen from Table 21, the effect of the decrease in load needed to reach a connection slip of $0{,}9 \cdot 0{,}15 = 0{,}135$ mm is not enough to offset the larger length l_{inj} over which creep takes place. As a result, the creep increases for increasing oversize of the hole, at equal initial deformation/slip. It should be noted that the creep model indicated by Eq. 38 cannot directly be used to estimate the creep deformation or strain, given that the stress distribution and redistribution is more complex than a uniaxial stress distribution. Table 22 proves that there is no linear correlation between the creep model and experimental results.

Table 21 – Rough schematization of the relative effect of bearing stress and length of bearing path l_{inj} on creep deformation for different degrees of hole oversizing

$\emptyset_{centre}$ (mm)	F_{LT} (kN)	σ_b (MPa)	$\bar{\varepsilon}_{cr} \sim \sigma_b^n$ (MPa^n)	l_{inj} (mm)	$\Delta\bar{l}_{cr}$ ($\cdot 10^3$ mm)	Relative (-)
22	132,7	166	3652	2	7,3	1
26	104,0	130	2412	4	9,6	1,32
32	86,5	108	1793	7	12,6	1,73
36	75,2	94	1436	9	12,9	1,77

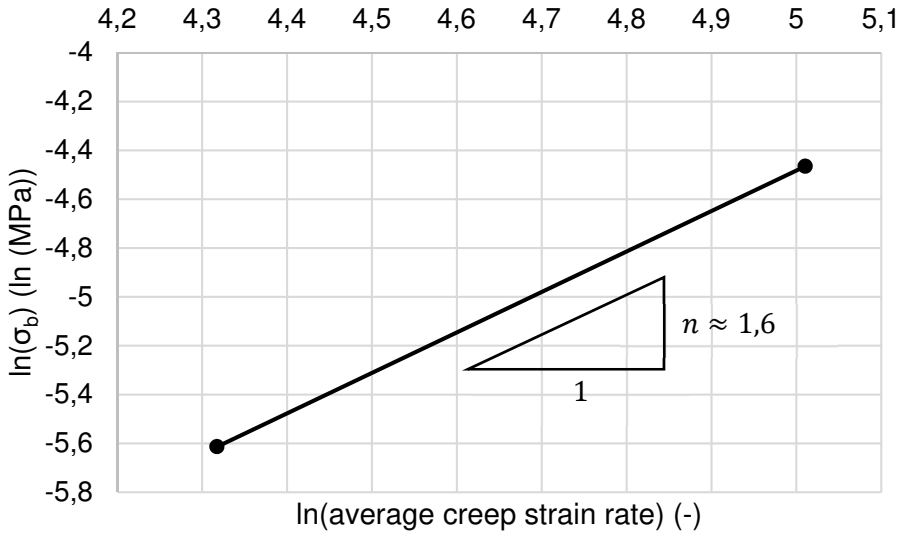

Figure 126 - Determination of stress exponent *n* based on long-term results at two different load levels on double lap shear connection with nominal clearance hole and M20 bolts (Li, 2017) [57]

Table 22 - Comparison between power law model and experimental results concerning relative creep deformation for different oversizing of centre plate holes

$Ø_{centre}$ (mm)	Relative creep deformation (-) at given t		
	Power law model	Experimental	Ratio Power law/Exp.
22	1	1	1
26	1,32	1,28	1,03
32	1,73	2,24	0,77
36	1,77	2,84	0,62

Given that the slip as a result of creep in the injection material dominates the total connection capacity with increasing oversize of the hole, it is suggested to look further into injection materials with a lower creep sensitivity, such as reinforced resin.

It was observed that the creep behaviour is non-linear on a linear slip and logarithmic time scale for non-reinforced resin-injected bolted connections, whereas a linear relationship was obtained for reinforced resin-injected bolted connections on the same set of axes. Figure 127 exemplifies two types of creep laws, power and logarithmic, hereby showing that as a result of the reinforcement the creep behaviour inherently changes.

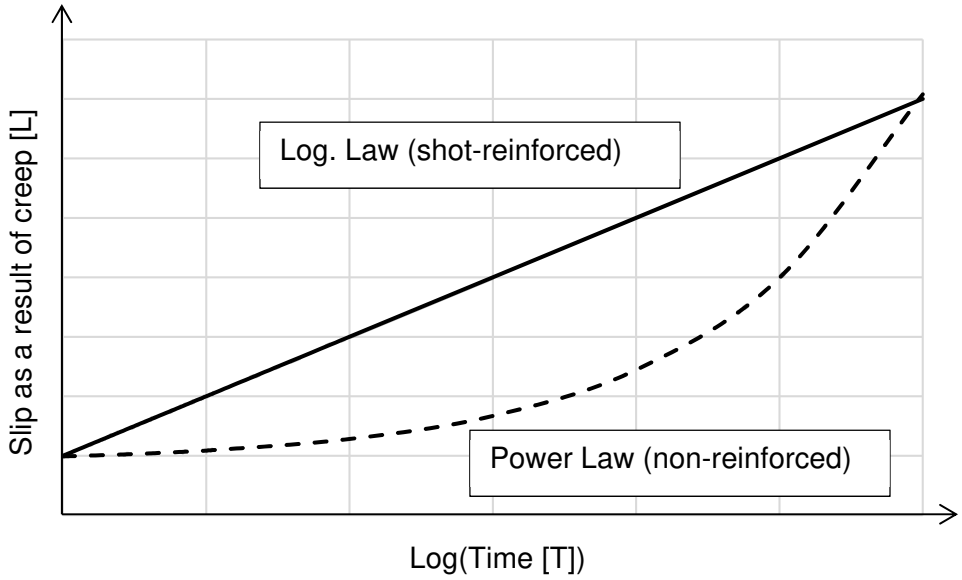

Figure 127 - Log(time) vs. linear creep slip, indicating the shapes of the curves for logarithmic and power creep laws. Magnitudes chosen arbitrarily.

7.7 Comparison between Experimental Results and EN 1993-1-8

As discussed in Section 2.1, EN 1993-1-8 contains a reduction factor k_s, to take account of the (negative) effects of oversize holes on the maximum allowable bearing stress. Unfortunately, no experimental tests could be carried out on specimen with bolt placement cf. EN 1090-2 [4] (bolts in most negative position with respect to connection slip). Hence, only a short-term numerical model of such connections is available. This linear numerical model is used to determine the relative load at $0{,}135$ mm of slip (CBG) for several hole diameters and is compared to the capacity according to EN 1993-1-8.

Although creep dominates the connection slip for increasing $Ø_{centre}$, it is not to be expected that the bearing capacity of the resin approaches zero, as currently implied by EN 1993-1-8. The true long-term relative bearing capacity will most likely be lower bounded by the capacity according to EN 1993-1-8, but will definitely be lower than the short-term bearing capacity found using the numerical model. In order to economically and successfully use injection bolts in significantly oversize holes, it is suggested to conduct more experimental research to find expressions for k_s that resemble the true bearing capacity as a function of oversizing. This is especially relevant, given that the current regulations are obtained using experiments with a maximal oversize $Ø_{centre} = 26$ mm (ECCS Recommendations, 1994) [5]

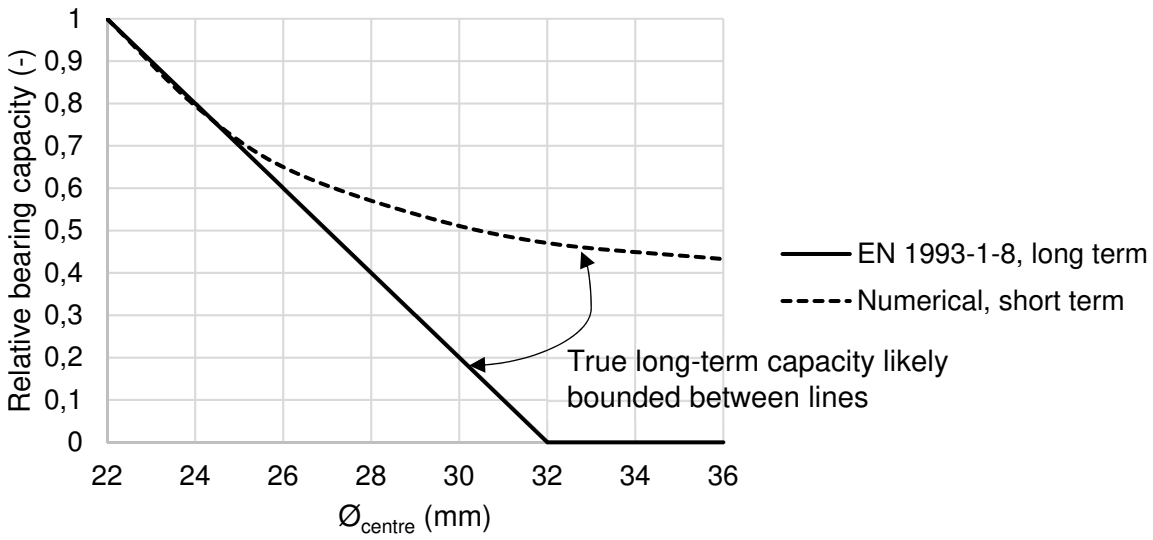

Figure 128 - Relative bearing capacity according to EN 1993-1-8 (long-term) and Numerical Model (short-term)

7.8 Benefits of Reinforced Resin-Injected Connections

In Chapter 6, the concept of reinforced resin-injected connections has been developed and tested. Based on these tests, it appears that reinforced resin-injected connections have certain benefits over their non-reinforced counterparts. Figure 130 illustrates the difference in short-term behaviour: the initial connection stiffness of the shot-reinforced is 71% higher than that of the non-reinforced connections. The creep behaviour of shot-reinforced connections under the 86% higher load is significantly less than that of the non-reinforced connections, as exemplified through Figure 129. A complete comparison is given through Table 23

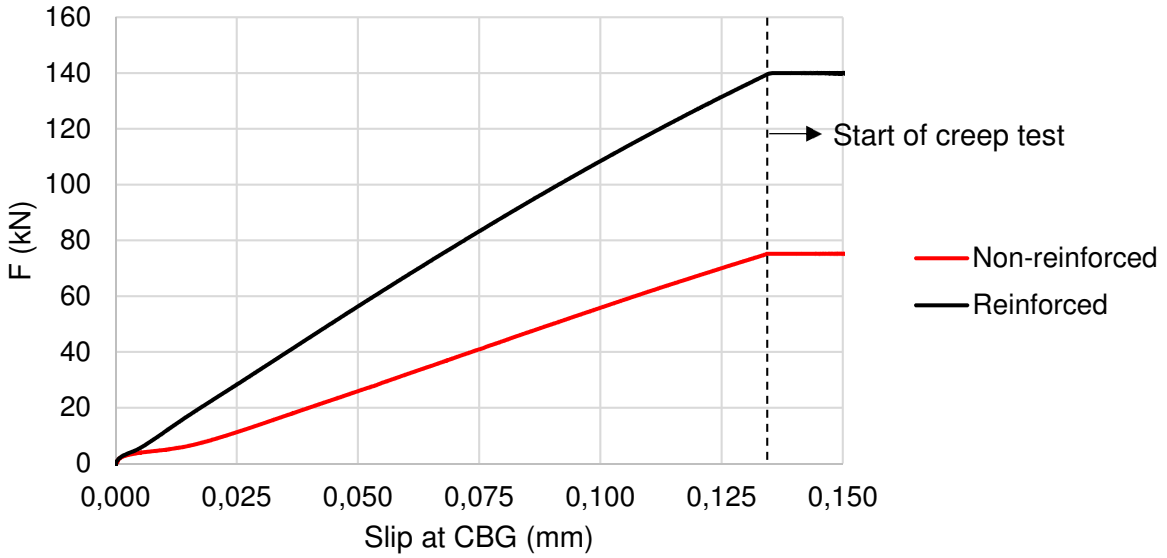

Figure 130 - Force-slip diagram for non-reinforced and shot-reinforced specimen (averaged)

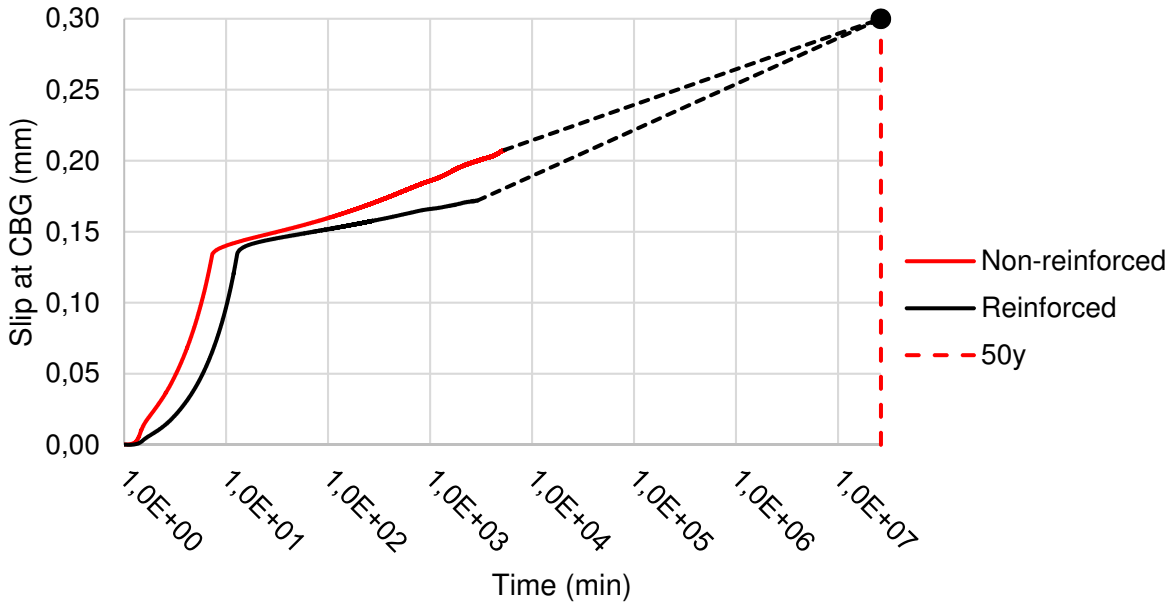

Figure 129 – Slip-time diagram for non-reinforced and shot-reinforced specimen (averaged)

Table 23 - Comparison between short- and long-term performance of non-reinforced and shot-reinforced connections

Connection Type	Initial connection stiffness $k_{ini}(\mathbf{kN/mm})$	Long-term load F_{LT} (kN)	Slip creep deformation after.. (mm)		
			24h	48h	72h
Non-reinforced	$5{,}8 \cdot 10^2$	75,2	0,0584	0,0677	0,0719
Shot-reinforced	$9{,}9 \cdot 10^2$ (+71%)	140 (+86%)	0,0381 (-35%)	0,0422 (-38%)	Not measured

As discussed in Section 6.3, both reinforced and non-reinforced resin-injected connections have a clear hysteresis is present in their respective load-slip diagrams, and the load level belonging to a certain slip level decreases for increasing amount of iterations. However, after a few iterations, the load level that can be reached at a certain slip level stabilizes. Hence, in this perspective there is no significant advantage of one connection type over the other.

Based on these results, it can be concluded that shot-reinforced connections have benefits in all structural ways tested for: higher load capacity with smaller time-dependent slip as a result of creep. However, it should be noted that no fatigue tests were carried out, meaning that in this perspective the relative performance cannot be determined.

7.9 Research Limitations

7.9.1 Study Design Limitations

Within the study conducted in this thesis, the experimental programme was only geared towards a specific test set-up, namely the test set-up from Annex G of EN 1090-2 [4]. This constraint means that connections with other geometrical characteristics, e.g. different l/d or t_1/t_2 ratios, do not necessary share the trends and results obtained within the experimental programme, for example due to other governing influences. However, generally it seems a good approximation to limit the maximum effective l/d ratio to $l/d = 3$, meaning that the difference in results is expected to be small. The effects of the ratio t_1/t_2, however, deserves more attention in future research, given that also in literature only limited information is available.

7.9.2 Impact Limitations

Within this thesis, the focus lay on only one type of grout and one type of resin. With respect to the resin, the choice is rather well defendable, given that this resin (Araldite/RenGel SW 404 + HY 2404) is the only resin allowed by the Dutch Ministry of Infrastructure (Rijkswaterstaat). Moreover, recent (unpublished) research has indicated that no epoxy resins are available on the market that provide a better performance. However, the grout was chosen arbitrarily, only looking at product sheet information and whether the manufacturer saw potential in the ability to inject his product through very narrow openings. This means that the impact of this thesis is largest for resin-injected connections, and that for grout-injected connections several other grouts should be obtained or designed, and tested for their performance.

Given the Study Design Limitations (section 7.9.1), the impact of this work only relates to very specific connection details. By carrying out more geometrically diverse experiments, the impact could be more significant, and lead to general recommendations in the design of injected bolted connections with oversize holes.

With regards to the creep tests, it should be noted that these have last for only a relatively short time (3 days – 2 weeks) compared to the deformation criterion at 50 years. Hence, all conclusions made in this report are only valid on the condition that the properties of the injection material do not degrade in time. Whether or not this is the case shall be further investigated, i.e. what degradation mechanisms described by e.g. Kajorncheappunngam (1999) [20] play a role in resin-injected connections.

7.9.3 Statistical Limitations

Only one specimen was tested per type of connection and test (short- and long-term). This results in a total of two connections, and thus two test results. Although two test results is not enough to have any value for a statistical analysis, the use of 4 LVDTs per test result decreases the influence of measurement errors. Moreover, the spread between the two test results was generally less than 5%. However, in order to create a design recommendation or design code, more tests are necessary to obtain any statistical significance.

8 Conclusions & Recommendations

8.1 Conclusion

Injection bolts are generally used to obtain slip-resistant connections by injecting a two-component epoxy resin into the free volume within the connection. Without precautions, it is not easily possible to demount such connections due to the adhesive bond between the resin and steel members. The formation of such an adhesive bond can be prevented by the use of a release agent, amongst which are wax-, silicon-, PFTE- and PVA-based products. If such products are used to coat the connection components, the connection can be demounted using hand tools (wrench, hammer).

An alternative to resin as an injection material is grout. The injectability of grout depends on the location of the washer with respect to the bolt, but this is not a limiting factor, given that special washer designs are available that prevent such injection problems (Qureshi & Mottram, 2012) [16]. Air inclusions were observed in the hardened grout, which are partially related to the formation of air bubbles as a result of super plasticising agents, and partially to the method of injection. Grout does not bond well to smooth steel, and thus no release agents are needed to allow for demounting of the connection.

In order to assess the influence of the oversize hole on the connection stiffness, experiments with $\mathrm{M20}$ bolts in holes with diameters of 22, 26, 32 and 36 mm were conducted. One of the effects of oversize holes in injected bolted connections is a reduced initial connection stiffness. Based on the experiments, a linear-elastic numerical model was calibrated. Based on this model, it could be concluded that connections with oversize round holes show larger connection stiffness than connections with slotted holes for the same longitudinal clearance, which is related to stress spreading in lateral direction. The effect of stress spreading becomes more significant for larger oversize holes. Hence, oversize round holes have the favourable characteristics of (1) providing the largest alignment potential and (2) the highest connection stiffness.

The use of injected bolted connections with oversize holes does not only decrease the connection capacity at a given slip level, but also leads to increased time-dependent slip as a result of creep of the injection material. The increased slip as a result of creep can be explained in its most basic form by the use of creep models. The creep of the injection material appears to govern the maximum load on the connection that can be withstood without exceeding the deformation (slip) limit of $0{,}3$ mm in 50 years imposed by $\mathrm{EN\ 1993\text{-}1\text{-}8}$ [3]. Creep tests were only conducted on resin-injected connections, given the uncertainty of successful grout injection using the chosen method.

The benefit of using a plate washer or cover plate is largest for injection materials with a higher Poisson's Ratio, since for such materials a higher confinement stress builds up. For epoxies, this benefit is roughly 20%, whereas this is much less for grout (6%), under the assumption of $\upsilon = 0{,}3\ (-)$ and $\upsilon = 0{,}2\ (-)$ respectively.

In an attempt to increase the initial connection stiffness and to reduce the creep deformation in connections with oversize holes, the free volume within the connection was filled with steel shot prior to injection with resin. The idea behind this concept is that the reinforcement transfers the load, whereas the resin provides a continuous matrix and protects the reinforcement against any detrimental external influences. Shot-reinforced resin-injected connections show a significantly higher load capacity $(+86\%)$ at $0{,}15$ mm of connection slip, and reduced creep deformation under this significantly higher load. The creep deformation can be expressed through a logarithmic creep law. Upon loading and reloading, the load capacity at a given slip level decreases slightly, but stabilizes after a few cycles, even at slip levels above the $0{,}3$ mm

slip criterion. Although the reinforcement (shot) is significantly stiffer than the resin, the connection must still be injected to prevent rigid body movement of the reinforcing particles. It is concluded that (shot-) reinforced resin may be promising to be used in injected connections with oversize holes.

Concludingly, it is advised to use round oversize holes and a release agent to create a demountable connection. In order to maximize the connection stiffness, a cover plate must be used. Reinforced resin as an injection material may (1) increase connection stiffness and (2) overcome the governing influence of creep on the connection slip. Given that the concept of reinforced resin is only in its early development, the full potential is not yet reached. It is suggested to find applications in specific structures/connections for this newly-developed material, in order to promote its further development.

8.2 Recommendations for Future Research

Based on the results obtained in this feasibility study, it is recommended to further investigate the following topics:

- Interaction between reinforcement and (resin) matrix in reinforced resin-injected connections
  - Purpose of such an investigation could be to improve the design of reinforcement, e.g. shape and gradation
- Development of a (compressive) creep model for the two-component epoxy resin Araldite/RenGel SW 404 + HY 2404, also in combination with reinforcement
  - To be used as input for Finite Element models of injected bolted connections, in order to assess the creep behaviour of a connection numerically. This can be done on plain specimen under uniaxial compression, or with additional tests with more variability in terms of load and geometry on injected connections using sophisticated software such as Isight [58] to automatically fit a material model.
- Execution of (reinforced) resin-injected connections with oversize holes
  - Current investigation is small-scale with well-defined and well-accessible injection and insertion channels. How can proper filling of the connection be assured in practice for different connection geometries?
- Fatigue strength of (reinforced) resin-injected connections
  - Tests are currently executed at TU Delft to assess the fatigue strength of non-reinforced resin-injected connections. To what extent does the addition of reinforcement in combination with oversize holes change the fatigue strength?
- Detailing and long-term + fatigue behaviour of grout-injected connections
  - Development of connection and execution details in such a way that (1) grout can be injected properly (2) without excessive air inclusions. Also the creep and fatigue behaviour of grout needs to be assessed to determine types of connections which would be appropriate to be grout-injected.

9 References

[1] RCSC, Specification for Structural Joints Using High-Strength Bolts, Chicago: RCSC, 2014.

[2] A. M. Gresnigt and J. W. B. Stark, “Design of Bolted Connections with Injection Bolts,” in *Connections in Steel Structures III: Behaviour, Strength and Design*, Oxford, Elsevier Science, 1996, pp. 77-87.

[3] European Committee for Standardization, “NEN-EN 1993-1-8: Design of Steel Structures- Part 1-8: Design of Joints,” Nederlands Normalisatie Instituut, Delft, 2011.

[4] European Committee for Standardization, “NEN-EN 1090-2: Execution of Steel Structures and Aluminium Structures - Part 2: Technical Requirements for Steel Structures,” Nederlands Normalisatie Instituut, Delft, 2011.

[5] ECCS, “European Recommendations for Bolted Connections with Injection Bolts,” ECCS Publication No. 79, Brussels, 1994.

[6] A. M. P. De Jesus, J. F. N. da Silva, M. V. Figueiredo, A. S. Ribeiro, A. A. Fernandes, J. A. F. O. Correia, A. L. L. da Silva and J. M. C. Maeiro, “Fatigue Behaviour of Resin-Injected Bolts: An Experimental Approach,” in *Iberian Conference on Fracture and Structural Integrity*, 2010.

[7] J. A. F. O. Correia, A. M. P. De Jesus, C. Rebelo and L. S. Da Silva, “Fatigue Behaviour of Single and Double Shear Connections with Resin-Injected Preloaded Bolts,” in *19th Congress of IABSE Stockholm 2016*, 2016.

[8] M. P. Nijgh, “Loss of Preload in Pretensioned Bolts,” Delft University of Technology, Delft, 2016.

[9] European Committee for Standardization, “NEN-EN 14399: High Strength Structural Bolting Assemblies for Preloading,” Nederlands Normalisatie Instituut, Delft, 2015.

[10] J. Kortis, “The Numerical Solution of the Bolted Connection With The Low-Quality Injection Bolts,” in *Proceedings of the 9th International Conference on New Trends in Statics and Dynamics of Buildings*, Bratislava, 2011.

[11] Tosec, “5 Factoren die de Prijs van Lasersnijden Beïnvloeden,” [Online]. Available: http://www.tosec.nl/wiki/kosten-lasersnijden/. [Accessed 9 1 2016].

[12] Inter-Composite, “Gelcoat Resin: Araldite SW 404 Resin with HY 2404 Hardener,” [Online]. Available: http://inter-composite.com/wp-content/uploads/2012/12/Araldite-SW-404-a-HY-2404.pdf.

[13] A. M. Gresnigt and D. Beg, “Design Bearing Stresses for Injection Bolts with Short and Long Duration High Loads,” in *Research and Applications in Structural Engineering, Mechanics and Computation*, Boca Raton, CRC Press, 2013, pp. 471-472.

[14] D. A. N. de Freitas, M. S. de Araújo and J. A. Cerri, “Propriedades Mecanicas de um Molde de Composito Multicamadas para Colagem Sob Pressao de Pecas Ceramicas,” in *CBECIMAT*, Joinville (Brasil), 2012.

[15] A. Koper, “Title not yet known (unpublished work),” Delft University of Technology, TU Delft, 2017.

[16] J. Qureshi and J. T. Mottram, “Resin Injected Bolted Connections: A Step Towards Achieving Slip-Resistant Joints in FRP Bridge Engineering,” in *FRP Bridges 20212 - NetComposites*, London, 2012.

[17] Sika Ltd., “Sikadur 30 - Adhesive for bonding Carbon Fibre & Steel Reinforcement,” [Online]. Available: http://resapol.com/wp-content/uploads/2015/05/Sikadur-30.pdf.

[18] D. Fernando, T. Yu, J. G. Teng and X. L. Zhao, “CFRP Strengthening of Rectangular Steel Tubes Subjected to End Bearing Loads: Effect of Adhesive Properties and Finite Element Modelling,” *Thin-Walled Structures,* vol. 47, no. 10, pp. 1020-1028, 2009.

[19] B. J. P. M. Carvalho, “Modelação por elementos finitos do comportamento de ligações aparafusadas sem e com resina injetada,” Universidade de Trás-os-Montes e Alto Douro, Vila Real, 2013.

[20] S. Kajorncheappunngam, “The Effects of Environmental Ageing on the Durability of Glass/Epoxy Composites,” Howell Information and Learning Company, Ann Arbor, 1999.

[21] C. A. Daniels, Polymers: Structure and Properties, Lancaster: Technomic Publishing Company Inc, 1989.

[22] T. Osswald, Understanding Polymer Processing: Processes and Governing Equations, Cincinnati: Hanser, 2010.

[23] M. Miravalles and I. Dharmawan, “The Creep Behaviour of Adhesives,” Chalmers University of Technology, Göteborg, 2007.

[24] L. P. Bouwman, “De invloed van de dikteverhoudingen van hoofd- en stuikplaten op de toelaatbare stuikspanning bij verbindingen met injectie-bouten,” TU Delft, Stevin Report 6-74-11, 1974.

[25] E. Ellobody and B. Young, “Design and Behaviour of Concrete-Filled Cold-Formed Stainless Steel Tube Columns,” *Engineering Structures,* vol. 28, no. 5, pp. 716-728, 2006.

[26] J. B. Mander, M. J. N. Priestley and R. Park, “Theoretical Stress-Strain Model for Confined Concrete,” *Journal of Structural Engineering,* vol. 114, no. 8, pp. 1804-1826, 1988.

[27] F. E. Richart, A. Brandtzaeg and R. L. Brown, “A Study of the Failure of Concrete under Combined Compressive Stresses,” *University of Illinois Bulletin,* vol. 26, no. 12, 1928.

[28] L. P. Saenz, “Discussion of 'Equation for the stress-strain curve of concrete' by Desayi, P. and Krishnan, S.,” *Journal of American Concrete Institute,* vol. 61, pp. 1229-1235, 1964.

[29] H. T. Hui and W. C. Schnobrich, “Constitutive Modeling of Concrete by Using Nonassociated Plasticity,” *Journal of Materials in Civil Engineering,* vol. 1, no. 4, pp. 199-216, 1989.

[30] European Committee for Standardization, “NEN-EN 1992-1-1: Design of Concrete Structures - Part 1-1: General Rules and Rules for Buildings,” Nederlands Normalisatie Instituut, Delft, 2011.

[31] H. Le Chatelier, “Sur les changements de volume qui accompagnent le durcissement des ciments,” *Bullet. de la société d'encouragement pour l'industrie nationale,* vol. 5, no. 5, pp. 54-57, 1900.

[32] Concrete Construction, “WHAT IS SHRINKAGE-COMPENSATING CONCRETE?,” 1 11 1999. [Online]. Available: http://www.concreteconstruction.net/how-to/what-is-shrinkage-compensating-concrete_o. [Accessed 12 01 2017].

[33] S. A. Kristiawan, “Strength, Shrinkage and Creep of Concrete in Tension and Compression,” *Civil Engineering Dimension,* vol. 8, no. 2, pp. 73-80, 2006.

[34] T. C. Powers, “Mechanism of Shrinkage and Reversible Creep of Hardened Portland Cement Paste,” *Proceeding of International Conference On the Structure of Concrete, Cement and Concrete Association,* pp. 319-344, 1968.

[35] R. Lin, “Shape Memory Alloys and Their Applications,” Stanford University, Stanford, 1996.

[36] J. Van Humbeeck, “Shape Memory Alloys: A Material and a Technology,” *Advanced Engineering Materials,* vol. 3, no. 11, pp. 837-849, 2001.

[37] University of Washington, “Applications for Shape Memory Alloys,” [Online]. Available: https://depts.washington.edu/matseed/mse_resources/Webpage/Memory%20metals/applications_for_shape_memory_al.htm. [Accessed 11 1 2017].

[38] MAPEI, “Mapefill - High-Flow Non-Shrink Cementitious Anchoring Grout,” [Online]. Available: http://www.mapei.com/public/COM/products/305_mapefill_gb.pdf. [Accessed 14 12 2016].

[39] Parex, “100 Newton Grout,” [Online]. Available: http://www.parex.co.uk/GetFile.ashx?file_id=1068. [Accessed 12 1 2017].

[40] L. P. Bouwman, “Het monteren, het injecteren en het demonteren van injectiebouten (Installation, injection and dismantling of injection bolts),” TU Delft, Stevin Report 6-72-14A, 1972.

[41] Epotek, “Tech Tip 22: Using Mold Release Agents with Epoxy Adhesives,” 2012. [Online]. Available: http://www.epotek.com/site/files/Techtips/pdfs/tip22.pdf. [Accessed 15 1 2017].

[42] H. J. Smits and L. P. Bouwman, “Investigation to the application of Seperating Liquids for Injected Bolt-Connections,” TU Delft, Delft, 1972.

[43] M. Veljkovic, M. Feldmann, C. Rebelo, M. G. Charalampos Baniotopoulos, V. Dehan and G. Nüsse, “HISTWIN+: High-Strength Steel Tower for Wind Turbines,” 2015.

[44] Y. Cheng and X. Ke, “Shear Strength of a Cold-Formed Steel Sheet in Bolted Connections Using Oversized Holes,” *Journal of Structural Engineering,* vol. 139, no. 5, pp. 860-864, 2013.

[45] R. N. Allan and J. W. Fisher, “Behavior of Bolted Joints with Oversize or Slotted Holes,” *Fritz Engineering Laboratory Report No. 318.3,* 1967.

[46] E. Chesson and W. H. Munse, “Studies of the Behavior of High-Strength Bolts and Bolted Joints,” University of Illinois, Urbana, 1965.

[47] M. Aublin, R. Boncompain, M. Boulaton, D. Caron, É. Jeay, B. Lacage and J. Réa, Systèmes mécaniques : théorie et dimensionnement, Dunod, 1992.

[48] C. Texeido, J.-C. Jouanne, B. Bauwe, P. Chambraud, G. Ignatio and C. Guérin, Guide de construction mécanique, Delagrave, 2000.

[49] D. Spenlé and R. Gourhant, Guide du calcul en mécanique : maîtriser la performance des systèmes industriels, Paris: Hachette Technique, 2003.

[50] T. Rugelj and D. Beg, “Uporaba Injektiranih Vijakov V Jeklenih Konstrukcijah,” *30. Zborovanja gradbenih konstruktorjev Slovenije,* pp. 171-178, 2008.

[51] PAGEL SPEZIAL-BETON, “V1HF Hogesterkte Gietmortel K90,” [Online]. Available: http://www.pagel.com/all/pdf/nl/v1_hf_nl.pdf. [Accessed 21 1 2017].

[52] Epotek, “Tech Tip 19: Understanding Mechanical Properties of Epoxies for Modeling, Finite Element Analysis (FEA),” Epoxy Technology Inc., Billerica, 2012.

[53] C. F. Gauss, “Recension der ``Untersuchungen über die Eigenschaften der positiven ternären quadratischen Formen von Ludwig August Seeber.'',” *Göttingsche Gelehrte Anzeigen,* vol. 1831, p. 1065, 1840.

[54] G. D. Scott and D. M. Kilgour, “The Density of Random Close Packing of Spheres,” *Journal of Physics D: Applied Physics,* vol. 2, no. 6, p. 863, 1969.

[55] G. W. Marshall and T. S. Hudson, “Dense Binary Sphere Packings,” *Contributions to Algebra and Geometry,* vol. 51, no. 2, pp. 337-344, 2010.

[56] S. D. S. Reis, N. A. M. Araujo, J. S. Andrade and H. J. Herrmann, “How Dense can one Pack Spheres of Arbitrary Size Distribution?,” *EPL,* vol. 97, p. 18004, 2012.

[57] J. Li, “Title not yet known (unpublished work),” Delft University of Technology, Delft, 2017.

[58] Dassault Systemes Simulia, “Isight - Automate Design Exploration and Optimization,” [Online]. Available: https://www.3ds.com/fileadmin/PRODUCTS-

SERVICES/SIMULIA/RESOURCES/simulia-isight-brochure.pdf. [Accessed 26 2 2017].

[59] B. Zafari, J. Qureshi, J. T. Mottram and R. Rusev, “Static and Fatigue Performance of Resin Injected Bolts for a Slip and Fatigue Resistant Connection in FRP Bridge Engineering,” *Structures,* no. 7, pp. 71-84, 2016.

[60] A. M. Gresnigt, G. Sedlacek and M. Paschen, “Injection Bolts to Repair Old Bridges,” *December,* pp. 349-360, 2012.

[61] X. L. Zhao, FRP-Strenghtened Metallic Structures, Boca Raton: CRC Press, 2014.

[62] K. Ravi-Chandar and Z. Ma, “Inelastic Deformation in Polymers under Multiaxial Compression,” *Mechanics of Time-Dependent Materials,* vol. 16, no. 2, pp. 333-357, 2000.

[63] [Art]. Wikimedia Commons.

[64] Screws & Fasteners, “Square Plate Washers M20”.

[65] H. Undrum, “Silicate- or Epoxy Zinc Primers - The Superior Protection,” Jotun AS, Sandefjord, 2016.

[66] E. Tazawa, S. Miyazawa and T. Kasai, “Chemical Shrinkage and Autogeneous Shrinkage of Hydrating Cement Paste,” *Cement and Concrete Research,* vol. 25, no. 2, pp. 288-292, 1995.

[67] C. Perabo, “Caplinq Blog: What Percentage of Carnauba Wax Spray is used in Epoxy Mold Compound?,” 7 5 2008. [Online]. Available: http://www.caplinq.com/blog/what-percentage-of-carnauba-wax-spray-is-used-in-epoxy-mold-compound_47/. [Accessed 15 1 2017].

[68] CSW, “Maeslantkering, stormvloedkering in de Nieuwe Waterweg. Tekening bovenaanzicht variant.,” Rijkswaterstaat, 1990.

[69] P. Vries, “Siroco - Bouwen met Staal,” 20 May 2016. [Online]. Available: http://www.bouwenmetstaal.nl/uploads/evenementen/techniekdag2016/05_Slip_resistant_connections_preload_in_bolts_pdv_May_2016.pdf.

[70] Citra Baru Perkasa, “RenGel SW 404 + HY 2404,” 2012.

[71] Home Depot, “Home Depot: HDX 160:20 Caulk Gun,” [Online]. Available: http://www.homedepot.com/p/HDX-160-20-Caulk-Gun-HD138C/202036534. [Accessed 24 1 2017].

[72] MIT (Massachusetts Institute of Technology), “Six-node wedge element / Eight-node brick element,” MIT, Cambridge (USA), 2014.

[73] SeminarsOnly, “Stone Mastic Asphalt,” 24 2 2016. [Online]. Available: http://www.seminarsonly.com/Civil_Engineering/Stone_Mastic_Asphalt.php. [Accessed 17 2 2017].

[74] E. W. Weisstein, “Kepler Conjecture,” MathWorld - A Wolfram Web Resource.

[75] M. H. J. Kroll, Artist, *Resin-injected preloaded bolts in the Maeslant Storm Surge Barrier.* [Art]. Het Keringhuis Publiekscentrum Water, 2017.

[76] M. Pakdil, “Failure Analysis of Composite Single Bolted-Joints Subjected to Bolt Pretension,” *Indian Journal of Engineering & Materials Sciences,* vol. 16, pp. 79-85, 2009.

Appendix A: Product sheet Araldite/RenGel SW 404 + HY 2404

Gelcoat Resin

Araldite® SW 404 Resin with HY 2404 Hardener

Filled epoxy system, abrasion resistant

Key Properties

- Easy to apply with brush or spatula, or by pouring
- Easy to use
- Covers sharp edges
- Cures rapidly at room temperature
- Outstanding mechanical strength
- Very hard, abrasion-resistant surfaces
- Very strong edges

Applications

- Foundry patterns
- Copy-milling models
- Foaming and concrete-casting moulds
- Tools and tooling aids

Typical product data

Property		Araldite SW 404	Hardener HY 2404
Appearance		blue, medium-viscosity liquid	yellow, transparent, low-viscosity liquid
Viscosity at 25 °C	mPa s	55,000 - 80,000	3,500 - 5,500
Density at 25 °C	g/cm^3	1.85 - 1.95	1.0 - 1.05

Processing

Mix ratio	Parts by weight
Araldite SW 404	100
Hardener HY 2404	10

Resin / Hardener mix at 20 - 25 °C

Viscosity		slightly thixotropic
Pot life (500 g batch)	min	25 - 30
Gel time, thin layer	min	40 - 45
Demouldable after	h	12-16

Properties

After cure for 7 days at 20 - 25°C

Property	Standard	Unit	Value
Density	-	g/cm^3	1.8 - 1.9
Shore D hardness	ISO 868	-	85 - 90
Compressive strength	ISO 604	N/mm^2	110 - 125
Flexural strength	ISO 178	N/mm^2	95 - 1 05
Flexural modulus	ISO 1 78	N/mm^2	9,000 - 9,500
Impact strength	ISO 179	kj/m^2	7.5 - 9.5
Deflection temperature	ISO 75	°C	70 - 75
Cold water absorption, 24h/23°C	ISO 62	mg	5.5 - 7.0
Boiling water absorption, 30 min	ISO 117	mg	30 - 40
Abrasion resistance (S/33 sandpaper strips, 500 P load)	NEMA	mg/100 rpm	8 - 1 5

Storage

The resin and hardener described in this instruction sheet have the shelf lives shown provided they are stored in a dry place at 18°C - 25°C and in the original sealed containers.

Resin which has solidified in storing owing to low temperatures can be re-conditioned by heating it to 70 - 80°C for about an hour and stirring it thoroughly. The resin must be allowed to cool to room temperature before the hardener is added.

Handling precautions

Caution

Ciba Specialty Chemicals' products are generally quite harmless to handle provided that certain precautions normally taken when handling chemicals are observed. The uncured materials must not, for instance, be allowed to come into contact with foodstuffs or food utensils, and measures should be taken to prevent the uncured materials from coming in contact with the skin, since people with particularly sensitive skin may be affected. The wearing of impervious rubber or plastic gloves will normally be necessary; likewise the use of eye protection. The skin should be thoroughly cleansed at the end of each working period by washing with soap and warm water. The use of solvents is to be avoided. Disposable paper - not cloth towels - should be used to dry the skin. Adequate ventilation of the working area is recommended. These precautions are described in greater detail in Ciba Specialty Chemicals publication No. 24264/3/e Hygienic precautions for handling plastics products of Ciba Specialty Chemicals and in the Ciba Specialty Chemicals Material Safety Data sheets for the individual products. These publications are available on request and should be referred to for fuller information.

Appendix B: Product sheet PAGEL V1-0HF

V1HF PAGEL SUPER HIGH STRENGTH GROUT

PRODUCTS

- **V1/30HF** PAGEL SUPER HIGH STRENGTH GROUT (0–3 mm)
- **V1/60HF** PAGEL SUPER HIGH STRENGTH GROUT (0–6 mm)
- **V1/0HF** PAGEL SUPER HIGH STRENGTH GROUT (0 mm)

PROPERTIES

- cementitious and chloride-free
- frost and deicing-salt resistant CDF-tested in compliance with DIN CEN/TS 12390-9
- controlled and even expansion
- microsilica modified
- impermeable to water and highly resistant against oils and fuels
- certified to fire protection class A1 as specified by EN 13501 and DIN 4102
- vapour permeable
- high fatigue resistance
- absorbs vibrations
- pumpable and easy to pour
- complies with the DafStb Directive (VeBMR) on the "Manufacture and use of cementitious concrete and grout"
- externally tested and factory quality controlled in compliance with the DAfStb VeBMR Directive
- **company is certified according DIN EN ISO 9001:2008**

FIELDS OF APPLICATION

- turbines, compressors
- wind turbines, cast joints
- portal and container transport systems
- **V1/0HF**: Lubemix for hoses
  Jointfiller for hybrid towers

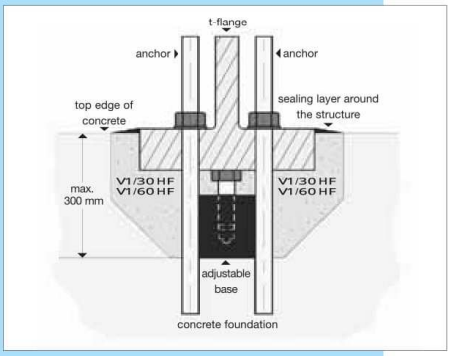

APPLICATION

SUBSTRATE: Clean thoroughly, remove all loose and unsound material such as cement slurry etc using a grit or water jet blaster or similar until the underlying grain structure is reached. The underlying substrate must have sufficient pull-off strength (i.m. ≥ 1.5 N/mm²).
Remove all of the rust from any exposed reinforcement bars with a sandblaster (Sa 2 1/2 as specified under DIN EN ISO 12944-4).
Wet the surface approx. 6–24 hours before grouting until capillary saturation.

FORMWORK: Attach in such a way that it is leak proof and robust. Seal around concrete base with, e.g. sand or dry mortar.

MIXING: The grout is supplied ready for use and only needs to be mixed with water. Measure out the quantity of water specified on the packaging and pour most of it into a clean and suitable mixing device (e.g. compulsory mixer). Add the dry mortar and mix for at least 3 minutes; add the remaining water and mix for another 2 minutes until it forms a uniform mass. Depending on the existing mixer longer mixing times may be required. Once the grout is ready mixed, apply immediately. If using a mixing and delivery pump and outputting material continuously, we recommend installing an agitator downstream of the mixing and delivery pump to ensure that the material is properly mixed. If using a mixing and delivery pump such as: PABEC II; we recommend the agitator: Putzmeister Dynamat.

MIXING WATER: Drinking water quality

GROUTING: The mixture must be poured from one side or corner only in one continuous pour. When grouting large areas, we recommend to pour the grout starting in the centre of the foundation plate, using a funnel or delivery house. On machine installations, cavities should be filled first (up to around just below the top edge) and then the base of the machine or similar.

CAUTION: On completion of the grouting, exposed areas must be immediately protected from premature water evaporation for a period of 3-5 days (wind, drafts, direct sunlight).

Methods that can be used to protect the grout: Misting the grout with water, covering it with foil and strips of felt, thermal insulation or a material that retains moisture,

O1 PAGEL EVAPORATION PROTECTION. When using **O1 PAGEL EVAPORATION PROTECTION**, observe the information on the Technical Data Sheet **O1 PAGEL EVAPORATION PROTECTION**.

Temperature limits for application (substrate, air and grout temperature): +5 °C to +35 °C
Applying the concrete in low temperatures and using cold mixing water will delay the concrete's strength development, require that it is intensely mixed and will reduce its flowability. High temperatures speed it up.

Protruding grout: Do not exceed the specified 50 mm when allowing grout to protrude and observe the structural specifications. When grouting dynamically stressed and prestressed base plates and machine foundations that are subject to high compression strengths at the edges, the grout should ideally be applied to be flush with the bearing plate, provided with a 45° edge using formwork or cut off flush with the bearing plate before it has set. This will prevent any stresses from becoming superimposed on one another and from becoming annihilated (observe static and structural specifications).

Non-iron metals: Cement and cementitious building materials may cause non-iron-metals (e.g. aluminium, copper, zinc) to loosen or come off where they are tied in. Please contact us for technical advice.

PAGEL-GROUT

Cement:
DIN EN 197-1 compliant
Aggregates:
EN 12620 compliant
Additives:
EN 450, AbZ, EN13263 compliant (quick ash, microsilica etc.)
Additional substances:
DIN EN 934-4 compliant

V1HF PAGEL SUPER HIGH STRENGTH GROUT

TECHNICAL DATA

TYPE			V1/30HF	V1/60HF	V1/0HF
grain size		mm	0–3	0–6	0
coating thickness		mm	30–300	40–400	–
amount of water	%	max.	9	9	20
consumption (dry mortar)		app. kg/dm³	2.30	2.30	1.836
density of freshly mixed mortar		app. kg/dm³	2.45	2.45	–
working time	20 °C	app. min	60	60	60
slump flow	5 min	cm	≥55	–	≥30
	30 min	cm	≥45	–	–
slump	5 min	cm	≥60	≥60	≥60
	30 min	cm	≥52	≥52	≥52
expansion	24 h	Vol. %	≥+0.1	≥+0.1	≥+0.3
compressive strength*	24 h	N/mm²	>70	>70	>60
	7 d	N/mm²	≥90	≥90	≥85
	28 d	N/mm²	≥130	≥115	≥100
	56 d	N/mm²	≥135	≥120	–
	91 d	N/mm²	≥135	≥120	–

All test data are guide values, proofed in our German manufacturing plants, - values from other manufacturing plants may vary.
* Grout compressive strength tested as specified by DIN EN 196-1; Concrete compressive strength tested as specified by DIN EN 12390-3
V1/30HF: Correl. compressive strength factor: Prism compression strength 40 x 40 x 160 mm : Cube compression strength 150 mm³ = 0.98

All of the test values provided correspond to DAfStb VeBMR – Directive
Tests of fresh and hardened grout at 20°C ± 2°C, storage of the test pieces after 24 hours until the strength test in water at 20°C ± 2°C. Higher or lower temperatures result in deviating properties and test results of the fresh/hardened grout. Depending on the temperature the consistency can be adapted by a slight reduction of the mixing water.

storage: 12 months. Cool, dry, free from frost. Unopened in its original packaging.
packaging: 20-kg bag, euro-pallet 960 kg, 1000-kg-Big-Bag
hazard class: no dangerous substance follow safety data sheet
giscode: ZP1

Exposure class according to:
DIN 1045-2 and EN 206-1
PAGEL – SUPER HIGH STRENGTH GROUT

	XO 0	XC 1 2 3 4	XD 1 2 3	XS 1 2 3	XF 1 2 3 4	XA 1 2 3	XM 1 2 3
V1/30HF	•	• • • •	• • •	• • •	• • • •	• •	•
V1/60HF	•	• • • •	• • •	• • •	• • • •	• •	•

Moisture classes in reference to concrete corrosion caused by alkaline silica reactions

moisture class	WO	WF	WA	WS
	dry	damp	damp · external alkali supply	damp · external alkali supply · strong dynamic stress
V1/30HF	·	·	·	·
V1/60HF	·	·	·	·

All of the aggregates used in PAGEL products are obtained from safe sources and correspond with the alkali sensitivity class E1 as specified under DIN EN 12620.

Classification according to DAfStb VeBMR - Directive
Product: PAGEL - GROUT

	V1/30 HF	V1/60 HF
flowability class	f1	a2
shrinkage class	SKVM 0	SKVB 0
early strength class	A	A
compressive strength class	C100/115	C100/115

CE
0921
PAGEL SPEZIAL-BETON
GMBH & CO.KG
Wolfsbankring 9
45355 Essen, Germany
11
110931
EN 1504-6:2006
Anchoring product
EN 1504-6: ZA.1

Pull-out	≤ 0.6 mm
Chloride ion content	≤ 0.05 %
Reaction to fire	A1

CE
0921
PAGEL SPEZIAL-BETON
GMBH & CO.KG
Wolfsbankring 9
45355 Essen, Germany
11
110932
EN 1504-6:2006
Anchoring product
EN 1504-6: ZA.1

Pull-out	≤ 0.6 mm
Chloride ion content	≤ 0.05 %
Reaction to fire	A1

PAGEL Spezial-Beton GmbH & Co.KG 45356 Essen
Werk Essen
VeBMR